A Hydrogen Hybrid Powertrain for the Union-Pearson Railway

by

Mehran Haji Akhoundzadeh

A thesis
presented to the University of Waterloo
in fulfillment of the
thesis requirement for the degree of
Master of Applied Science
in
Chemical Engineering

Waterloo, Ontario, Canada, 2019

AUTHOR'S DECLARATION

I hereby declare that I am the sole author of this thesis. This is a true copy of the thesis, including any required final revisions, as accepted by my examiners.

I understand that my thesis may be made electronically available to the public.

Abstract

Canadian legislation attempts to regulate particle emissions released from the rail transportation sector. Assessment of the impact of rolling stock is the key to perform such regulations. Different strategies have been proposed to evaluate the health risks of mobile emission sources. Popular methods in measuring health assessment of rolling stock were reviewed in this study. Hydrail was proposed as an alternative option helping Canadian legislation to regulate emission generated from this mode of transportation. The feasibility of developing Hydrail technology is investigated in this study.

As a case study, the drive cycle of the DMUs working on the Air-Rail link's tracks of Great Toronto Area (GTA) was extracted. A theoretical model was implemented to estimate the duty cycle of the train as it was not possible to access the DMU's throttle data. According to the duty cycle estimator subsystem, the annual emission released from the track is calculated. To assess the health risk on people, 32 places which are located near the track were collected, and the locations were extracted using Google Earth. These places include hospitals, schools, and social community centers. The concentration of three types of pollutants was locally approximated in the 32 places, using Gaussian air dispersion modeling method. To implement the model, commercial software, AERMOD, was used. To contemplate the health effect of the trains, the estimated pollution concentrations were compared with the air quality standards. The Hydrail was introduced as an alternative technology to reduce the health impact of the rail sector. The benefits and drawbacks of the technology were introduced in detail.

Finally, a hydrogen powertrain is designed in this study with respect to the estimated duty demand. This should be considered as the first subsystem of an end-to-end Hydrail design platform for this 25 Km long rail route. A frequency-based power management scenario was applied to the developed powertrain to control the power flow between energy sources. A sensitivity analysis was performed to approximate the system dynamics. The proposed power management scenario will be capable to optimally keep the system working in its optimal working region whenever it will become integrated with a real-time high-level global optimization subsystem.

Acknowledgments

First and foremost, I would like to express my deepest levels of sincere gratitude to my supervisors, Professor Michael Fowler, and Professor Kaamran Raahemifar. Professor Michael Fowler's motivations had directed me through the knowledge process when I was a newcomer to Canada. The ability to direct my research in the way that I believe it has an impact was fundamentally promoted by Professor Fowler. Professor Raahemifar has great patience and a clear mind, and he has shown me what I could achieve since the last five years. I want to thank him for his patience and supports. Besides my advisors, my special thanks to Professor Ting Tsui and Roydon Fraser for helping me during my master, more specifically when professor Fowler was in recovery. Also, I would like to convey my strong feelings of appreciation for my whole academic life supportive supervisor, Dr. Madjid Soltani, who has been directing me during my studies. In addition to my beloved supervisors, I had the chance to be supported with three more reference points, professor Saeid Amanpour, professor Mohammad Mahjoob Jahromi, and Dr. Alireza Shiri and I would like to express my strong feelings of appreciation to have their encouragement.

I would also like to thank my best friend, the lead of the research group, Dr. Ehsan Samadani, who has advised me in finding the path in my research. Working with Ehsan was my opportunity to understand the mean of patience and cooperation. I would also like to convey my special thanks to my kindest supportive friend, Dr. Satyam Panchal. He is one of the nicest people I have ever seen in my life. Dr. Kamyar Rouindej was the man who spent lots of time motivating me in different typical and unusual ways. I want to thank him for his incredible supports. Moreover, I offer my deepest thanks to Dr. Hadi Adibi for all his assistance and constructive feedbacks.

Last but not least, I would like to thank the key driver for my life's success, my family. I am very lucky to have such a great family who raised me with a love of science and supported me in all my pursuits and my life in general. Without my father and mother's constant moral support, it would not have been possible to finish my master degree. My brother, Mohsen, and my sister, Sarah, has turned out to be my best friends, and their understanding and encouragement have been present throughout my education.

Table of Contents

List of Figures

List of Tables

Chapter 1: Introduction, Research Objectives, and Outline

1.1 Introduction

In 2009, the Medical Officer of Health (MOH) requested from the Board of Health of Toronto (BHT) to conduct review research. The research was an approximation of all the health-related studies were carried out by the Metrolinx about the expansion of the Georgetown service. The main concern was the potential excess of health risks associated with the increased train traffics. Diesel exhaust and the main components are associated with major health risks. However, Metrolinx assessment showed a significant health risk associated with the rail routes and the recommended solution to protect the near tracks residencies' health was the electrification of the Georgetown South Service [1].

Two of the recommendations of the MOH to the BHT and Metrolinx are the main objective of concern in this manuscript. These two recommendations are allocated to the Metrolinx by the BHT. The first one was to conduct a health impact assessment study due to approximate the contribution of each train line to the total and annually diesel exhaust emissions and evaluate the impact of emission reduction achieved by the Georgetown Service electrification. On the other hand, the second one was to electrify the Georgetown south service as soon as possible [1].

In response to the allocated recommendations, Metrolinx intended to modify the electrified and non-electrified portions of Go network and enhance infrastructures as a program named "Regional Express Rail" (RER). The program is planned to be started in 2025, and the target is the locomotives and Electric Multiple Units (EMUs). In this regards, hydrogen fuel cell locomotives seem to be the first candidates of Metrolinx renovation [1].

1.2 Motivation and Research Objectives

A key parameter in feasibility investigation of hydrogen fuel cell EMUs is to figure out if the technology can support the expected performance of Metrolinx, BHT, and MOH. With the aim of such feasibility study, the following points should be evaluated, and the answers might show the path:

1. Components sizing and functionalities of a Hydrail system through an end-to-end model. End to end means that the system should be designed as an integrated complex system including rolling stocks as well as hydrogen production system and the other mandatory subsystems.
2. The electricity needed to produce the required hydrogen.
3. The hydrogen production scheduling in off-peak times to avoid extra production costs.
4. Optimal designed rolling stock in different sizes of which satisfying the Metrolinx requirements.
5. Refueling stations requirements supporting the daily hydrogen demand.

The main objective of this project is divided into two parts according to the BHO's recommendations to the Metrolinx and also Metrolinx modification intention. However, the first part is to identify the health risks in terms of three different types of mobile sources of air toxics, PM, NO_x, and HC. As a very simple scenario to evaluate the environmental impact of the track, in this part of the research, the concentration of these pollutions are calculated for 32 different places near the track, and the results are compared with the standards. Candidate places are hospitals and schools, which has more vulnerably at-risk occupants inside. The output results of this simple model, which did not consider detailed factors such as building downwash, does not show a significant impact for this single track with low traffic range based on the proximity standards. Although such a result was expected according to the literature [2], the analysis should be thought as a justification for track electrification in high traffic load railways. However, the output of the study, as future work, will be utilized in optimizing dedicated powertrains to be installed on any rolling stock working within high load tracks. However, the inconsistency of analysis for only one DMU should not lead to eliminating this important side from the designing progress of such end-to-end multidisciplinary concept like Hydrail. The second part of this thesis, as the main part, includes a semi-empirical model of a hydrogen hybrid powertrain which is represented to be used as a base platform for future studies. The benefits and the challenges of hydrogen rolling stock comparing to the electrified ones are explained in details in chapter 2. Accordingly, modeling of hydrogen locomotives should be performed at the first step of implementing such multilayered integrated system which has to be optimized in a systematic holistic platform. To construct a platform and prepare it as a host for the other subsystems, a comprehensive sensitivity analysis was conducted. Since the main challenge in Hydrail system development, at this level of accuracy,

is the energy flow and consumption, the sensitivity analysis of the powertrain, in this thesis was performed based on energy view and the results are represented in terms of degradation and durability of the fuel cell and battery. In implementing the power management algorithm, a rule-based frequency-domain power management system was implemented.

1.3 Thesis Outline

Chapter 2 is focused on the background of two parts of this thesis. In this chapter, the concept of mathematically modeling of air pollution will be represented. The air pollution regulation strategies are approximated in detail and the concept of Hydrail, as a recently proposed regulatory scenario, is defined, and the cons and pros are described in detail.

In chapter 3, the Gaussian air dispersion modeling method is applied to calculate the local emission concentration. An energy consumption estimator subsystem is developed in this chapter. The model receives the drive cycle and the characteristics of the track, as the inputs, to estimate the conventional DMU's power demand. The emission rate of the UP Express DMUs is calculated based on the simulated energy consumption rate. The emission rates were utilized as the AERMOD inputs to estimate the concentrations. The results were finally interpreted in this chapter, and the necessity of implementing a Hydrail platform was approximately assessed for the UP Express tracks.

Chapter 4 involves implementing a causal model to simulate the flow of energy between different components of the powertrain. The powertrain composed of five different subsystems. The battery module, the fuel cell module, the energy estimation subsystem, the power splitting subsystem, and the high-level supervisory controller.

Chapter 5 is dedicated to comparing the conclusion of this thesis and discuss the potential future works.

Chapter 2: Literature Review and Background

This chapter aims to demonstrate a detailed introduction in terms of emission modeling and the related practical techniques in this field. As the second part, the concept of Hydrail powertrain is presented as an air emission regulating mechanism.

2.1 Recent Air pollution

A revolution in the air pollution discipline happened during 1900-1925. Although both the air emission and engineering control have been changed a lot during these years, no impressive changes happened to the societies attitude, regulation, or even legislation. However, by the natural urban population growth, the problem gradually tended to become a perilous challenge while regulation legislations showed to be mandatory. At this stage, the major activity to clean the polluted environment was a big switch from the steam motors to the conventional electric motors. Such a switch was the shift of the concentrated sources of smoke and ash from boilers to the coal power plants. However, the significant difference between technology was used at the beginning of the period and the end of the period was that at first the coal was fired handy; In the middle of the period, it was fired in stokers, and at the end of the decay, the coal firing was completely abolished.

In terms of rolling stock, the steam locomotives came to the larger cities at the start of the period. By the end of this period, the air pollution burden of railroads in metropolitan areas was transferred to the local electric power plants, when almost all the urban tracks became electrified. Such a move from burning fossil fuels in tracks to making railroads electrified developed regulating legislation which brought a big decrease in ash levels in urban areas.

2.2 Evolution of Intraurban Air Dispersion Modeling

Living in big cities might cause serious side effects on human health. Accordingly, in the concept of air pollution, there is a meaningful trade-off between the distance to intra-city roads and the health effect. In this regard, the development of precise models of pollution exposure assessment within cities should be a prospective in health study research [3]. To measure the pollution variation in the scale of small areas using surrogate measures like the distance to the pollution source, it is not applicable to use locally installed monitoring stations to extract the mandatory data

to be used in health risk assessment calculations. Consequently, it would be of interest to implement applicable models with the aim of using Geographic Information System (GIS) data and integrate it to the data extracted from the short-term monitoring instruments located near the Region of Interest (ROI). The output of such models would then be utilized to be integrated with geologically referenced human health datasets. The health risk, however, will be assigned personally in place.

Recently, the interest in calculating pollution exposure assessment has been increased due to several reasons. The first one is the fact that the contribution of transportation in pollution generation has been growing rapidly and the new technologies should be offered to regulate the generated emission [4]. The studies on the background concentration of distinct intraurban ultrafine particles have recognized elevated concentration levels of ultrafine particles until about 300 m far from highways [5]. As the second reason, although the regulation of the pollution in small scale might be of interest in developing such models, it would be important to quantify the health effect. As an example, the cardiopulmonary mortality due to the cardiopulmonary diseases was quantified for a cohort of 5000 people. It was shown that near the major roads, the relative risk should be 1.95, 95% CI 1.09-3.52. The background pollution was interpolated in that study using the data were generated by the monitoring sites of governments. In that study a simple exposure measurement scenario was used, i.e., buffers, which means that the development of a more robust exposure metrics should be represented to give more impressive results. Another reason for the interest might be the advanced technics have been presented in the field of statistical analysis of exposure with the aim of recently developed GIS techniques [6]. Such innovative technics have boosted the exposure calculation time of research, which previously was impossible or taking many years to be accessible. Nowadays, integration of atmospheric, dispersion and time activity models with GIS capability were introduced more complex and precise types of intra-urban exposure models [7]. In this regard, we have identified six types of analytical exposure calculation models. In most cases, using one types of these models instead of another brought a huge implementation cost and time. These models are included, but not limited to 1. Proximity-based [8]; 2. Statistical Interpolation based methods [9]; 3. Regression models [10]; 4. Dispersion models [11]; 5. Emission-metrological integrated models; and 6. Hybrid models [10-[12]. In the following, we have divided this subheading into three parts. In the first session, a brief review of the literature is performed to find the impressive models have been established on the intra-urban

exposure assessment. Some examples are applied from Hamilton, Canada, to enrich the review. The evolution of the models was qualitatively analyzed according to the key criteria important to health effect assessment. At the last part, we disclose the conclusion and evaluate future studies.

2.2.1 Proximity Models

To approach the interurban air pollution issue, evaluating the proximity to emitting sources are the first step since it is mandatory to figure out the health risk in terms of the distances to a pollutant source. Figure 1 demonstrates a road buffer which can be utilized to evaluate the health risks of proximity to the combination of different sources considering only the respiratory uptake pathway represented as research performed in Hamilton, Ontario, Canada [13]. A "1" is assigned to the respondents in the proximity of the source route, and "0" is the logical value assigned to those who are not, instead. However, in the mentioned research, the health impact of asthma risk factors on children's health were observed using an empirical model [14].

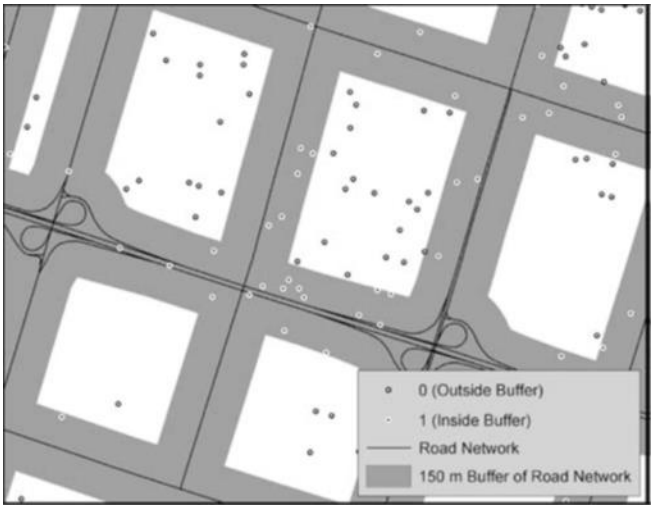

Figure 1: A buffering schematic view to measure the proximity-based on logics [13]

2.2.2 Interpolation Models

Interpolation methods are stochastic and deterministic models. These types of models are based upon geostatistical techniques. At the first step, the target air quality and contaminants are measured using distributed air monitoring stations. The main objective of these types of models is to estimate the pollutant concentration at sites far from monitoring stations due to the observed local air information. Technically, a mesh grid is generated at the location of the interest and the

estimates are obtained locally at the center of the network. Kriging method introduced and accepted as a popular geostatistical method of this category [9]. The Kriging's interpolators are estimating the best magnitudes of the variables at any point of the mesh grid [15]. The major contribution of this procedure is that the method generates both the predicted magnitudes and standard deviations which called Kriging variance at the location without any monitoring stations. The standard deviations are approximate the uncertainties in three-dimensional predictions of these locations. So the places with the lowest reliability can be identified in this method [15]. Kriging models are strongly dependent on the spatial datasets to estimate a continuous contour of pollution concentration. In a noisy dataset or further random errors, two types of responses are shown based on this algorithm; First and second-order effects. In the first- order which is called as the global trends, the missing data are approximate based on the entire study area. I contrast, the second approach uses a distance-dependent function to resolve the error or missed data.

2.2.3 Land Use Regression Models

These types of models are obtaining pollution concentrations in terms of the traffic patterns of the location as well as surrounding land use. Technically, the model estimate concentration, as a response variable y, using predictors all around the location S, which called the buffers. There is a regression mapping to technically predict the exposure assessment due to the local traffic pattern of the area of interest. Least square regression method is used in this model type to predict surface pollution based upon the monitoring stations data and some exogenous independent variables.

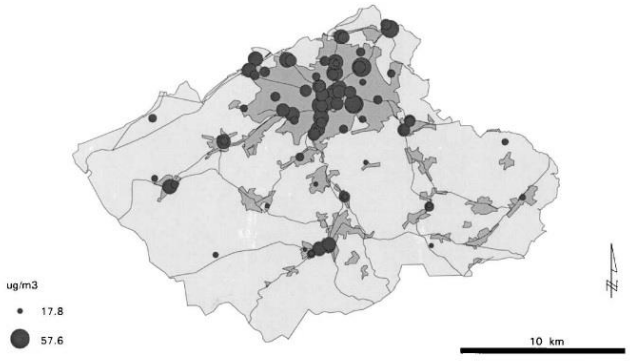

Figure 2: A popular mapping in the land-use regression model to assess the exposure [15].

2.2.4 Dispersion Models

These types of models are using Gaussian plume relations. They utilized metrological, emission rate, as well as topography data to deterministically estimate spatial exposure and concentrations. With the aim of GIS techniques, air dispersion modeling comes more reliable and precise. Such combination gives the opportunity to have the population distribution as well as the empirical data extracting from monitoring systems. Analyzing these two types of information in a combination of the real-time traffic patterns, road geometries, and the terrain information, these models offering more realistic results than the other types of the air pollution modeling platforms has been mentioned so far. So far, different types of pollutions are modeled with the aim of Air dispersion models like SO2 [16], NOx [17], CO [18], TSP [17], etc. To calibrate these kinds of modeling platform, the background pollution concentration data are usually used of which are observed by monitoring systems [17]. These monitoring stations are installed in the vicinity of the region of interest. However, pollution data are categorized into two types of stationary and mobile sources. In a point inside of the region of interest, several released factors should be collected like the annual mass emission rates, height of stacks, temperature, the velocity of emission, etc. these data are observed annually basis or by patterns of emission which show the hourly emission rates. About mobile sources, traffic emissions are usually estimated based on standard emission factors based on different vehicle types. All in all, after the data are provided, and the model calibrated, the output is the concentration at the place of interest [19].

2.2.5 Integrated Meteorological-Emission Models

In these types of models, chemical modules, as well as meteorological information, are integrated to simulate the dynamics response of atmospheric pollutants [20]. In these models, timely meteorological data are applied to the chemistry modules. It is not mandatory that chemistry modules are being fed to meteorological modules as well (a bi-directional coupling) since the chemistry may have a tiny impact on meteorological factors. IME models are beneficial for locations that do not have significant observations defining characteristics of the key meteorological fields required for air quality application. The information is released upon these types of models are dependent on the physics of the model, the data availability, the mesh grid resolution, and the land scheme. These types of models have a high cost of implementation and

data set requirement. The drawback of these models is that they are not able to be linked to air quality and health. However, they have the potential for those places with large populations.

2.3 The Impact of Light Rail Transit on Emission Generation

Rail transportation systems are commercially appeared in the UK from 1804 to 1812. Steam locomotives were the first generations running on cast tracks. The oldest subway is the London Underground (LU), which is opened in 1863. Trains were even developed ten years before the first gasoline engine was commercially invented [21]. Nowadays, both of these transport modes are considering as major sources of mobile emission sources. However, the huge amount of legislation is done to regulate particle emissions released from such a rail transportation system. Although the research on wear particles released from rail transportation has begun since 1909, there is no available regulation mechanism invented on the high concentration levels of particles released in environments. These mass particles have raised serious worries between researchers are working on air quality [22].

It can also be mentioned that the exhaust's output contaminants contain CO, NOx, and PM emitting from rail sectors are less than released emissions released from the other transport fashions like road, aviation, or even shipping [24]. Rail transport, like the other sectors, involves diverse particle emission types. Exhaust and non-exhaust pollutants are two groups of particles emitted from the rail vehicles. Several kinds of research have addressed these particles recently. However, in this session of the thesis, the current researches and standards are introduced of which has the concern of regulating the emissions released from the rail transportation sector.

2.3.1 Renewable Line-Haul Locomotives

Each type of energy sources has unavoidably an environmental impact. To decrease the environmental impact, the energy conversion intensity should be improved. However, improving efficiency, which is meant for less usage of sources, is equal to the less associated pollution. Due to the importance of regulating air pollution produces out of the railway transportation sector, governments have set-up their agenda clean rail initiatives. The problem is under serious crisis and complex as it has a large scale in the railway's domain with critical air emissions in terms of two kinds of emission sources: (i) conventional diesel engines installed on rolling stocks and also (ii) electric power plants supporting electricity for electric rolling stocks. However, mentioned clean

initiatives referred in a great number of the improvement of the emission specifications of diesel fuel locomotives and rolling stocks. Many programs are concentrated on the implementation of catalytic reduction platforms on rolling stocks. As another opportunity, diverse types of diesel blends like biodiesel have been alternatives of which considered much more in the past years. On the other hand, the most impressive clean rail opportunity has been introduced in the last decade is the introduction of hydrogen trains. Hydrogen economy, as well as the methanol economy, has been the topic of several types of research so far. Moreover, ammonia fueled rolling stocks were also presented as another alternative fuel to the hydrogen economy. However, major funding opportunities are invested in natural gas rolling stocks. Similar to the NG, compressed gas and liquefied methane were paid lots of attention. Consequently, pilot projects have been implemented in the past decades covering mentioned alternatives as clean rail systems. Between these alternatives, natural gas showed much cleaner than diesel in terms of emissions, more especially due to the GHG per kW of shaft power.

2.3.2 Hydrogen Hybrid Locomotives

The energy crisis from the 1970s affected the thought of the scientific community about the hydrogen economy. From the first time heard about storing hydrogen in large scales, the 1970s, the economics showed that hydrogen-fueled transportation is much better than transportation-based electricity. Even before the 1970s, another concept was introduced namely “small scale hydrogen storage,” to support power generation demand of vehicles as well as power generators of small scale. Hydrogen as an energy carrier can reduce environmental impact and cause sustainability. Sustainability is improved when hydrogen is generated out of renewable sources of energy. However, the hydrogen fuel’s environmental impact is also reduced throughout sort of fact; 1) Fossil fuels should not be consumed, and hydrogen combustion emissions, in ICEs, should not contribute to the global warming issue and should not generate any substantial wastes. 2) At the hydrogen utilization scale, the corresponding processes should be more efficient than the progress performing under traditional fuel usage.

For example, the fuel cell can provide efficient and sustainable alternatives than conventional energy technologies because of two main reasons:

- Their compatibility with the other renewable sources of energy which makes them appropriate for fate energy security; and,
- The diversity of hydrogen-based options and technologies supports flexible arrays of options.

For the reason that using hydrogen gives the opportunity to have control over conventional energy systems, it would be more sustainable even if hydrogen is produced from fossil fuel sources.

2.3.3 Hydrogen rolling stocks history

To start a survey on the hydrogen rolling stock platforms, it would be a good idea to introduce the international organizations working on hydrogen energy sides. Table 1 acknowledge such sample list of the worldwide associations. The concept of the hydrogen economy, however, became well known by 1980s. On the other hand, Russia started to publish research outcomes in Hydrogen Energy with the application in nuclear technology periodicals showing a systematic scientific effort for developing a hydrogen economy from nuclear energy. By the end of the 1990s, many of the fundamental problems of hydrogen production, transportation, distribution, storage, utilization, materials, and safety were solved.

Table 1: International hydrogen energy consortiums [34].

Organization	Year	Description
IAHE	1974	International Association of Hydrogen Energy is the leader of initiating the hydrogen energy foundations.
ISO	1990	To implement standards related to the hydrogen energy
NH_3FA	2003	Ammonia fuel organization. To promote ammonia as a source of hydrogen.
CHFCA	2009	Canadian hydrogen and fuel cell association which is seeking for the ways of adopting hydrogen infrastructures in CANADA.

An impressive component which can represent the hydrogen economy is the hydrogen rolling stocks. As shown in Figure 3, a hydrogen rolling stock integrates with the natural resource, water cycle in the way that the hydrogen is generated from water resources by implementing sustainable production methods. However, in a railway transportation platform, it seems feasible to reserve

hydrogen onboard. Steinberg and Scott [25] proposed a comparison between fuel and energy consumption rail sectors using different types of renewable propulsion modes as well as hydrogen, against a conventional diesel-electric rolling stock. As a result, it was revealed that the alternate hydrogen train would strongly compete with the other locomotive, electric train. The compete taking place on the hydrogen side in case the provided hydrogen is generated in a sustainable pathway. Technically, electrified rolling stocks can transfer the input power to the wheels with more than 85 % efficiency. As a result, these types of trains are considered as one of the most efficient vehicles of transportation sector when compared with automobiles, buses, or airplanes. The major disadvantage of the electrified rolling stocks is the fundamental cost of implementing infrastructures as the main Burdon. The trains are also facing limited flexibility as they cannot work on the tracks without the pantographs. On the other hand, Table 2 gives a summary of typical hydrogen locomotive initiatives.

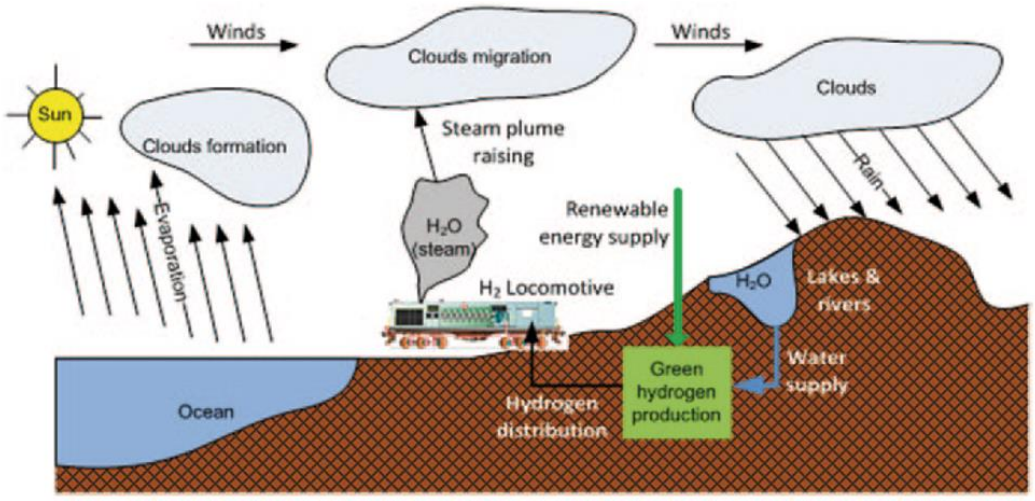

Figure 3: The integration of hydrogen railways with the natural water pathways [23].

Table 2: Hydrogen rail initiatives [23]

Country Region	Year	Description
USA	1992	DoE promote a hydrogen fuel cell program in transportation with the application in Locomotives
North America	1990	A consortium was founded to develop a prototype of a hydrogen locomotive with the application in military
Japan	2001	Japan's railway research center started a program to implement hydrogen locomotives. Two locomotives of 1 kW and 30 kW were implemented.
Quebec	2002	A hydrogen mining locomotive was built in Quebec.
European Union	2005	A program named "FELICITAS" extended for more than three years. This project aimed to fabricate hydrogen trains for marine and urban tracks.
Denmark	2005	A feasibility study carried out on the hydrogen trains. The governments were arranging the study.
Taiwan	2007	A mini hydrogen rolling stock was implemented by a Taiwan community called Taiwan FC partnership.
Germany	2008	ARKONA Train was a project held by the regional environment ministry. The goal was to convert the conventional trains to hydrogen-fueled trains.
UK	2008	A feasibility investigation of the hydrogen rolling stocks safety and standards.
Ontario	2008	University of Ontario Institute Technology performed research about the hydrogen locomotives in Toronto
USA	2009	BNSF unveiled the first hydrogen switcher locomotive
China	2010	A hydrogen PEM Light Rail Transit vehicle was implemented in China.

According to Table 2, in 1992, the Department of Energy (DoE) started to develop a big scale program on fuel cell with the application in rolling stock, hydrogen technology. The program aimed to introduce an alternative renewable, and also help energy saving and air quality improvement in the rail transportation sector [26]. A consortium in North America was established in the 1990s to develop a prototype of a hydrogen fuel cell battery switcher locomotive for the military-base rail applications [27]. Hydrogen fuel cell locomotives were tested by Japanese Railway Technical Research Institute (RTRI) by 2001 [28]. In this regards successful tests were released: a mini LRT running with 1 kW power demand generated using fuel cells (2001); a mini

locomotive with the powertrain of 30 kW in 2004. In Quebec (Canada), a mining locomotive demonstrated. In European Union, a project started in 2005 named FELICITAS aiming at development of hydrogen fuel-cell-driven trains capable of meeting the exacting demands of heavy-duty transport for road, rail, and marine applications. The project duration has been of 3 years, and it was a part of the Sixth Framework Program of the European Research Area. Also in 2005 the Hydrogen Innovation and Research Center (HIRC) of Denmark performed a feasibility study for hydrogen train and its application in Europe. In Germany, a feasibility study supported by the Environment Ministry of the region Mecklenburg–Vorpommern has been completed and favorably reviewed for the implementation of a hydrogen train in Ruegen (Germany's largest island). The project aims to convert the diesel operated "Arkona Train" to a hydrogen drive. The Rail Safety and Standards Board (RSSB) of the UK performed a feasibility study of a hydrogen train, including a comparison with other alternative modules. It recommends that Auxiliary Power Units (APUs) are much simpler and less expensive for carrying out train demonstration trials.

The University Ontario Institute of Technology (UOIT) is the leader in hydrogen fuel cells with the application in locomotives in Ontario. A significant feasibility investigation was performed on the utilization of hydrogen fuel cell locomotives in the Greater Toronto Area (GTA). About 100,000 passengers are weekly transferred by GO Transit Lakeshore corridor. In the Lakeshore corridor, conventional diesel-fueled locomotives are working with fuel consumption rates of approximately 5 L/km. These locomotives are pulling/pushing overall 10 to 12 carriages with up to 1540 passengers during peak hours. Utilization rate projections for the lakeshore corridor expected to be grown by 90 % for the Lakeshore Eastbound and 65 % for Lakeshore Westbound between 2007 and 2031, respectively. A sensitivity analysis was taken place to calculate the expected capital investment for rolling stock in terms of accepted operational costs for a hydrogen train, with the variability of feedstock prices. According to general estimates [29], the initial capital cost for train electrification in 2007 was in the order of 5.9 billion Canadian dollars. The operation of the electrified corridor varied between 78 and 145 $/train-km, projected to 2015, while hydrogen operation had a cost varying between 79 and 151 $/train-km, with a capital cost varying from 12.5 to 16 %, respectively. According to the estimations from [66], the prime mover is on the order of 0.09 GJ/km, resulting in the prediction of fuel efficiency between 53 and 58 %. One drawback of fuel cell trains is the required refurbishing at approximately 5000 h of operation; much less when compared to a diesel engine that requires a complete overhaul every 15,000–25,000 h of operation,

although continual advances are being made to improve fuel cell durability. Figure 4 provides a comparison of averted emissions based on different power sources, against the annual distance traveled by train. In terms of the hydrogen-fueled trains and according to the energy resource utilized to produce the hydrogen demand, which might be nuclear, Ontario mix, or SMR, utilizing a heat recycling pathway in the thermal powerplant might results the lowest level of averted GHG emission, even in the order of 0.04 $kg \times km^{-1}$. The higher efficiency of the PEMFC, from the other side, complements the performance of thermochemical hydrogen production, yielding the lowest GHG emissions at the prime movers. Such reduction would be on the order of 0.04 $kg \times km^{-1}$ (345 tonnes by 2015, and 488 t by 2031).

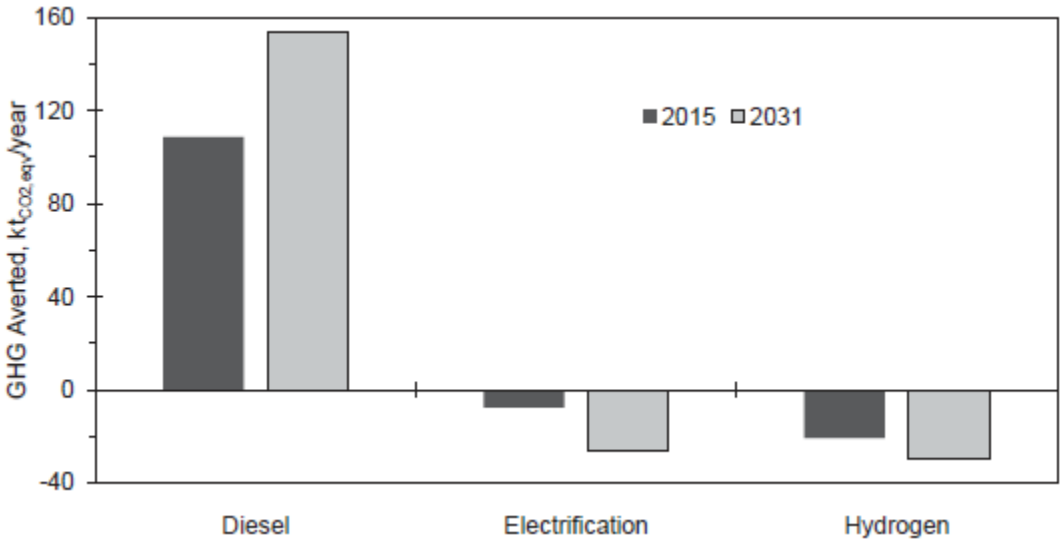

Figure 4: Averted GHGs in Rolling Stock Application [23].

In this case, CO_2 emission would be impressively reduced compared to the rolling stock are fed with the diesel alternatives. However, based on these results, it's obvious that the GO program for implementing the Hydrail routs has several environmental advantages. Besides these advantages, there are also drawbacks related to the cost as well as the short lifecycle of the PEMFCs [23]. On the other hand, electrification of the GO trains might be affected by the CO_2 regulation legislation of Ontario established for the Ontario electricity mix. As the mix should supply the fossil fuel portion, when the GO program will become executed, an intrinsic uncertainty in the increase of the operational cost of trains should be considered. The uncertainty should also be integrated with another uncertainty for the fuel cell degradation rates. In this case, an increase in GHG emission

intensives might be expected in the future. In terms of the Fuel cell degradation costs, as the technology will become mature, it should be expected the intensives will be decreased.

Chapter 3: Air Pollution Modeling and Health Assessment

3.1 Introduction

The development of emission regulatory strategies by renovating urban transportation sectors could be interesting for the governments, more specifically in North America. As a modernizing scenario, Light Rail Transit (LRT) systems are already used commonly in their fanfare fashions between vehicle and bicycle lanes of great urban cities. After the first successful experience in North America, Edmonton 1978, the Province of Ontario released their big move plan in November 2008; a $17.5 billion investment for implementing the rapid transportation system in Greater Toronto and Hamilton Area (GTHA) [49]. Approaching such a sustainable plan needs several research studies evaluating the efficiency of implementing LRT in an urban area. The first issue to be evaluated is how would the LRT systems affect the air quality regarding the decrease in pollution and helping to reduce mobile source-related pollutions.

Air monitoring networks are responsible for measuring air quality and also finding the compliance of the timely logged quality assessment with the existing standards. There are different innovative methods to calculate the air quality and evaluate or estimate the pollution conditions, both off-line and on-line [30]. A good measurement method should be integrated into an emission characterization scenario to assess the Mobile Source Air Toxics (MSATs) released from the sources. Such integration might result in a good indication of how an individual pollution source might contribute to the total regional pollution condition [31]. From another side of the view to prove the claim that the urban LRT has a tremendous effect on the air quality, an important issue should be answered initially. The issue is to technically evaluate achievable health assessment by implementing innovative sustainable technology instead. To answer this question, there are two types of problems should be answered first. However, as the first part of studies, it should find out how does it desirable to switch from technology to the other one. In terms of LRTs, it is mandatory to recognize the mobile source air toxics (MSATs) first to figure out how much the conventional locomotives affect air pollution and cause a health risk. In the field of finding Toxic Air Contaminants (TACs), the United States Environmental Protection Agency (EPA) has already released a list of more than 1000 compounds are identified in the exhaust or evaporative emissions. As the second question, which is the main concern in this study is to evaluate how much an individual source might individually contribute to the net transportation-related health impact.

Hydrocarbons, oxides of nitrogen, and photochemical ozone precursors are emitted from the mobile sources of air pollutions and heavy haul diesel vehicles. These pollutant sources are the dominant sources of Nitrogen Oxide (NO) as well [18]. There are two approaches to estimate the mobile source generated emissions. The first one is to combine the estimated average emissions per distance traveled, which should be extracted in the unit of normalized distance per vehicle. In the second approach, which is a fuel-based scenario, a model should be developed, which is representing the "emission index" using the appropriate emission factor [18]. These data are used to be extrapolated and show the fleet's emission production. In such calculations, the fleets might be categorized into two groups of light and medium- heavy-duty vehicles. Recently, in both of the light and heavy-duty vehicles, Exhaust Gas Recirculation (EGR) system reduces the generated Nitrogen oxides (NO_x) [18]. Also, in these types of vehicles exhaust gases are treated by three-way catalysts which can oxidize CO and HC to H_2O [18]. Moreover, the remained HC is captured through the evaporative emission control system [18]. However, it's an important issue to find the emission inventory and use the data to find the pollution contribution of mobile sources.

To find whether the LRT infrastructures could affect the local air quality, it is worth to evaluate the "Mohring effect" [32]. The concept is argued that the use of LRTs will reduce air pollution through motivating automobile travelers to use LRTs [32]. To proof this concept, it should be assumed that the public attends these facilities. So it was shown that to evaluate the effect of the LRTs on the mobile source-related air pollution, five types of pollutants should be monitored which can potentially be good candidates to represent the footprint of the LRTs in the air pollution. These chemicals are Carbon monoxide (CO), Ground Level Ozone (O_3), Particulate matter (PM), and Sulfur dioxide (SO_2) [33]. In this study, the author had access to both emission and metrology data of different zones of Taipei. Those five mentioned criteria pollutants were grabbed from the stations. As the results, they found out that by opening the Metro in Taipei, 5 to 15 percent of CO tailpipe pollutant was reduced. Also, they found that there is a little change in ground ozone level after opening the Taipei Metro so ground ozone does not affect by LRTs. Accordingly, their calculations evaluated a positive change in the level of these types of pollutants. The authors were not complete their calculations for the other pollutants since they did not have access to high-frequency data of those two other pollutants. In another study, the authors indicated that the Black Carbon (BC), and PM are the main candidates to assess the locomotive impacts on air pollution in the vicinity of the railyards [34]. In this study, they used two pollution monitoring sites near the

Inman and Tilford railyards. They measured the air pollutants with a multiangle absorption photometer, a tapered element oscillating microbalance, and also an "NDIR 41i" analyzer from April to December 2011. They gathered the information and used Wavelet, regression, and image processing to calculate the fuel-based Emission Factor (EF) using Carbon Balance Method (CBM). Also, using these three techniques, they could subtract the background concentrations out of the pollutions comes from a variety of railyard sources like drayage trucks, cranes, welding facilities, or switcher locomotives. The outputs of these analyses were showed meaningfully comparable for the two railyards. However, by using metrological data from December 2010 to December 2011, they showed that the railyard's diesel-electric engines have an average per-gallon fuel-based EF of 2.8 and 0.2 g for BC and 6.0 and 0.5 g for PM, respectively [34]. Also, the average per-gallon fuel-based EF for the railyard was calculated as 0.7 and 0.03 g for BC and 1.5 and 0.1 g for PM. The average emissions of 1.7 and 0.1 for the PM and 0.8 and 0.1 for the BC were estimated for the railyards [34].

Go Transit System (GTS) has seven rail lines in the Great Toronto Area (GTA) with diverse transit schedules. Between these routes, Lakeshore west urban Diesel Multiple Units (DMUs) are the keys in the public transportation system with 60,000 daily ridership. The Union Pearson Express (UPE) line is placed on the Go Kitchener rail route of which possessed several common parts with the Go Lakeshore line. This part of the GTS, however, began its operation in 2016. Before the route started its operation, the Toronto Public Health (TPH) released a risk assessment report, in 2009, concerning the impact of installing required DMUs. Based on the study, it was indicated that the Air-Rail link should be pulled by new locomotive types meeting the Tier 3 standards. However, Tier 4 DMUs were installed in the route and had been transporting passengers so far. Although the trains were satisfied with the TPH expectations, the intention of the route electrification seemed a good way to approach the communities concerns, which were the air pollution [35]. However, in this chapter, the environmental impact of the current Tier 4 locomotives was calculated. Although we did not access to experimental data to validate our calculations, there are two main strategies to figure out this issue. The first one is that we used the certified report released from Cummins which showing the engine information are utilized in the DMUs working in the route of interest. The second way of approach was using the AMS/EPA Regulatory Model (AERMOD) as an approved Gaussian dispersion model has been developed by the U.S. Environmental Protection Agency (EPA).

In the second part of this chapter, we have represented our mechanistic model of longitudinal movement of the Union-Pearson locomotives. The output of this model was validated with the train's specifications. In section 3, the hospitals and schools are already located near the rail route were characterized, and the locations were extracted. Using the method χ/Q ("Chi-over-Q") we could calculate locally emission factors for the different pollutant in 32 places near the route. However, the locomotives were simulated as the line area sources of emission, and the 32 places were characterized through appropriate receptors in AERMOD to calculate the factors for NO_x, HC, and PM. In section 4 of this chapter, the cumulative health risk assessment is derived based on the concentrations. The outputs of the AERMOD software are used to calculate the cumulative cancer risk and Chronic Hazard Indices (CHI) in section 5 of this chapter. Finally, the applicability of implementing the hydrogen locomotives as an option is evaluated through the resulted outputs.

3.2 Energy Demand

3.2.1 Benchmarking

Analyzing the demanded driving cycle is the first step in sizing a hybrid powertrain. Once the drive cycle is extracted, the emission released by the prime mover can be evaluated based on the demanded duty cycle and the emission factors and also the desired topology. This approach would be considered as the efficient one when the throttle signal output of the locomotives is not available experimentally. However, the current UPE's prime movers "Nippon Sharyo diesel multiple units (DMUs)" are used as a benchmark for our calculations. Table 3 shows the specifications of a self-propelled DMU train. The provided information corresponds to each DMU, whether the trainset is an A-car or C-car. An "A-car" configuration consists of two DMU cars, and a C-car configuration consists of three DMU cars synchronized to operate together.

3.2.2 Drive Cycle

Cyclic energy and power demand can be calculated using a drive cycle. For our work, the UPE drive cycle was extracted using the "Speed Tracker" mobile application with a one-second data-sampling rate, as shown in Figure 5. This application uses the global positioning system (GPS) data to save the time-dependent velocity of the vehicle on its path. In UPE route, each trip takes 25.5 min, and the train has 10 min of idling at the Union and Pearson stops. From the graph, it

turns out that the maximum train speed on the route is 127 km/h, which corresponds to the train specification information [36].

Table 3: Self-Propelled Diesel Multiple Unit (DMU) Train Specification [36]

AAR Wheel Arrangement	**2-B**
Train Length	25.91 m
Track Gauge	1435 mm
Train Height	4.3815 m
Tare Weight	74,842.741 kg
Seating Capacity	60 (56 + 2 wheelchair)
Maximum Acceleration	0–32 km/h, 0.56
Maximum Deceleration	1.1176 (Normal) 1.12 (Emergency)
Maximum Speed	128.75 km/h
Number of Powered-axles	1 axle/each car
Power Output	567 kW
Peak Torque Response	3084 Nm

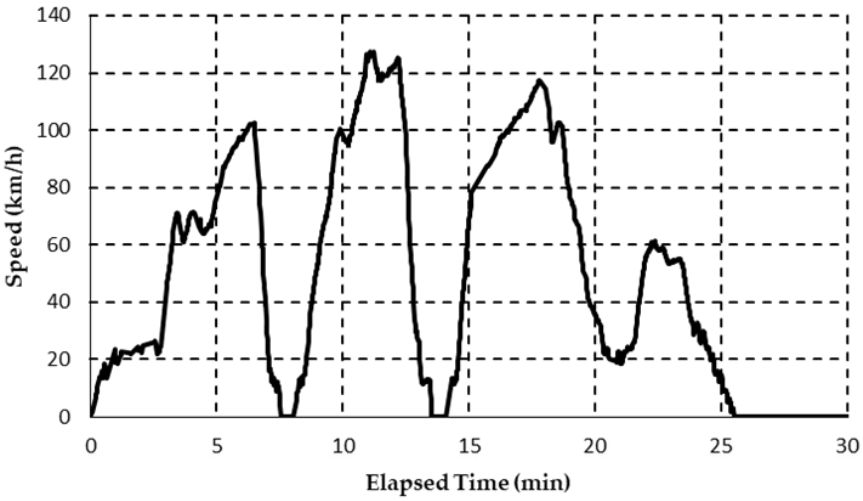

Figure 5: Union Pearson Express (UPE)-extracted reputable drive cycle.

Figure 6 shows the route altitude versus time through a UPE route derived from the data output of the Speed Tracker application. The change in the training altitude occurs because of the difference in the altitude of Toronto (with an average of 76.5 m) and Mississauga, Ontario, Canada, where the Pearson Airport is located (with an average altitude of 156 m).

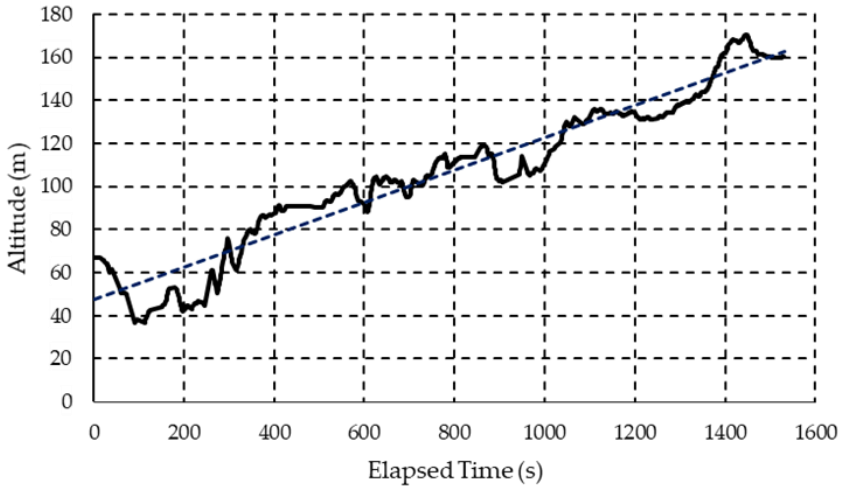

Figure 6: Altitude of the UPE route.

3.2.3 Duty Cycle

The duty cycle shows the relationship between power demand and time [37]. Duty cycle calculation can be done based on two types of data: "time-at-notch" measurement data and "route simulation data" [38]. In the former method, an event recorder is a preliminary instrument that is used to monitor the train's power demand. Hence, the parameters of interest are estimated based on statistical analysis. The latter is only used when the drive cycle is highly repeatable, and the simulation can be undertaken through analytical methods [39]. To calculate the duty cycle, it was assumed that the locomotives showing a longitudinal dynamic response similar to a truck falls into the class 8 category based on EPA Standards. This way, we implemented an analytical model published for the performance metrics required for semi-trucks [40]. The main goal for a locomotive is to transport the payload in a specific distance with a certain cost. The energy demand to run a class 8 truck can be estimated based on the standard dynamic model shown in the following [40]:

$$Ep = \left[\frac{1}{2}\rho C_d A v^3 + C_{rr} W_T g v + t_f W_T g v Z\right] / \eta_{bw} + \frac{1}{2} W_T v a \left(\frac{1}{\eta_{bw}} - \eta_{bw}\eta_{brk}\right)\left(\frac{D}{v}\right) \quad (1)$$

The equation is a combination of four parts of aerodynamic drag, frictional force, road gradient, and inertial force. In the implemented model, the regenerative force was considered as a combination of these forces except for the gradient force and was explained in detail in the following chapters. However, in this equation C_d refers to the drag coefficient, v is the average velocity, C_{rr} is the rolling resistance, W_T is the weight, and Z is the road gradient. In (1), the term D/v is the drive cycle time, which should be used in the modeling procedure. To calculate the weight of the train, it was assumed that the passengers have an average weight of 65 kg (per person). A C-car configuration is modeled in this study. As a result, the train should be able to transfer 175 (3 × 58 + 1) passenger in each trip [35]. It is also assumed that each passenger carries a 5 kg load into the car. Hence, the total weight of a full train can be estimated as 236,779 kg. Moreover, (2) was used to calculate the track grade from Figure 7.

$$\text{Track grade: } \theta = \tan^{-1}\frac{\Delta h}{\Delta d} \quad (2)$$

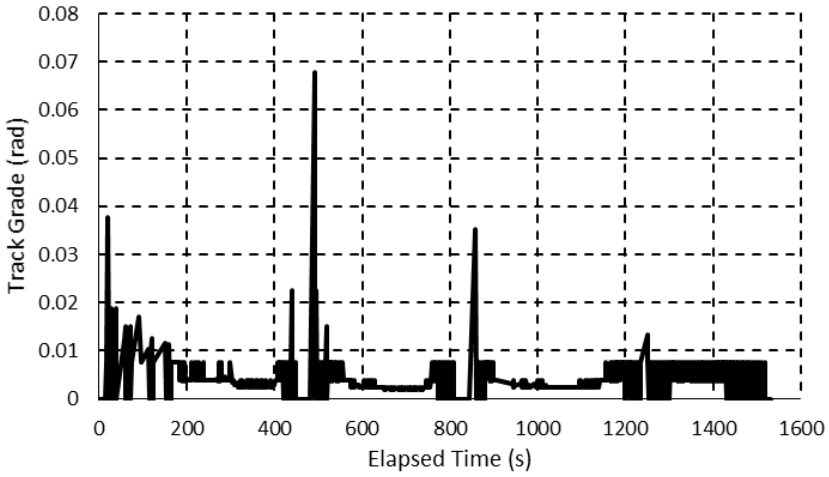

Figure 7: Time variant normalized grade.

The model was implemented in Simulink, MATLAB 2017, and it was shown in detail in Appendix 1. The main goal of developing the model was to design a hydrogen hybrid locomotive. The model was described in detail in chapter 4 of this theses. However, only for a brief introduction, the model includes five different subsystems. The subsystems include the high-level control, power demand

estimator, power splitting unit, battery subsystem, and fuel cell and hydrogen calculation subsystem. The DMU drive cycle is the input of this model. In the calculation of the duty cycle, as it was mentioned, the expression of different resistance power sources is shown in (1). The timely inertial power demand is shown in Figure 8. Power demand was calculated for a C-Car type DMU. In this figure, the peak of the inertial power demand is 500 kW. It can be obtained from this figure that the portion of inertial power resistance increased as time reaches to the last part of the drive cycle. The reason for such an increase can be explored in the combination of the acceleration and velocity at the last portion of the drive cycle. In (1) the last component of the equation is the inertial power demand, and velocity and acceleration are the only variables in the equation. Figure 9 shows the timely acceleration of the DMU during one trip of the drive cycle. As the other part of resistance forces, also Figure 10 shows the timely aerodynamic resistant power obtained from the model. The first part of (3) shows the aerodynamic force. This part of the derivative is a function of the drive cycle, drag coefficient, DMU's frontal area, and also density of the air. Except for the velocity, the other factors are fixed parameters, and this is the reason that the overall shape of the aerodynamic resistant power is similar to the drive cycle.

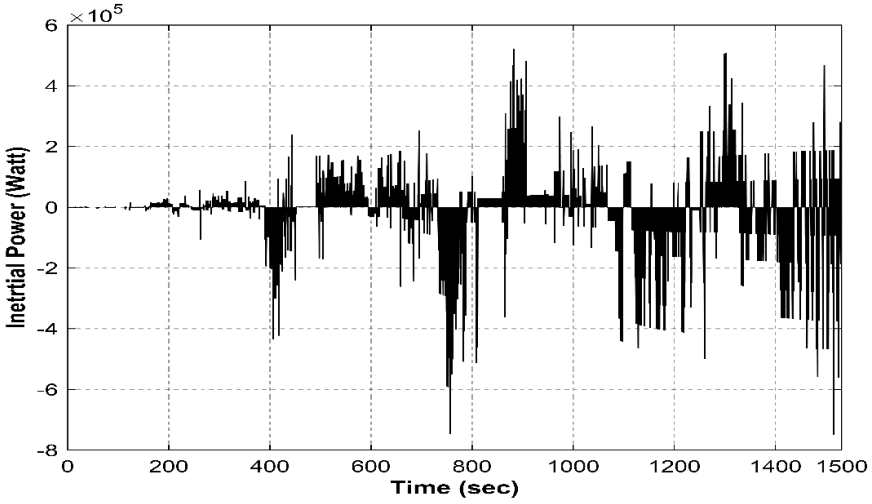

Figure 8: Inertial Power Demand versus Time.

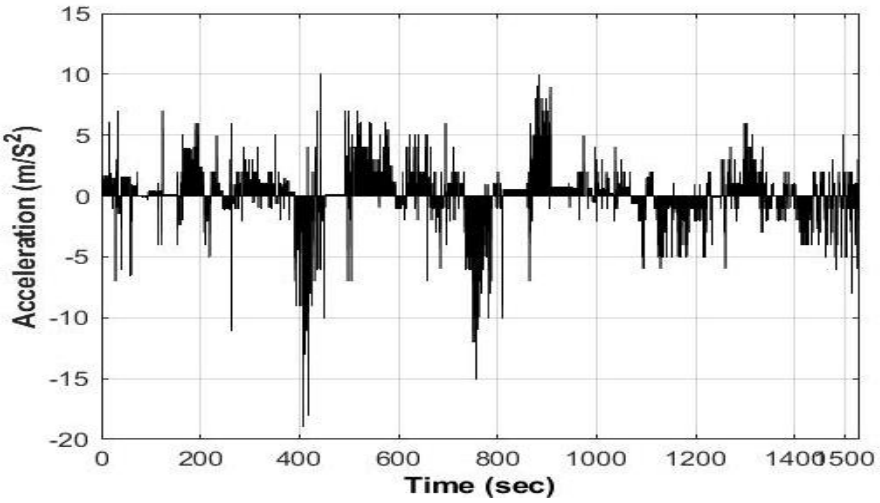

Figure 9: DMU's Acceleration versus Time.

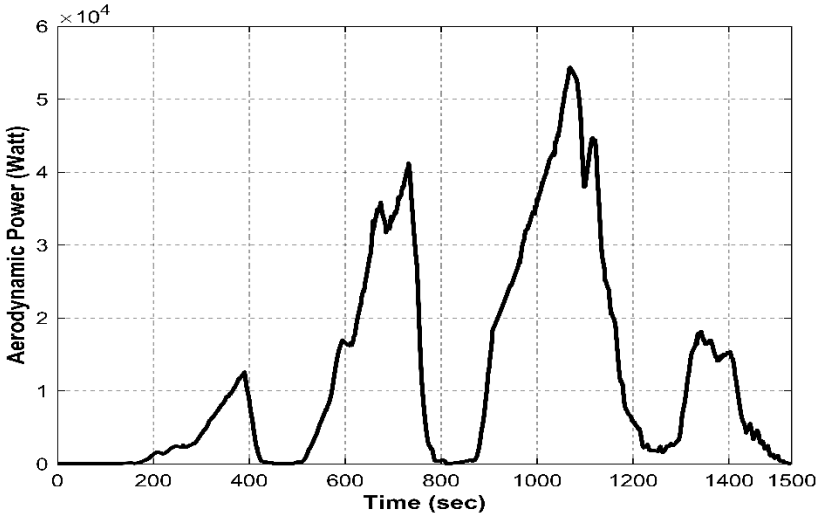

Figure 10: Aerodynamic Force versus Time.

The maximum of this resistance force is expected to happen in 1071 second during the trip. Rolling resistance is the third source of power consumption considered in (1). This portion of the resistive power is smaller than the other portions. The maximum amplitude of this power is 481.6343 watt and is estimated to happen in the 673S. To calculate the rolling resistance, it was assumed that the rolling resistance is similar to the ones that have been represented in articles for the locomotives. So, the defined value was chosen as 0.000015 based on the report published in 2015 [41]. Figure 11 shows the timely rolling resistance power consumption value during each trip. The gradient resistant power was also simulated as a part of the (1). Figure 12 shows the gradient resistance

power. The maximum gradient power happens at 859 seconds of the journey. To make our calculations more complex, we assumed that the locomotive was equipped with a regenerative braking technology. In this regenerative braking technology, which will be discussed in more details in chapter 4 of this assentation, it was assumed that the only power could not be utilized as alternative energy is the gradient power. So the gravitational force was subtracted out of the other portions of the resistive powers, and the remains were applied to the regenerative braking in a specific power regeneration algorithm. Figure 13 shows the total regenerative power. Finally, total power demand which is the summation of the four sub-components was calculated, and Figure 14 shows the total power demand according to the UP Express DMU's drive cycles. After finding the timely power demand, timely energy consumption would be calculated integrating the power demand over trip time. In evaluating the energy demand, both timely and total energy demand which is shown in Figure 15 and Figure 16, the time step was choose fixed at 0.01 second. This value allowed synchronizing this block with the other subsystems of our model which was described in chapter 4 in more details.

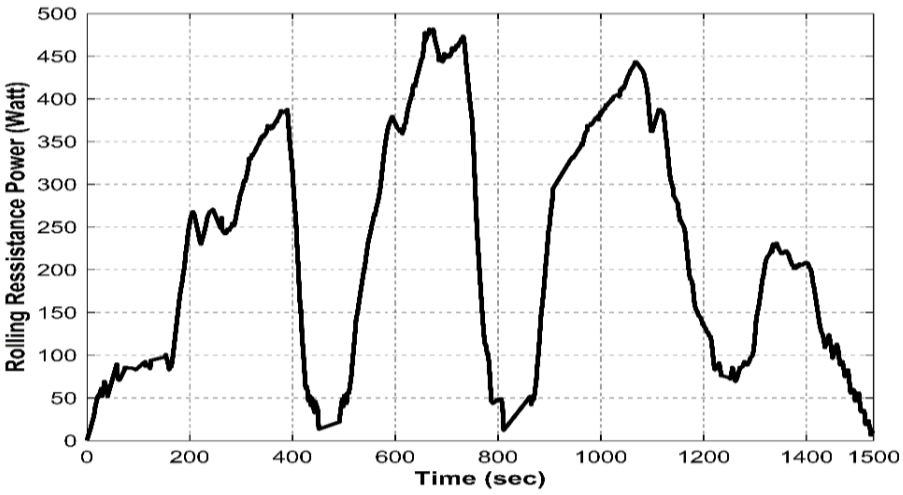

Figure 11: Rolling Resistance Power versus Time.

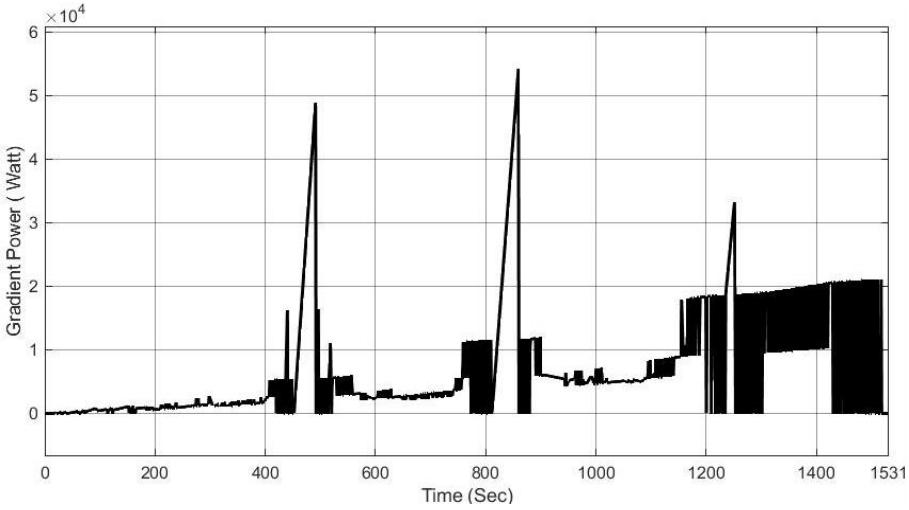

Figure 12: Grading Resistance Power versus Time.

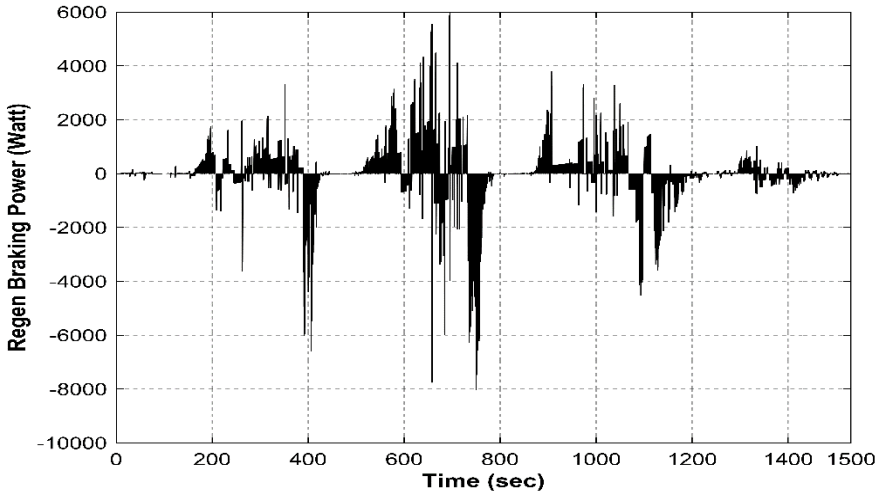

Figure 13: Regenerative Braking Power versus Time.

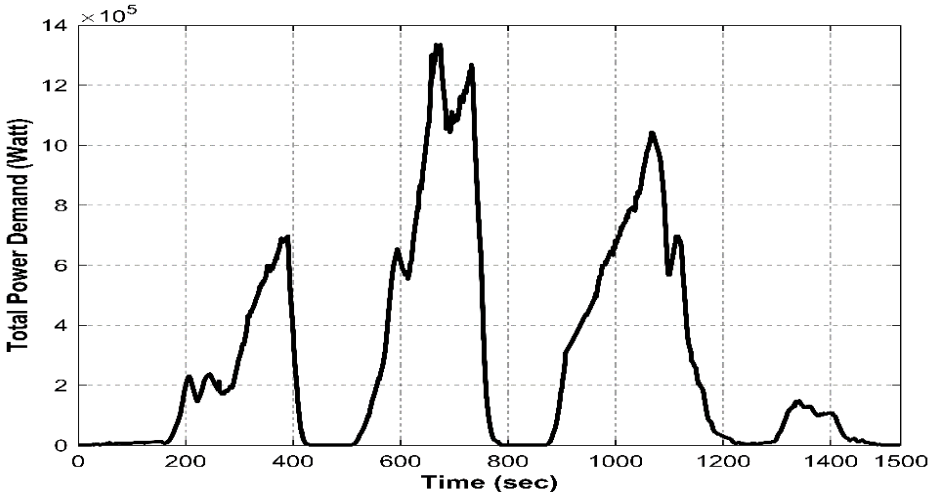

Figure 14: Total Power Demand versus Time.

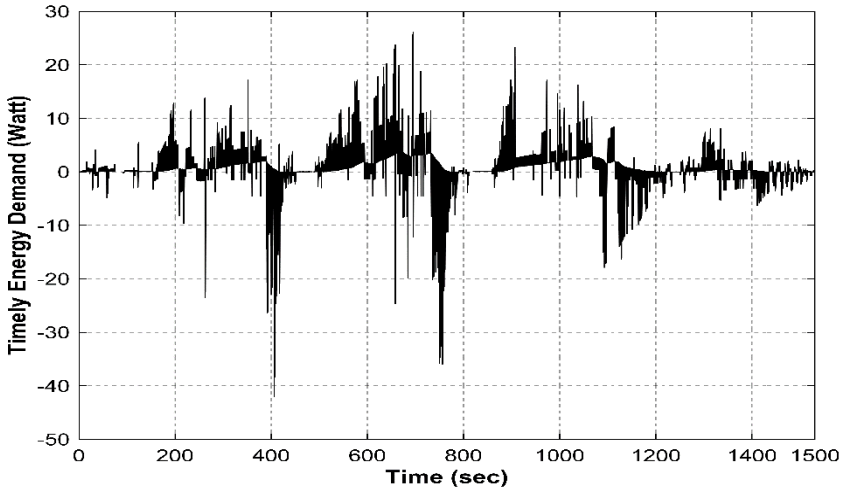

Figure 15: Timely Energy Demand versus Time.

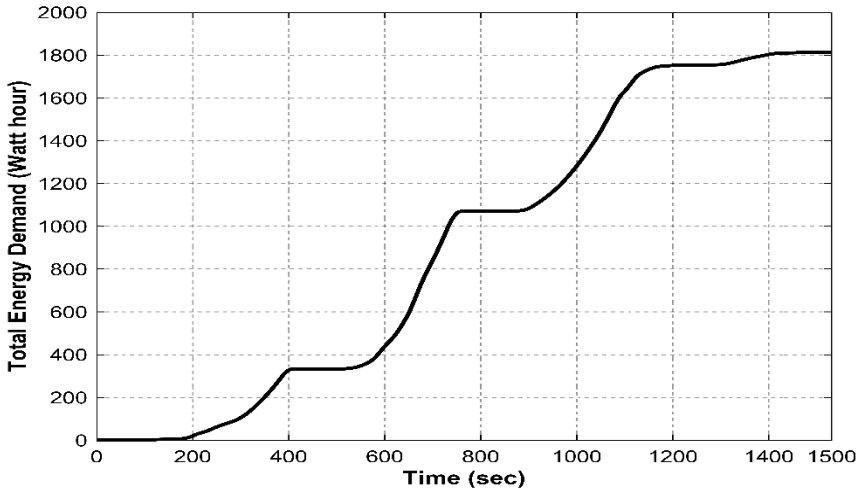

Figure 16: Total Energy Demand versus Time.

3.2.4 Validation

We compared our results with the Nippon Sharyo DMU specifications. The "2-B" prime mover has two trucks, and the wheel assemblies are installed on each of its three cars. The "2" truck is installed under the front of the unit and contains two idler axles in a row. Also, there is a "B" bogie located under the rear of each car which has two powered axles. According to Table 4, each bogie of the current locomotives is equipped with a QSK19-R prime mover. Based on the engine specification data, the output power of the engine is 567 kW. By comparing this value with the calculated power demand, 400 kW of peak power demand, in this paper, a safety factor of 1.4 is observed showing an acceptable deviation.

Table 4: The Modified preliminary prime mover and final drive specifications.

Component	**Value**	**Component**	**Value**
Max. Power Out	567 kW	Torque	6764 Nm
Max. Speed (Engine)	3139 rpm	Max. Angular Velocity	335.10 rad/s
Power Out Ratio	4.48	Max. Wheel Angular Velocity	78.21 rad/s
Torque Ratio	4.48	Final Drive Value	2.61
Speed Ratio	1.52	Max. Road Wheel Torque	8384 Nm

3.2.5 Emission Calculation

In this session, the methodology for emission calculation was developed, which is the first step in the health impact assessment. The Toxic Air Contaminant (TAC) emission is quantified, firstly in this session. Then, the utilized air dispersion and concentration algorithm are represented in the next part. Children, elderly, and pregnant women are considered as the most vulnerable groups of society at risk of traffic-related pollutions. About 30 places, including schools and hospitals near the Union Pearson rail route, were characterized, and the impact of the individual rail route was compared to the air emission standards. The DMUs are using the Go lakeshore and Go Kitchener tracks adjacent to diverse type of residential buildings and constructions. The route is shown in Figure 17. The DMUs are emitting Diesel Particulate Maters (DPM) which are identified as TACs by the board of health of Toronto [1]. Diesel exhaust contains diverse types of particles and mixtures. It is a complex of several organic and inorganic compounds which are harmful and can cause serious side effects when they became uptake via an organ. Age and type of diesel is the most important parameter approximates the types of emissions released from trains components.

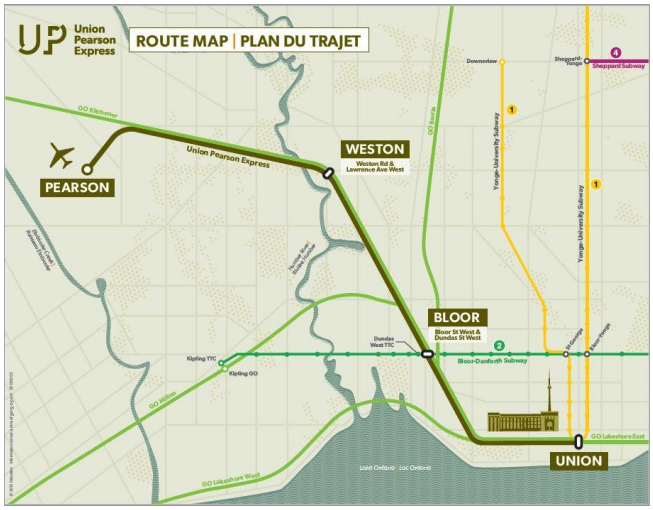

Figure 17: Union Pearson Express Route. [42]

3.3 Typical Toxics Air Contaminants as Diesel Particulate Matters

The 1, 3 butadiene, formaldehyde, benzene, and polycyclic aromatic hydrocarbons (PAHs) are the most common toxics have been identified between hundreds of chemicals may be distinguished in the gas phase of a diesel plum.

- Formaldehyde is a carcinogen. The highly reactive chemical can quickly irritate to the nose, eyes, skin, throat, and lungs at fairly low levels of chronic exposure;
- Benzene is also a carcinogen, and the chronic exposure can get disorder of the blood; and,
- Exposure to the 1, 3 butadiene can cause side effect in lymph and blood system and cause harmful diseases such as Leukemia. It can also affect the reproductive and developmental system as well as the lungs.

A report published in 2002 which listed substances should be put as a priority of reduction in Toronto [45], [46].

3.4 Toxics Air Contaminants Emission Quantification

To evaluate the dispersion and compare the impact of local TAC concentrations in different places, Table 5 describes the methodology was used to estimate the rail route emission in this research. This emission rate calculation methodology is based on the California Air Resource Board (ARB). To find the E_r, as well as E_i, the parameters shown in Table 6 should be filled according to the Union-Pearson DMUs. Since the real fuel intensity data, which should be logged throughout the throttle's control units, were not available, the simulated duty cycle represented at the beginning of this chapter was used to estimate the fuel intensity of the Nippon Sharyo's DMUs.

Table 5: Emission Calculation Methodology [47], [48].

	Source	**Methodology and Formula**	**References**
Metrolinx (ARL)	Exhaust (Running) Exhaust (Idling)	Er = EFr×VMT Ei=EFi×Stops×TPS	Caltrain 2014. BAAQMD 2011.

E_r: Running Emission ($gr \times day^{-1}$)

EF_r: Running Emission Factor (gr×day-1×Km-1)

VMT: Distance Traveled (Km)

E_i=Idling Emission ($gr \times day^{-1}$)

EF_i= Idling Emission Factor ($gr \times hour^{-1}$)

Stops = stops per day

TPS= Time Per Stop at Union and Pearson

Fuel intensity and fuel efficiency of the DMU's were calculated based on the calculations were done so far. The outputs of the mechanical power estimation subsystem were power and energy, which were verified based on the DMU's specification data. Table 6 shows the estimated fuel

intensity and efficiencies. To verify the estimated intensities, the outputs of the model was compared with the stochastics have released in the technical report [41]. Table 6 shows an acceptable coincidence between the simulated theoretical fuel intensity and the average fuel intensity of the locomotives published as the report.

Table 6: Fuel Consumption Index for the UP Express Trains According to Two Different Scenario.

[1] Fuel Intensity Rail-VIA Corridor West of Toronto kWh×(Seat ×Km)$^{-1}$	**[2] Fuel Intensity UP Express Nippon Sharyo DMUs kWh×(seat × Km)$^{-1}$**	**[3]Fuel Efficiency Rail-VIA Corridor West of Toronto Estimated (Seat-Km× gal^{-1})**	**Fuel Efficiency UP Express Nippon Sharyo DMUs (Seat-Km× gal^{-1})[5]**
0.21043	0.2761	193.413	147.41
[1] A represented energy intensity for Rail-VIA Corridor West of Toronto fleets [41].			
[2] Based on the simulation were presented in this chapter. Also, Nippon Sharyo trains have 175 seats weighted 236.8 (tons).			
[3] In that study, it was assumed that the trains are equipped with diesel-electric powertrains. The calculations were based upon the seat configuration, which does not depend on ridership; So, the seat-miles per gallon was preferred as the fuel efficiency type. The dimension conversion was carried on assuming diesel LHV as 40.7 (kWh×gal^{-1}) [41].			

The calculated fuel efficiency was converted into the fuel consumption index as described in Table 7. To quantify the emission throughout the estimated fuel consumption index, three important pollutants were targeted in this study, which are PM, NO_x, and HC. Emission factors for the pollutants were substituted into the calculations performed based on two reports published by the Toronto Medical Officer of Health [1], and EPA [49]. In calculating emission factors, ideal conditions were assumed, which means that all the efficiencies were set to be 100% which means that brake horsepower tends to be engines rated power. However, Table 7 shows the different EFs for PM, NO_x, and HC, which are 0.03, 1.3, and 0.14 (g/hp-hr) respectively. However, EFs in gr/hr is calculated using an appropriate conversion factor. The conversion factor was calculated in the mechanical power estimator subsystem using the rated energy consumed during each trip. All the efficiencies were considered to be 100%, and the calculated conversion factor was 21.3 (hp.hr/gal). This conversion factor show coincidence, 14% error, with the conversion factor, represented for a small line-haul train in the EPA report [49], which is 18.2 (bhp.hr/gal). Finally, the estimated

emission factor for the criteria pollutants, PM, NO_x, HC are shown in Table 7 as 0.64, 27.76, and 2.99 (gr/Km), respectively. Figure 18 indicates the rated fuel intensity (Kwh×Seat-Km^{-1}).

Table 7: Fuel Consumption Index for the UP Express DMUs

Train Tracks	**Fuel Consumption Index gal×(seat-Km)$^{-1}$**	**Train Seats Numbers[1]**	**Standard Emission Factor (gr×bhp.hr^{-1})[2] [1]**	**Conversion Factor[3] bhp-hr×gal^{-1}**	**(PM, NO_x, HC) EF (gr×Km-1)[4]**
Northbound	6.78×10^{-3}	175	(0.03,1.3,0.14)	21.3	(0.64,27.73,2.99)
Southbound					

[1] A C-car configuration Nippon Sharyo DMU with 58 seats/car.

[2] Standard emission factors for the TIER 4 locomotives. These factors are released by Toronto board of health [1].

[3] This conversion factor is calculated based on the theoretical model of energy consumption, which is 21.3. The conversion factor for a small line-haul train is 18.2, according to the report released by EPA [60]. However, Simulated conversion factor has a 14 percent difference with the EPA released conversion factor.

[4] Emission Factor (EF) multiplied by the Conversion Factor (CF).

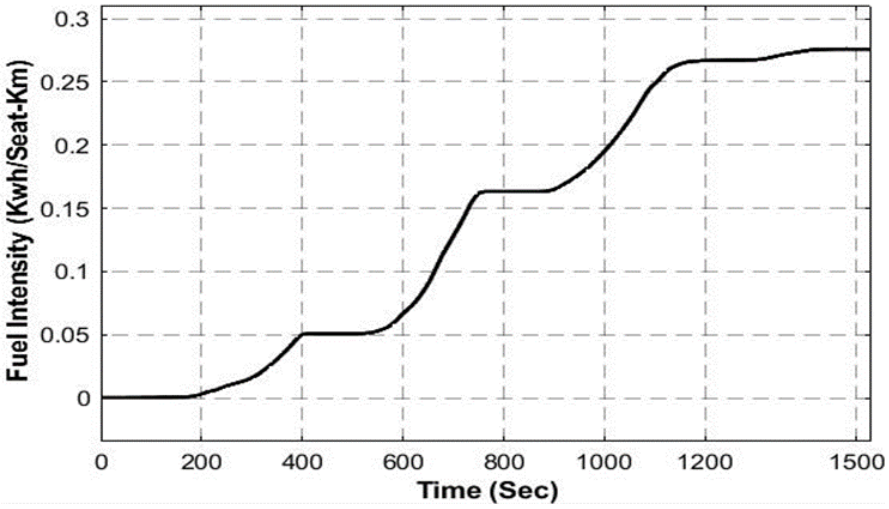

Figure 18: Rated Fuel Intensity (Kwh×Seat-Km^{-1}).

The daily activity of the trains is shown in Table 8. Using the emission factors and the Daily distance traveled for each train, it was shown that the emission rate for the trains in a weekday is

(2430, 105380, 11530) gram per day for (PM, NOx, HC). These values are also calculated for a weekend day, which is (2303, 99906, 10761) for (PM, NOx, HC). These emission rates are calculated based on emission factors provided with the Bay Area Air Quality Management District (BAAQMD) [2]. Annually emission of the track was also shown in Table 10.

Table 8: UP Express Emission Calculation (ı) [1]

	Service	**Activity**	**Travel Time**	**Total Daily Operating Time**	**Total Stops**	**Idle Time× Train^{-1}×Trip^{-1}**	**Total Run Time**
		Trains×day^{-1}	Min×train^{-1}	min		min	
weekday	Metrolinx (ARL)	154	35	5390	616	22	25
weekend	Metrolinx (ARL)	146	35	5110	584	22	25

Table 9: UP Express Emission Calculation. [1]

Distance Traveled	**Average Speed**	**Emission Rate Assumptions**	**Daily Emissions Running (PM,NO$_x$,HC)**
Km×train^{-1}	Km×hr^{-1}		gr×day^{-1}
24.65	59.16	EF×VMT	(2430,105380,11530)
24.65	59.16	EF×VMT	(2303,99906,10761)

Table 10: Annually emission release out of UP Express DMU's.

Weekday (Kg)	**Weekend (Kg)**	**Weekly (Kg)**	**Monthly (Kg)**	**Year (tone)**
(2.4,105.4,11.5)	(2.3,99.9,10.8)	(16.6,726.8,79.1)	(66.4,2907.2,316.4)	(0.88, 38.45,4.2)

3.5 Gaussian Air Dispersion Modeling

The UP Express route points were extracted using Google Earth, and the points were imported into the AERMOD software, source pathway. The track was introduced through around 600 surface area sources. Each surfaces square footage, as well as its center point, were imported to AERMOD via an excel sheet. The different sources create the track in a way to follow the concept of Unitized Emission, or "chi over Q," which means the emission rates were defined as a multiple of uniting. The aim of characterizing each source in terms of it's surface and center point geometry was to employ the effect of the DMU's duty cycle on emission rate by assigning different emission rates,

as a percentage, to each of the 600 area sources defined in the model. To assign a rate to each source, the distance of each center point was measured out of the start point of the track, which is the Union or Pearson stations. In our case, we measured the distance onetime from the Union station, when the DMU is reaching through the northbound track, and then Pearson station when the DMU is reaching through the westbound track. After the distances of each source from the start point were approximately figured out, the consumed diesel was calculated based on the timely duty cycle, which was shown in Figure 14. A table was constructed to assign an emission rate to the center point of each source. Emission intensity was calculated based on the developed model. The energy intensity was converted to fuel consumption rate and then subtracted to the total fuel consumed by the DMU from the start point to the center of the emission source. The progress was then replicated for all the area sources on the track. The resulted intensities were divided by the total diesel fuel demand for each trip, and the excel sheet was imported to the AERMOD importing assigned intensities to surface area sources. It was also assumed that the entire idling emissions emitted in the first and last parts of the track. So two point sources were put on the first and last stops of the route. Figure 18 shows the track path was filled up by 600 pieces of the line area sources and two-point sources at the first and last points of the track.

To define source parameters, the released height was assumed to be 5 m. Moreover, the initial vertical dimension was set to be 1.4 m. The track width, which the turbulent flow is happening inside, is assumed to be 9 m. The conversion factor in calculating the plum height was set to be 1.7. The factor is multiplying by the vehicle height. A factor of 0.5 was defined to obtain the released height.

To find out the health impact of the DMU's in terms of pollution emission, the places with much more vulnerable risks were identified. More than 34 hospitals and buildings with such vulnerable occupants were characterized, and their locations were extracted using google earth. Table 11 shows the latitude and longitude of these points.

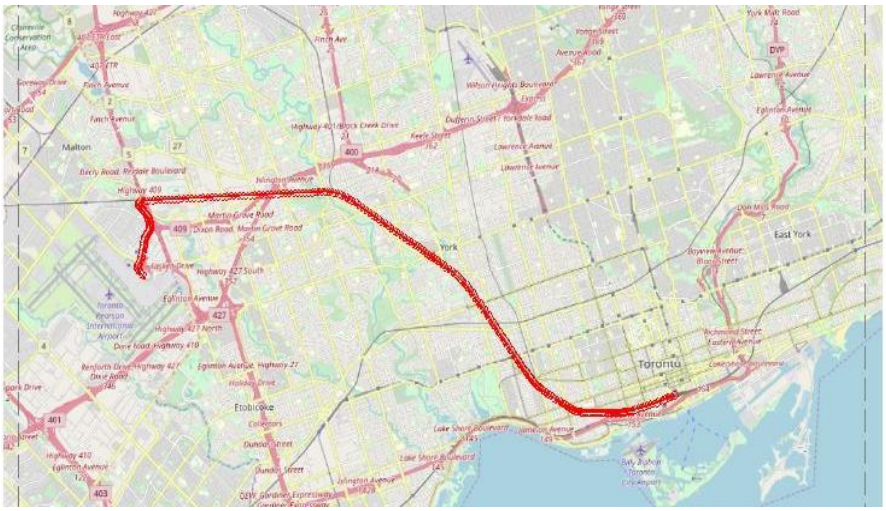

Figure 19: Source points imported as the AERMOD source pathways.

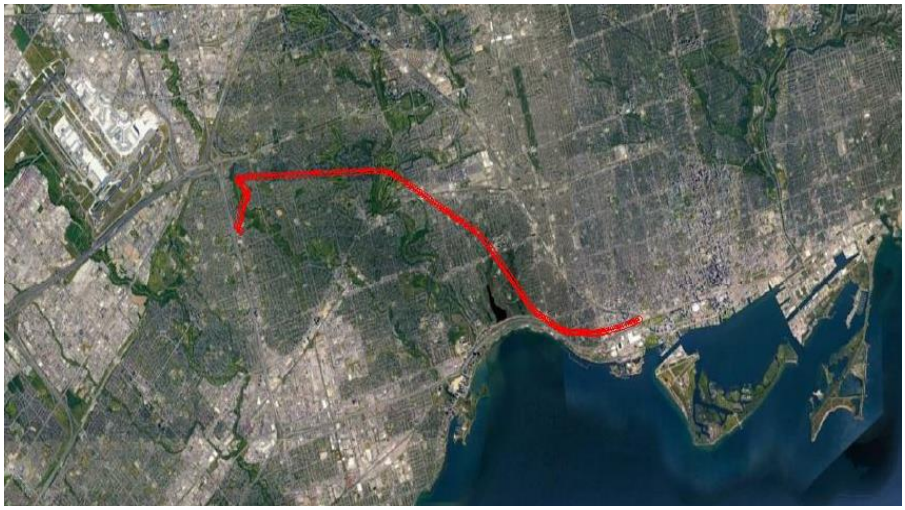

Figure 20: UP Express path with line area emission sources.

A uniform Cartesian grid of receptors with the resolution of 250×250 m^2, without a flagpole, was applied to the Region of interest in the site domain. The domain was a circle of 15 Km with the center point located on (622346.00 m E, 4834425.00 m N). Uniform polar receptor grid was also defined as the receptor pathway to locally measure concentrations with different heights of the mentioned 32 risky areas. Dimensions, number of rings, and direction radials were assigned to the receptors according to each place's dimension. Accordingly, flagpole heights were assigned to each receptor. Since the uptake pathway of interest was choose to be inhalation, the flagpole height chose in a way to appropriately represent occupant's heights. So the human's overall height was assumed to be 1.5 m. In this context, it was also assumed that each story of a building has 4.3 m

height. To put it simply, a good choice for a receptor to measure concentration on the third floor, the appropriate flagpole height is assigned to be 14.4 m. Figure 20 shows the location of the uniform polar receptors with the flagpole heights of 1.5, 5.8, 10.1, and 14.4 m.

Table 11: Location of the places at more risk near the UP Express route.

Easting	Northing	Place Description
630440	4833855	Kaplan Toronto
630074	4833794	CSI Training Center
629802	4833581	Kids & Company - Day care center
628906	4833297	City Kids Early Learning & Child Care Centre - Child care
628073	4833344	Downtown Kids Academy - Day care center
627329	4833065	Rider Training Institute
626724	4833784	Alexander Muir/Gladstone Ave Junior and Senior Public School
625408	4833947	Westminster Feedback - Point of interest
625666	4834420	École secondaire Toronto Ouest - High school
625038	4834620	Toronto Aikikai Martial arts school
624776	4834819	MakerKids Bloor West Village
624782	4835603	St. Luigi Catholic School - Catholic school
624448	4835969	Saint Rita Catholic School - Elementary school
624208	4835763	Toronto Dundas St W YMCA Child Care Centre
624111	4835807	Lucy McCormick Senior School
624448	4835969	Saint Rita Catholic School
622711	4837426	Santa Maria Separate School - School
622499	4837508	St. Oscar Romero Catholic Secondary School
621924	4837940	Dennis Avenue Community School
621715	4838058	Our Lady of Victory Church
621834	4838174	Toronto Public Library - Mount Dennis Branch
621509	4838891	The Learning Enrichment Foundation LEF
621003	4838577	Student Life Education Company Inc. The
620659	4839553	Prodigy Learning Centre
619846	4839834	C R Marchant Middle School
619741	4839558	Weston Christian Academy
619634	4839698	P.T. Montessori School
619476	4839630	CML Healthcare Inc.
619846	4839834	C R Marchant Middle School
619196	4839968	St John the Evangelist School
619231	4839881	H J Alexander Community School
614615	4840093	Community MicroSkills Development Centre

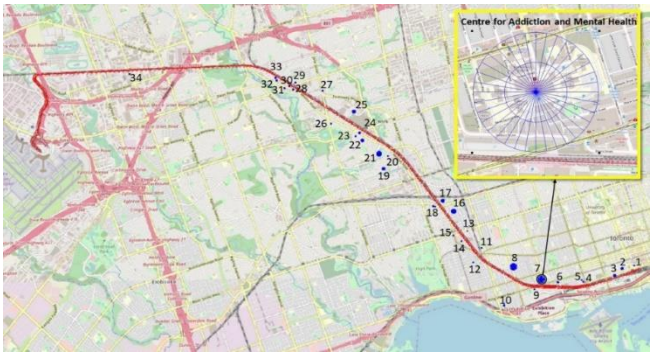

Figure 21: Receptors were imported to the AERMOD-View receptor pathway.

3.5.1 Metrological Data Input

Upper and surface metrological information were implemented to set up the air dispersion model. The metrological data for the year 2000 were collected from Environment Canada. The regional data was prepared for use in AERMOD modeling. The surface metrological data were collected from the station corresponding to the upper air data collection located at Toronto (Latitude: 43.67, Longitude: -79.6, Height above sea level: 65 m). There were approximately 5% missing data filled by the data logged from the other station were closed to the base station or were interpolated by the raw data extracted from the Toronto station. To generate the metrological datasets, it was assumed that the surface conditions are the same in all directions. These surface conditions are shown in Table 12. The metrological data, both upper and surface data, were processed via the metrological preprocessor software package "AERMET."

Table 12: Emissions conditions were used in AERMOD.

Season	**Parameters**		
	Albedo (A)	Bowen ratio (B_0)	Surface roughness (Z_0)
Winter	0.35	0.5	1
Spring	0.18	1.5	1
Summer	0.18	1.5	1
Fall	0.18	1.5	1

Figure 22 shows the wind rose diagram was generated by WRPLOT View for the year 2000 from the metrological data collected from Environment Canada. The wind rose diagram shows the distribution of the wind speed and direction in a specific location.

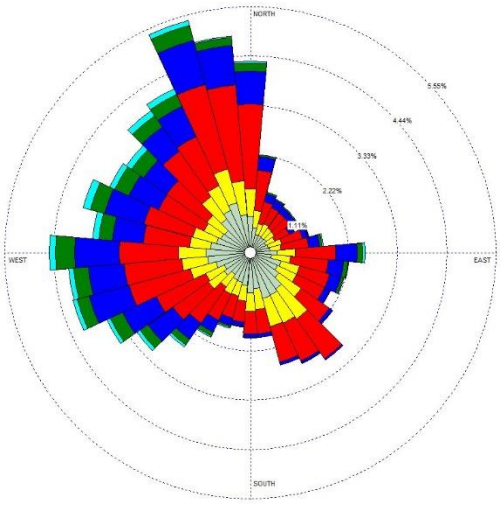

Figure 22: Wind rose for the year 2000.

3.5.2 Results and discussion

A model was set up in AERMOD using different pathways. Measured concentration was shown in Figure 23. The significant concentration between all the defined receptors around the track happened in the latitude (m) 619634.00 and longitude (m) 4839698.00 with the daily concertation value of (0.006, 0.2665, 0.0290) ug/m^3. Table 13 shows the concentration in each receptor. Figure 25, Figure 26, and Figure 27 also show the weekday, weekend, and total concentrations for PM, NO_x, and HC according to the receptor number.

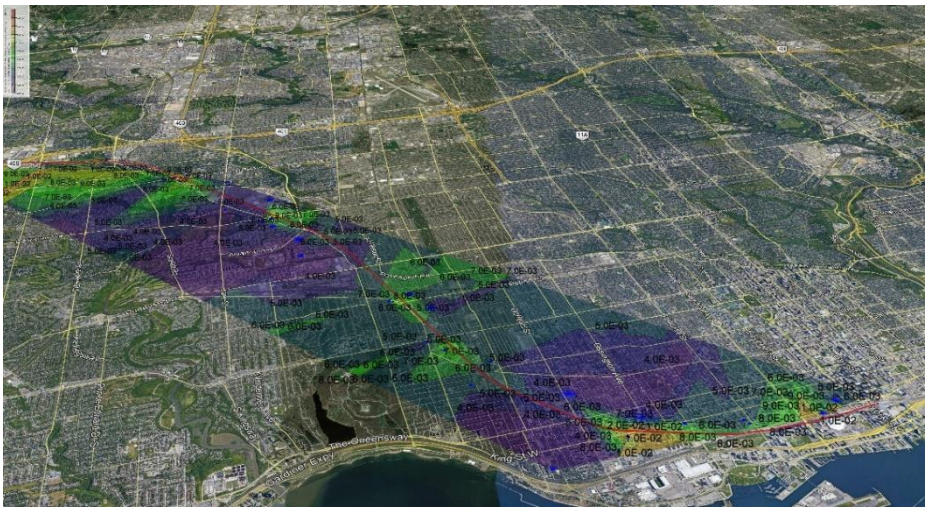

Figure 23: Concentration contour.

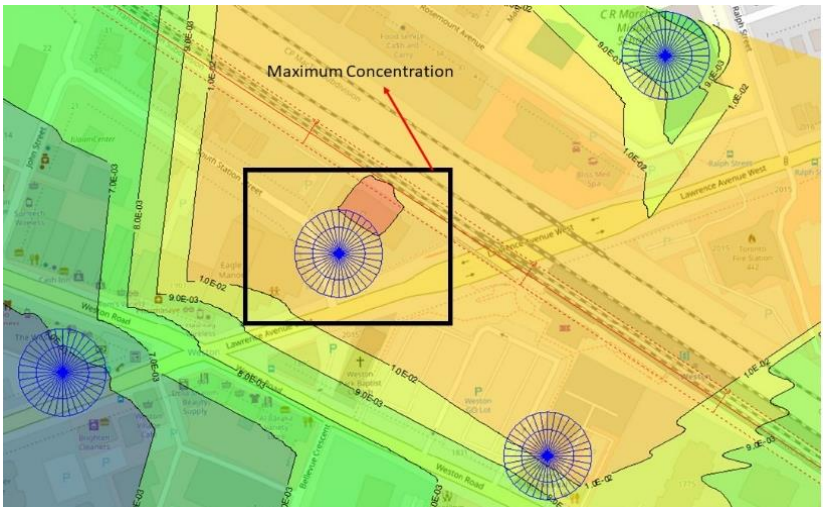

Figure 24: Maximum concentration between receptors.

Table 13: Concentration at different receptors.

Description	**UPO1**	**UPO2**	**UPO3**	**UPO4**	**UPO5**	**UPO6**	**UPO7**	**UPO8**	**UPO9**	**UPO10**	**UPO11**
PM	0.0040	0.0020	0.0044	0.0054	0.0049	0.0081	0.0033	0.0037	0.0037	0.0060	0.0036
NO_x	0.1714	0.0885	0.1916	0.2340	0.2143	0.3493	0.1413	0.1601	0.1585	0.2583	0.1570
HC	0.0187	0.0096	0.0209	0.0255	0.0234	0.0381	0.0154	0.0174	0.0173	0.0281	0.0171
Description	**UPO12**	**UPO13**	**UPO14**	**UPO15**	**UPO16**	**UPO17**	**UPO18**	**UPO19**	**UPO20**	**UPO21**	**UPO22**
PM	0.0043	0.0055	0.0054	0.0047	0.0040	0.0030	0.0041	0.0032	0.0065	0.0033	0.0026
NO_x	0.1867	0.2387	0.2339	0.2019	0.1740	0.1307	0.1781	0.1407	0.2820	0.1419	0.1139
HC	0.0203	0.0260	0.0255	0.0220	0.0190	0.0142	0.0194	0.0153	0.0307	0.0155	0.0124
Description	**UPO23**	**UPO24**	**UPO25**	**UPO26**	**UPO27**	**UPO29**	**UPO30**	**UPO31**	**UPO32**		
PM	0.0033	0.0087	0.0145	0.0041	0.0061	0.0059	0.0064	0.0137	0.0098		
NO_x	0.1432	0.3791	0.6284	0.1769	0.2665	0.2575	0.2775	0.5941	0.4229		
HC	0.0156	0.0413	0.0685	0.0193	0.0290	0.0281	0.0302	0.0647	0.0461		

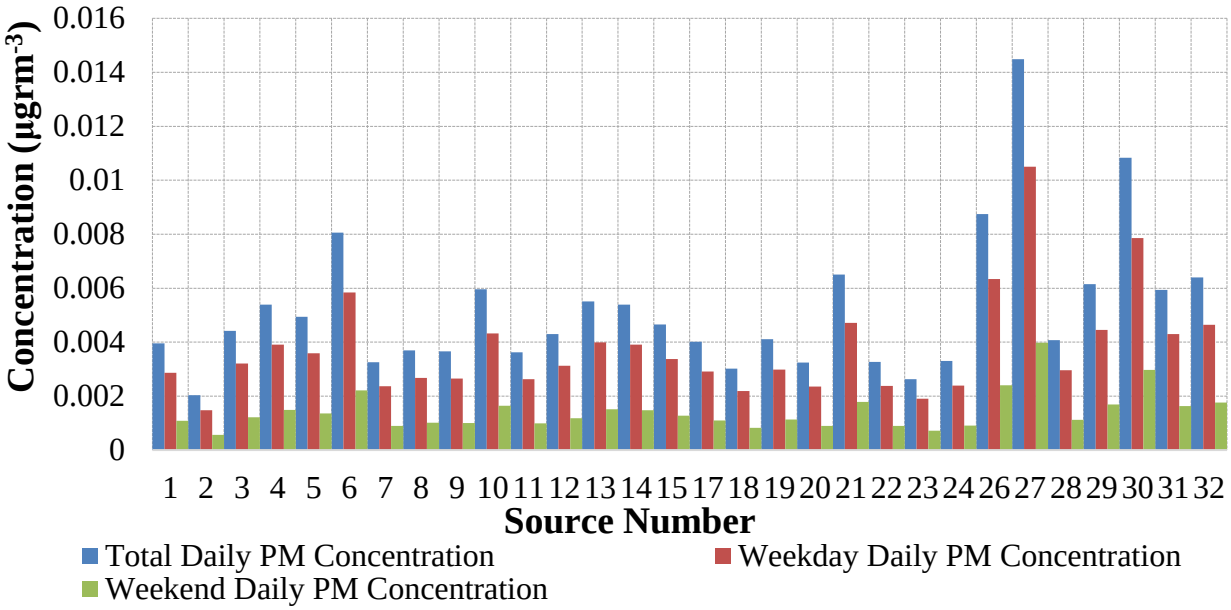

Figure 25: PM Concentration in Each Receptor (µgr/m^3).

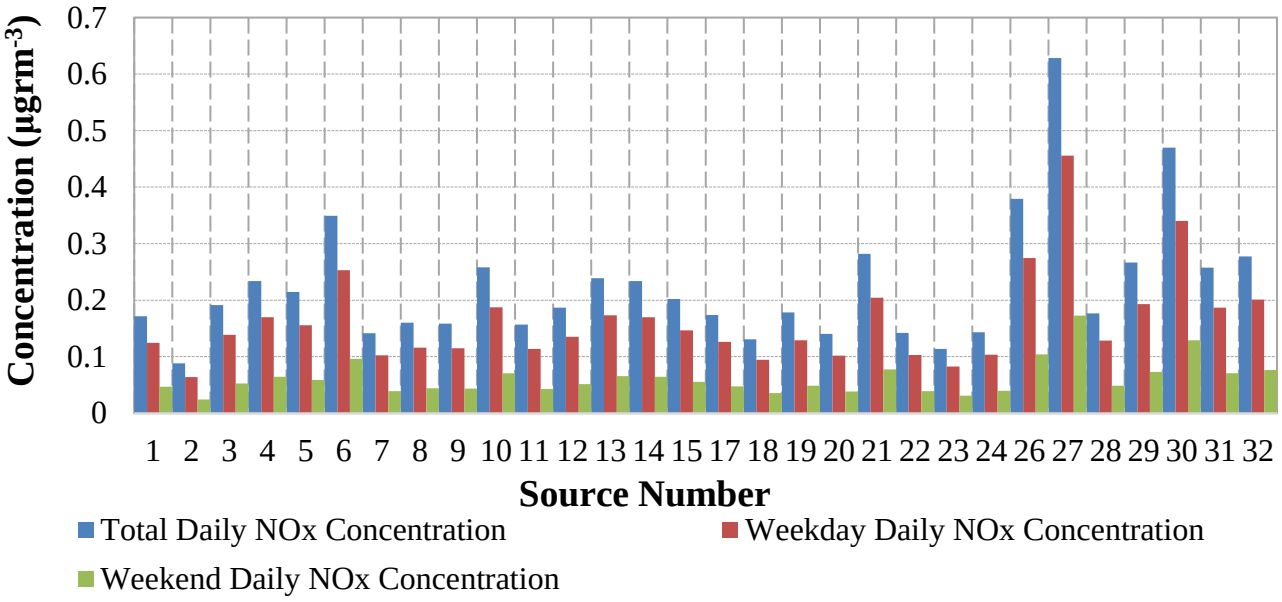

Figure 26: NO_x Concentration in Each Receptor (µgr/m^3).

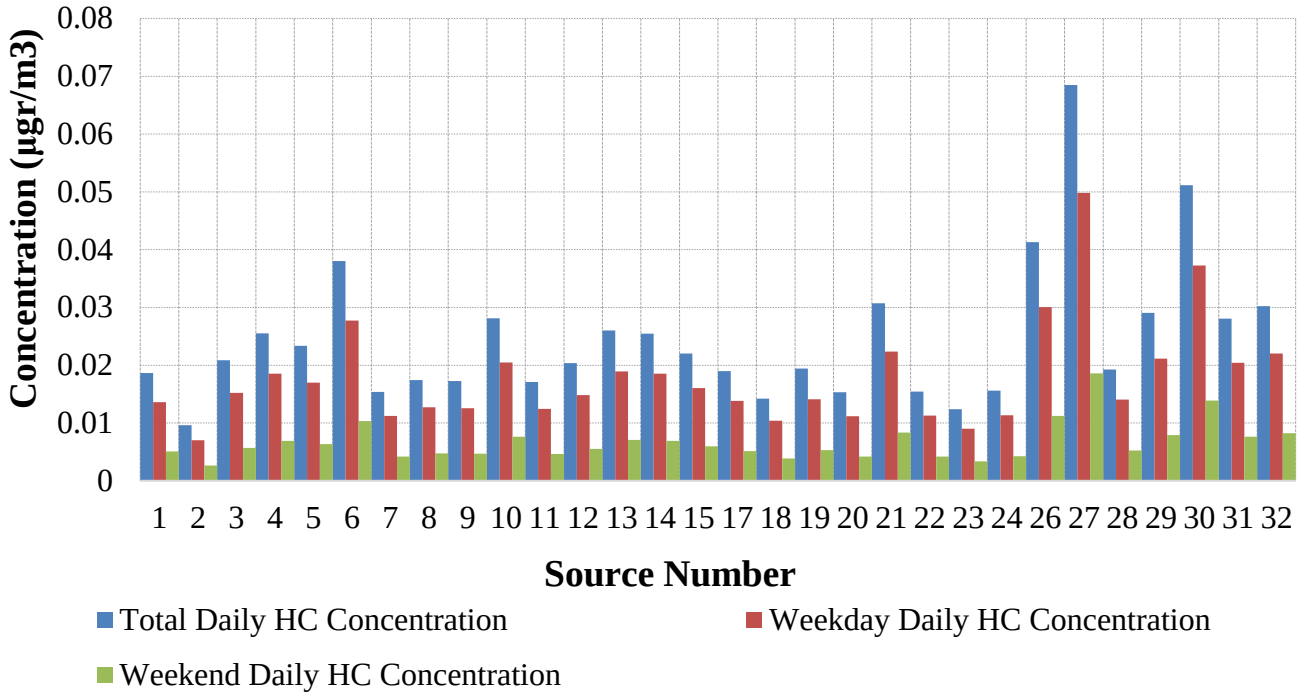

Figure 27: HC Concentration in Each Receptor (µgr/m^3).

3.6 Summary

The traffic-related air pollution of the UP Express track was examined in this chapter of the theses. The calculations were performed based on a subsystem implemented to introduce the power demand of the UP Express DMUs. Daily, weekly, monthly, and annual traffic of the track were approximated evaluating the fuel consumption index for the rail route. Emission factors released by EPA is showing good levels of fidelity with the Cummins specifications released for TIER 4 engines similar to those installed on UP Express DMUs. Using appropriate emission/conversion factors and simulated fuel intensity, the fuel efficiency of the DMUs approximated in terms of seat-Km/gal. The value was compared with the standard intensities published in high fidelity reports, and the scale was impressively verified. Total daily emission in gr/day, gr/month, and gr/years were determined for weekend and weekday.

On the other hand, two types of communities with vulnerable high-risk occupants, which are hospitals and schools, were locally specified with their locations via google earth. Receptors were introduced in AERMOD, and the daily local concentration was calculated in receptors closed to the tracks on three tailpipes pollutants of PM, NO_x, and HC. After calculation and regarding to the

Canadian Ambient Air Quality Standards (CAAQS) values which are shown in Table 14 for the three factors, although the pollution concertation generated with the current DMUs are located at the safe level for two factors of PM and NO_x, it turned out that the 24 h concentration for HC, Benzo(a)pyrene, is not located in the safe zone. The value for the receptor with the maximum concentration close to the track is 0.0290. However, the portion of the contaminants in the exhaust was not available for the specific engine, and the claim about the safety of the diesel engines need more calculations and analysis which was not in the scope of this study.

Table 14: The 24h concentration thresholds for the three candidate pollutants based on CAAQS. [177]

Management level	PM	HC	NO_x
Threshold (Healthy)	10 µgr/m^3	0.00005 µgr/m^3	200 µgr/m^3

Chapter 4: A Hydrogen Powertrain for the UP Express Route

4.1 Introduction

Nowadays, the transportation sector is in a globally serious challenge. Environmentalists concerns are due to excessive fossil fuel consumption, belongs to the motorized vehicles, have already been converted to a serious challenge. Criterion pollutants emitted from the exhausts of the vehicles should be thought as the principal cause of greenhouse gas (GHG) emission and global warming. Increasingly excess of fuel consumption rate can resonate such global side effects. In the lower scale, as it was mentioned before, exhaust gasses contain several types of chemicals which are thought as hazards. These two reasons might be enough to be considered as a cause of proposing alternative fuels. These alternatives are usually targeting the sustainability, economy, and conservation of energy systems. Prevalent alternatives are biodiesel, natural gas, propane, hydrogen, ethanol, etc. [50]. The concept of Hydrail came from these definitions. Hydrail is a generic definition of the rail vehicles using onboard hydrogen to supply a portion of their duty demands.

Rolling stock, as an approved class of transportation sector, are representing the best advantages in terms of economic, environment, social, and energy intensity. Occasionally, the rail transport sector represents a congestion-free transportation opportunity with high levels of safety. These options are concurrently along with a reduced emission generation as well as better per passenger fuel intensity. As the other option, the land use per traffic portion is more reasonable for the sector. Rail transportation is almost utilized in freight applications. Cargos can be delivered by the light and heavy haul rolling stock. Like the other options, goods might be transported through trams and monorail vehicles. However, three modes of rolling stock are used in today's transportation which are unit trains, carloads, as well as intermodal mode [51].

In terms of life cycle assessment of rail transportation sector, distinctive numerical methodologies are utilized in train modeling and environmental risk calculations. Hydrogen seems to be praised in the heavy-duty cycle transportation sector amongst the other alternatives. Hogerwaard [52] proposed a model which thermodynamically approximated the efficiency and environmental impact of hydrogen hybrid locomotives. In that study, the performance of hydrogen hybrid rolling

stock was compared against the conventional diesel electric-powered trains. In the study, efficiencies were calculated based on energy and exergy rules. On the other hand, Hoffrichter [52] proposed a model of a fuel cell powertrain for a hybrid locomotive. The powertrain utilized compressed hydrogen in two distinct pressure of 350 and 700 bar. The pressurized hydrogen was assumed to be reserved in metal-hydride tanks. As a result, they concluded that the hybrid hydrogen rolling stock is 34% more efficient than the conventional baseline which was a diesel-electric rolling stock. Abdelrahman [53] implemented a model of a train using power demand datasets were logged from Bombardier's train's throttles. The simulation was carried on for powertrain with an average power demand of 40 kW. The hydrogen consumption and tank dimensions were characterized by different energy storage scenarios. The prototype was implemented for the first time in North America, and it turned out the prototype can be scaled up for any transit platform in the world. Din [55] developed a Hydrail model to analyze energy consumption as well as life cycle GHG emission generation. In their study, a British class 150 conventional diesel-powered train was chosen as the baseline, and the calculations performed based on the train's specification. A comparison was reported on the GHG emission and energy consumption rates of two different hydrogen powertrains. The first powertrain was a hydrogen-only fed powertrain, and the other was the hydrogen hybrid powertrain. As a result, 44% energy consumption reduction was observed for the hydrogen-only powertrain and 60% consumption reduction approximated for the modeled hydrogen-hybrid train. It was also shown that in hydrogen-only powertrain, downstream carbon-dioxide emission was reduced by 59% which was 18% lower than the CO_2 reduction taking place in their simulated hydrogen-hybrid powertrain. The emission consumption reduction of 77% was observed in the last powertrain. Washing [56] simulated the energy demand and emission production of two distinct powertrains. Hydrogen-electric and conventional diesel-electric. He showed that the hydrogen hybrid powertrain is 34% more efficient than the conventional diesel-electric light rail trains. The results of the simulations are also indicated that the hydrogen-hybrid trains are technically feasible to run on the Blue Line Extension LRT platform in Charlotte, North Carolina. Preliminary simulation of the S70 electric train as the baseline which was working on the Blue Line Extension tracks set up the initials for the development of the conceptualized hydrogen-hybrid locomotives. However, the output of the conceptually designed train was then compared with the baseline.

According to the brief literature review, it turned out that the hydrogen and hydrogen hybrid powertrain concept is technically relevant in rolling stock application. On the other hand, a brief analysis was performed in previous chapters to evaluate the health impact of the UP Express DMUs. It also approximated that the DMU's emitted hydrocarbons, as a criteria TACs, reaches the critical concentrations, in some sources, based on CAAQS and OAAQC standards. However, with such a violation, the necessity of developing a Hydrail platform in a city like the Great Toronto Area (GTA) is manifested. Implementing a Hydrail system is end-to-end progress. To develop an end-to-end designing platform and implement the technology on a customized scale, a designing scenario should be created both in theoretical and practical levels. A high-level model of a hydrogen locomotive was developed in this chapter, Figure 28. The model consists of five different subsystems which were explained in detail in the following chapter. This chapter aims to approximate energy consumption as well as the durability of the energy storage systems as a response to the dynamic of the load. Splitting power demand between different energy sources within a frequency domain scenario is a recently proposed method in power management of hydrogen hybrid locomotives [57]. This scenario was explained in detail in the following sessions. The power management strategy was also implemented as a part of the high-level control subsystem to generate diverse power splitting modes and distribute it between the components.

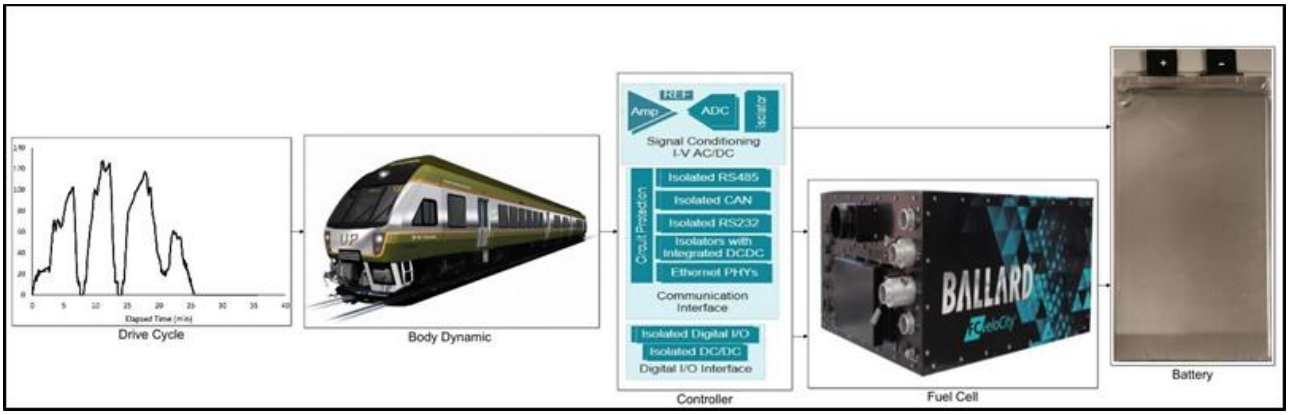

Figure 28: A Model of Union Pearson DMUs.

4.2 Degree of Hybridization

Locomotives have different chassis configurations depending on the number of drive axles [59]. Although diesel-electric drivetrains are seemed to be the earliest types of electric powertrains, these vehicles, when are implemented in a centralized configuration, Figure 30, fail the concepts

of hybrid vehicles. The concept of series and parallel hybrid electric vehicles would resolve the conflict. In a centralized diesel-electric rolling stock the mechanical engine is replaced by an electric motor drive, and the mechanical part maintains the concept of a range extender. In this case, the train's powerplant generates the demanded electricity to feed the motor drive. Diesel-electric locomotives in this configuration belong to the series hybrid electric classes according to the popular method of classification of a hybrid electric vehicle. However, to the best of author's knowledge and apart from the series-parallel concepts, there is no specific available classification for the rolling stock in terms of the degree of hybridization for the concentrated configuration.

In this study, the rolling stock of interest belongs to the distributed power generation category, Figure 30. Inspired by the hybrid electric vehicles with two axles and depending on the size and characteristics of the installed powertrain, a distributed configuration rolling stock may be classified into any of the four different groups of micro, mild, full, and plug-in Hybrid Electric Locomotive (HEL) which is shown in Table 15 [60].

In a micro-hybrid scenario, a micro start-stop controlling unit is installed on an HEV which can automatically shut off the powertrain in each idling modes. Similarly, in a distributed configuration with medium power capacity, Figure 29, which is similar to the UP Express DMUs, the thermostat controlling unit might be work with different characterizations according to the engine type and size. The reason for such contrast is that there is a trade-off between the engine size and its agility [61]. However, in such adaptive thermostat power management control, which might be more complex in distributed rolling stock application, optimal rules should be extracted defining the efficient region of the engine's "efficiency map" during each idling period. In a HEL application and depending on the state of the system, the engine might be set to the "on" mode at an idling moment [61].

On the other hand, a mild HEV is a vehicle which has electric traction machines mounted on their axles. These machines are connected to the Internal Combustion Engine (ICE) through the ground, which means that no mechanical coupling is available between the two sources of torque except the road. This concept may need some modifications in terms of the rolling stock applications. In a typical diesel-electric rolling stock with both distributed and concentrated configuration, the engine is not mechanically coupled to the traction motors. In a stand-alone rolling stock, the power ranging from approximate changes between 300 hp to 6000 hp [54]. There are multiple engines,

and power sources are connected in different embodiments. From another side of view, the power of different traction motors should be controlled independently. The multitype power sources, as well as power consumers, are connected in parallel to the main bus. As an example, in the most popular configuration, a traction motor connected to a fixed ratio transmission. The motor is powered, on the other side, by two or more diesel engines, as the range extender. Regardless of the type and amounts, which can be different in rolling stock, range extenders should be connected to an AC or DC bus. These range extenders might be controlled commonly or individually. Accordingly, in a mild HEL, the main bus voltage controls the amount of energy flow between diverse power sources. Regulating the voltage and current of the main bus is a challenging part, which causes diversity between mild-hybrid HEL fleets.

The full hybrids are the third types of HELs in our classification. A larger battery pack gives a unique characteristic to this types of locomotives, which is an independent electric trust force, and it gives the option to operate on only battery mode. So the range extender is generating the demanded duty cycle. However, the powertrain can use the energy storage system for only limited driving ranges. The powertrain of this topology, similar to the mild and micro HELs, cannot become connected to the electricity grid. Plug-in configurations, as the fourth groups of HELs and similar to the overhead catenary rolling stock, are introduced to keep the rolling stock more renewable.

Table 15: Powertrain Configuration in HELs.

Degree of Hybridization	Power Source	Power Flow
Micro	Electric-ICE	Parallel
Mild	Electric- Fuel	Series
Full	ICE-Hydraulic	Electric traction motors
Plug-in	ICE-Pneumatic	Series-parallel

4.3 Different Topologies for locomotives

Similar to the degree of hybridization, diverse types of topologies have been introduced for rolling stock in the literature. Indeed, topologies for innocent rolling stock were creatively designed in different styles before the standard topologies had been introduced recently [62]. Today, the standard topology for high efficient rolling stock is to utilize different numbers of wheels in similar diameters as a propulsive system called “Bogie” [63]. Such a unified discretized strategy is

rationally viable from diverse points of view, such as economy [64]. In addition to the wheel configuration, there are other characteristics in rolling stock, such as the available power sources, power flow control and distribution, and size of the rolling stocks.

This study aims to look at a specific type of rolling stock from the energy point of view. Figure 29 shows a classification of the rolling stock based on the size and power supply capacity of its powertrain [65]. According to Figure 11, as the output of our mechanical power estimation subsystem, and based on the classification carried out in Figure 29, the UP Express DMUs are distinguished as Monorails.

There is also another popular classification in terms of the type of utilized power sources, Figure 30. Between two categories, in the first type, a configuration of locomotives are pulling the coaches. On the other hand, in the second type, Electric Multiple Units (EMU), are generating demanded power in the different distributed platform. Although the distributed power systems are more efficient comparing to the concentrated platforms, there are some issues due to passenger comforts, pantograph performance, and maintenance [65]. The further classification was shown in Figure 30, due to the power sources type.

Until 1990, trains used dc traction systems even though the electricity was generated by an onboard diesel engine. This type of onboard power supply was not appropriate to be employed in EMUs due to technical limitations. In these types of traction systems, a diode rectifier was utilized to control the power flow vector during the cruise or brake time steps. Meanwhile, with practical accomplishment in semiconductor science, the control of such drivetrains was switched into another field like the vector field and phase-based motor speed control. As an example, in this period, thyristors played a key role. Around the 1990s, induction motors showed impressive robustness while they were highly cost-effective. These two reasons plus the tendency to use pulse width modulation based converters came over the high-performance diesel-electric powertrains. Although achievements were impressive in gate turn-off controlling of high impedance thyristors, i.e., 4.5 kV/4000 Ampere [66], issues were remained in switching frequencies higher than 500 Hz [67]. Innovations of high voltage IGBTs almost solve this limit for up to 1.5 kHz [67]. Recently, improvements in cooling systems, innovation in semiconductors technology, and developing efficient high-speed drive systems, led to a relevant revolution in traction converters, which means standard integrated IGBT based induction motor traction systems.

Comparing the advantages of the two categories can be meaningful, and it can reveal which category might be appropriate for a specific topology. For example, highly acceleration demand, as well as an increase of passenger capacity, is the design criteria for an LRT rolling stock. For these types of Rolling stocks, low voltage (600-750 V) dc traction motors are fed with third rail or overhead line is the best option [68]. DC- AC traction converters receive the dc power from the DC line and generate the desired voltage vector in amplitude and frequency to drive the motor in its efficient power rating requirement. A similar configuration is used for light-duty rail vehicles, such as metros, DC EMUs, and trams. On the other hand, induction motors with customized IGBT drivers are the dominant traction architectures for the heavy haul electric rolling stocks. In these types of locomotives, a transformer is installed onboard to reduce the pantograph voltage to a secondary voltage appropriate for a four-quadrant converter. A dedicated power circuit, a DC link-capacitors as well as second-harmonic filters, is installed after the converter. Converter output is pumped into the circuit, and the alternative voltage/alternative frequency power is generated to feed the motors. The working voltage and frequency in these locomotives are changed from 600 V to 3000 V [69]. The prime mover in a heavy haul diesel locomotive is an IC diesel engine which supplies the power in a designed rotational speed to feed two synchronous generators installed onboard. The generators and multiple traction motors, as well as a power supply circuit, are responsible for regulated traction power. This train is not capable of providing regenerative braking opportunity.

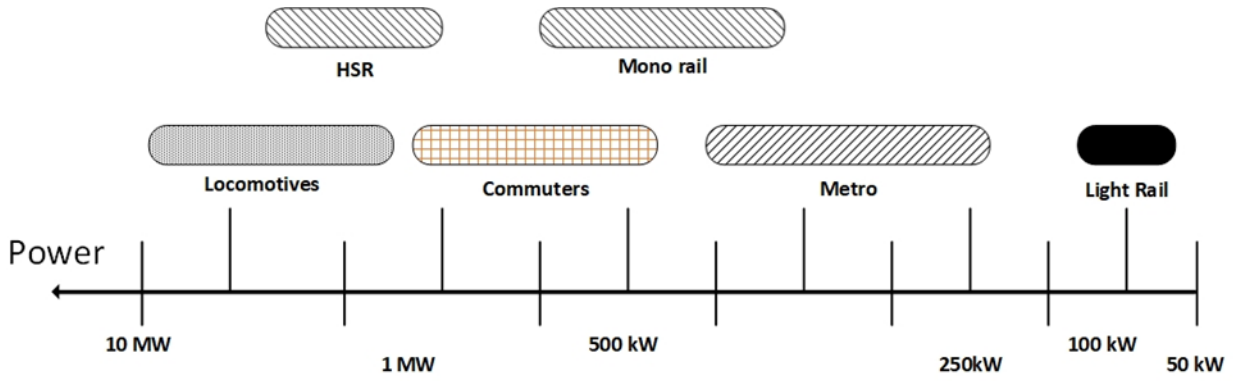

Figure 29: Classification Based on Size versus Power Supply Capacity.

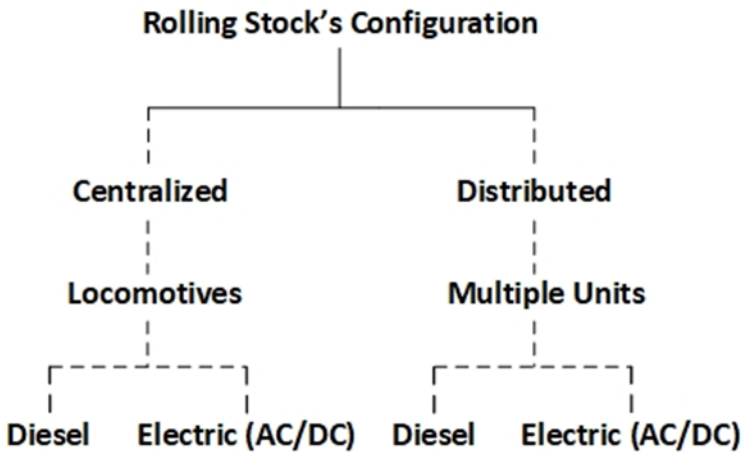

Figure 30: Classification Based on Power Distribution between Power Sources.

4.4 On-Board Energy Storage System (Hydrogen Economy)

Some advantages of installing onboard energy storage systems are included, but not limited to:

- Energy intensity improvement;
- Peak power management;
- Improving the traction/braking dynamic more specifically in high accelerated regions.
- Voltage regulation;
- Regulating power supply infrastructure; and,
- Eliminating the need for catenary/third rail infrastructures.

Although installing an onboard hydrogen storage system have its benefits, the method of reserving hydrogen is a challenge and should be realized quickly in the Hydrail application. The problem is the high-pressure demand at one end of the system. Reaching such pressure is extremely costly, and also it has its safety codes to be implemented. The cost of compressed hydrogen under 35 MPa is approximated 40 to 500 $USDkg^{-1}$ [70]. Ammonia is a valuable option to overcome such a challenge. The proof is that more than 17.65% of the liquefied ammonia in normal temperature is hydrogen [71]. There are also some other benefits for using ammonia-based onboard hydrogen production systems, as one end of an end-to-end Hydrail platform [72]. Modeling the hydrogen production system is not in the scope of this thesis, but as an important pathway, it should be noted that to develop a liquefied hydrogen Hydrail platform, producing a fully active catalyst to achieve

a high level of round-trip efficiencies at the ambient temperatures can result in an impressive pathway in terms of hydrogen economy [73].

However, through the diverse types of renewable energy storage technologies and regardless of the production pathway, hydrogen is the most prominent technique to store energy, in the shape of electricity, for a long duration. This would give an opportunity to define the concept of power to hydrogen as another end of the Hydrail system. The concept of green hydrogen should become a major business case in terms of the re-electrifying huge amount of renewables [74]. A growth market rate in the value of €4.2 bn in Europe was estimated to be happened by 2025. Since the electricity price is the major factor in the development of the green hydrogen concept, such development might result in the installment of electrolyzers with a cumulative capacity of more than 2.8 GW [74]. However, profitable business in this area needs an overall electricity price of lower than 50 € MWh^{-1} [74]. Table 16 shows a summary of profitability for three different business [74]. In this table the primary market, net electricity cost, capital expenditures, and H_2 cost and prices were shown in 3 different scenarios for different years.

Table 16: Different business cases.

	Semi Centralized		**Light Industry**		**Large Industry**	
	2017	2025	2017	2025	2017	2025
Primary Market ($Toneyear^{-1}$)	270	950	900	900	3230	3230
Average Net electricity price (€×MWh^{-1})	44	45	38	47	17	26
Nominal system size (MW)	2MW	12MW	6MW	6MW	40MW	40MW
CAPEX (k€×MW)	3660	1900	1760	1400	1480	960
H_2 Cost (€×kgH_2^{-1})	6.7	4.1	3.5	3.4	2.4	2.3
H_2 price (€×kgH_2^{-1})	7.0	6.0	5.0	5.0	1.8	2.6

In the Hydrail application and the case that the conventional compressed hydrogen pathway is utilized to empower the platform, the benefit margin of the hydrogen in the hydrogen refueling stations should be the key factor in approximating the price needed to be produced. Table 17 summarizes the accepted price for different application of transportation sector [74]. Such stochastics should be developed for Hydrail depending on the types of fleets, technical and operational constraints, typical demands, and some other factors [74].

Table 17: accepted price for different application of the transportation sector.

Application	Forklift	Bus	Fuel Cell Vehicles
User	Private operator	Bus operator	Private operator
Hydrogen Production	Truck Delivery or on-site production	on-site production	Truck Delivery or on-site production
Usage rate	2 to 3 times per day	250 km×day^{-1}×bus	100 km×day^{-1}×car
Fleet Size	50	10	50
H_2 Consumption	33 t×year^{-1}	154 t×year^{-1}	16.5 t×year^{-1}
Delivery Pressure	350 bar	350 bar	350 bar
Refueling Schedule	Whole day	1 per day	Whole day
End user price	11-12 €kg^{-1} (16.19-17.66 CADkg^{-1})	6-7 €kg^{-1} (8.83-10.3 CADkg^{-1})	9-10 €kg^{-1} (13.25-14.72 CADkg^{-1})
Station price	6-7 €kg^{-1} (8.83-10.3 CADkg^{-1})	4-5 €kg^{-1} (5.89-7.36 CADkg^{-1})	5-7 €kg^{-1} (7.36-10.3 CADkg^{-1})

4.5 Chapter Outline

A mathematical model of a hybrid electric locomotive with a hydrogen fuel cell as a range extender is developed in this chapter. The model consists of five different subsystems, which are mechanical power demand estimator subsystem, battery subsystem, fuel cell subsystem, high-level control subsystem, and frequency-domain power split subsystem. In mechanical power demand estimation subsystem, as it was shown in the previous chapter, a baseline model of the DMU was constructed according to the baseline topology showed in Figure 31. In this figure, the left side topology shows the bogie with an installed QSK-19R engine. The engine produced with Cummins and the nominal rate of the engine is 500 kW. The characteristic of the engine was summarized in chapter 3. On the other hand, the right figure shows the typical hybrid topology was developed in this study. Figure 32 shows the topology of interest in this chapter. A hydrogen fuel cell range extender was installed in an embodiment with a connection to the battery packages. A frequency-domain power-split control system distributes the power demand between the two different energy storage systems. A high-level control scenario is controlling the flow of power in the powertrain.

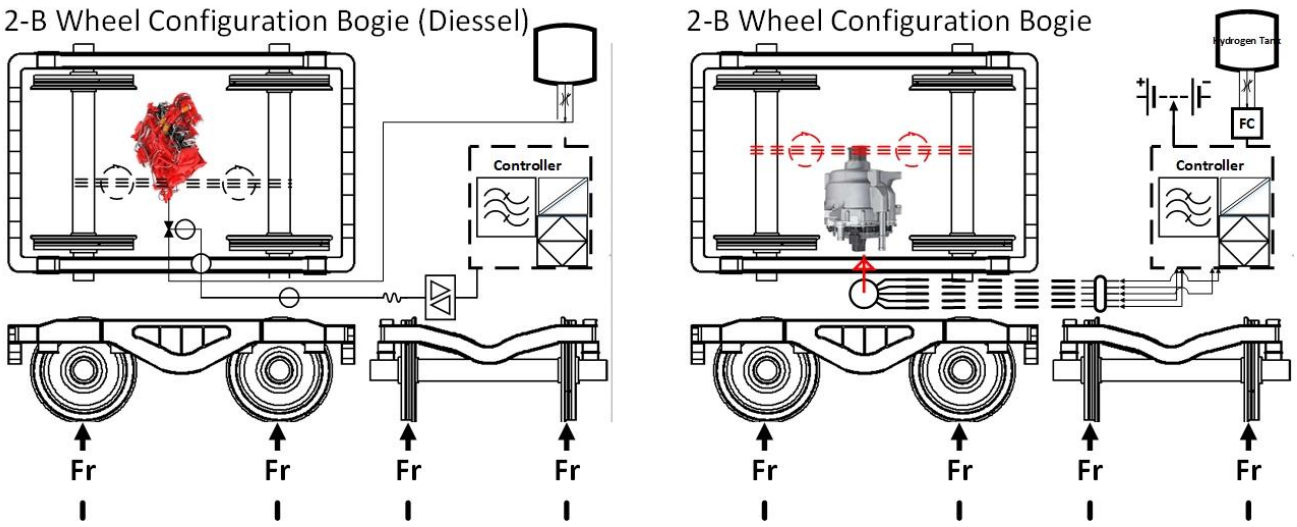

Figure 31: Baseline Topology representing one bogie of the UP Express DMUs.

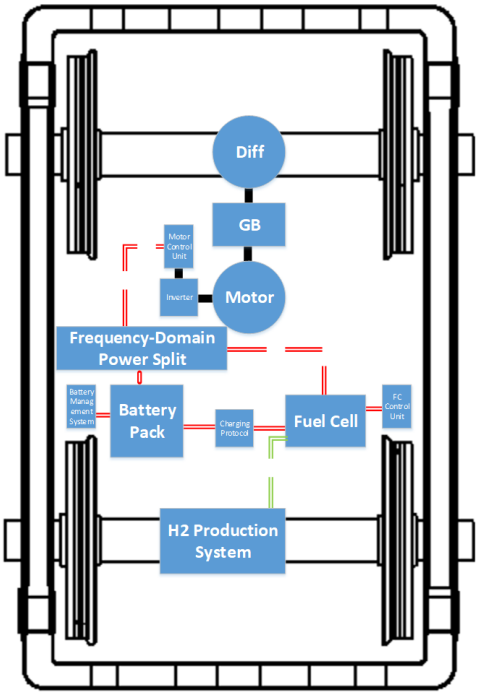

Figure 32: The Mild Hybrid Hydrail Topology of Interest.

After validating the resulted power demand, the output demand was applied to the frequency-domain power split subsystem. In this subsystem, the power demand is splitting according to the frequency content of the demanded power. The distributed power portions are then applied to the battery and the fuel cell subsystems to evaluate the dynamics of these two subsystems according

to the input loads. Owing to the drive cycle frequency content, applying entire frequency content to the fuel cell is not applicable as the starvation happens in the fuel cell membrane [75]. To avoid such a significant issue, a power management scenario was implemented in our model to split the demanded duty cycle due to the applied drive cycle's frequency content. The subsystem, however, called the frequency-domain power splitting subsystem. Since four subsystems are integrated into the model to simulate the sensitivity of each subsystem to a cut off frequency, an energy management control is needed to control power flow based on the different parameters of the system. So, a high-level rule-based power management control subsystem was implemented to control the flow of the power between the subsystems.

4.5.1 Contributions

1. A mathematical model of a hydrogen fuel cell powertrain was developed in this study. To the best of author's knowledge, such study has not been performed for the Union Pearson rail route. A battery pack, as well as a configuration of fuel cell stacks, were modeled to simulate the energy flow response of the system based on the real drive cycle applied to the model. In this regards, the drive cycle was converted to a duty cycle in our mechanical power estimation subsystem, as explained in the previous chapters of this study. Then the power applied to the other subsystems of the model to analyze the sensitivity of the system.

2. To preventing premature fuel cell damage, which results from gas starvation issues [75], a frequency-domain splitting power management system was implemented in our model. The power management system consists of the power splitting subsystem as well as a high-level rule-based controller. In the power splitting sub-model, a third-order IIR filter was implemented to filter the power demand based on frequency content. In the high-level control, the controller receives feedbacks throughout the other subsystems and control the energy flow. The cost function in the control system was the battery state of charge and the level of hydrogen in the tanks. To the best of the author's knowledge, there is a limited number of studies evaluating the effect of factors such as H_2 consumption, durability, leakage, etc. in terms of the cut off frequency.

3. Degradation models were implemented for the battery and fuel cell subsystems to show the long term durability response of the system. Since the goal was investigating the feasibility as well as the sensitivity of the Hydrail platform, the model utilized in this subsystem was not such a low-

level detailed one, and it was observed that a simple causal model could catch acceptable dynamic of the system.

4. A regenerative braking algorithm was implemented to contribute to the estimated power demand. Quantification of this portion of the power and implementing an algorithm to utilize the power in charging modes in an engagement with the power splitting block's output were seemed to be promising in Hydrail application as this portion of the power was controlled, in the lower levels, throughout a thermostat controlling scenario.

4.6 Battery Subsystem

Battery state of charge estimation is a key parameter in Hybrid electric vehicles. In a HEL, it's important for the controller to have a real-time estimation of battery state of charge. Basically, a HEL, like HEV, has three phases of operation. Charge sustaining, charge depleting, and idling modes of operation. In Charge depleting mode, a HEL is drawing current throughout the battery package. So, parts of energy demand are contributed through battery packs. Once the battery SOC is reached to its minimum level, the control strategy should switch the mode to charge sustaining mode. In this mode, the current vector is switched to the opposite direction, and the battery started to be charged. This scenario is the simplest scenario between those vehicles without regenerative braking mechanism contributing to the power supply loop. Moreover, in vehicles with regenerative braking, another strategy should be implemented. The controlling strategies are mentioned in detail in the next session of this part. However, SOC estimation in HEL is an important issue.

Battery models for locomotive applications need to be especially robust as HEL batteries are often exposed to dynamic and aggressive current draw profiles while working across a wide range of temperature and state-of-charge values. These changing conditions have a significant influence on battery performance parameters and thus need to be accounted for in a robust battery model [79]. Failure to do so will result in imprecise state information causing poor battery performance or worse yet, damage to one of the most expensive life components of the vehicle.

The focus of this session is to describe the development of an empirical performance model for one type of battery, A123 Systems lithium-ion cell. The reason for choosing such a battery cell was the previous experience in using this battery in an HEV competition called "EcoCar." An accurate model is needed for these A123 batteries. The development of the model involves first

collecting empirical battery data through standard reference performance tests. From here to the end of this part, all the data were used from our previous paper [79]. However, a model algorithm should be developed in Matlab to utilize the empirical data and predict battery performance. Finally, the model predictions should be validated through comparison to experimental data collected during the performance tests.

The developed empirical battery model was based upon the equivalent circuit diagram, Figure 33.

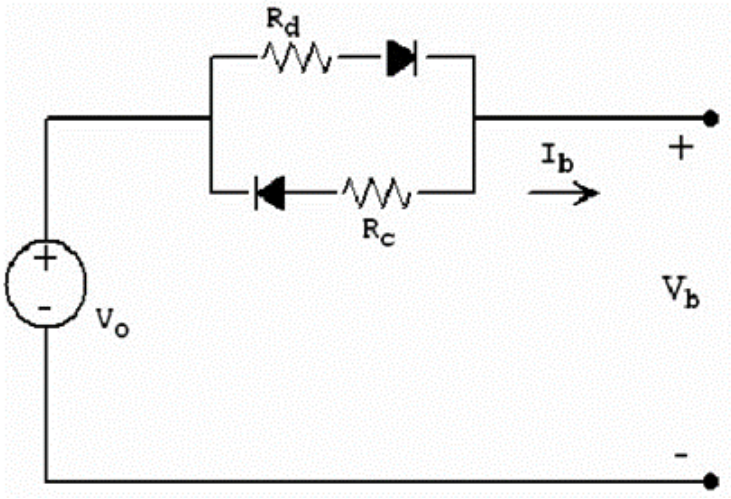

Figure 33: Battery model.

The model consists of a battery with open-circuit voltage (OCV), and two types of internal resistance (Rd) and (RC). These two resistors are put to account for different resistance values under discharging and charging, respectively. These two parameters model all forms of internal resistance including internal ohmic and polarization resistances. The diodes shown imply that during charging or discharging, only one of the resistances (Rd) or (RC) will be used. The battery terminal voltage (Vb) is represented as the open-circuit voltage plus the voltage rise or drop across the resistor.

To develop the model, empirical data, including open-circuit voltage as well as charge and discharge resistance determined through standard battery performance tests. To make the model more robust, these data will be collected across varying current draws, SOC values, and operating temperatures. Once acquired, this data should be utilized as look-up tables. In the model developed in our study, the A123 cells are utilized as the battery module to be sized as battery packs.

Therefore, the ultimate goal is to develop an accurate cell performance map that can eventually be scaled up to a pack level model and utilized in Autonomie as part of the HEL model developed in this study. The overall pack model will help in providing valuable battery state information to ensure optimal performance of the HEL.

4.6.1 Battery Cell Information

The cells being modeled are the A123 Gen 1.5 20 Ah Lithium-Ion Prismatic Cells. These batteries contain lithium-iron-phosphate cathode chemistry which is intrinsically safer than lithium cobalt chemistries due to the stronger phosphorous oxygen bond. The cell has a nominal voltage of 3.24V with a maximum and minimum cut off voltage of 3.6V and 2.0V respectively. It is rated for a maximum 10-second discharge pulse of 200A or 10 ℃ for a maximum discharge power of approximately 650W [79]. The most important cell specification and parameters are summarized in Table 18.

Table 18: Specifications for A123 20Ah Li-Ion Cell.

SPECIFICATION	VALUE
Capacity	20.0 Ah
Nominal Voltage	3.24V
Nominal Energy	64 Wh
Energy Density	135 Wh/Kg, 245 Wh/L
Mass	0.48kg
Power @25 ℃, 10sec, 50% SOC	650 W
Dimensions	165 x 227 x 7.05mm

4.6.2 Battery Data

4.6.2.1 Charge and Discharge Capacity

Selected results from the static capacity tests of the A123 cell are shown in Table 18. As expected, the charge capacity is slightly greater than the discharge capacity across all temperatures, which is partly due to the constant current-constant voltage method for charging as compared to the constant current discharge. Also, charge and discharge capacity decrease sharply below 0°C. Lower temperatures slow the electrochemical reactions within the cell, which increases internal resistance and as a result decreases the battery's usable capacity.

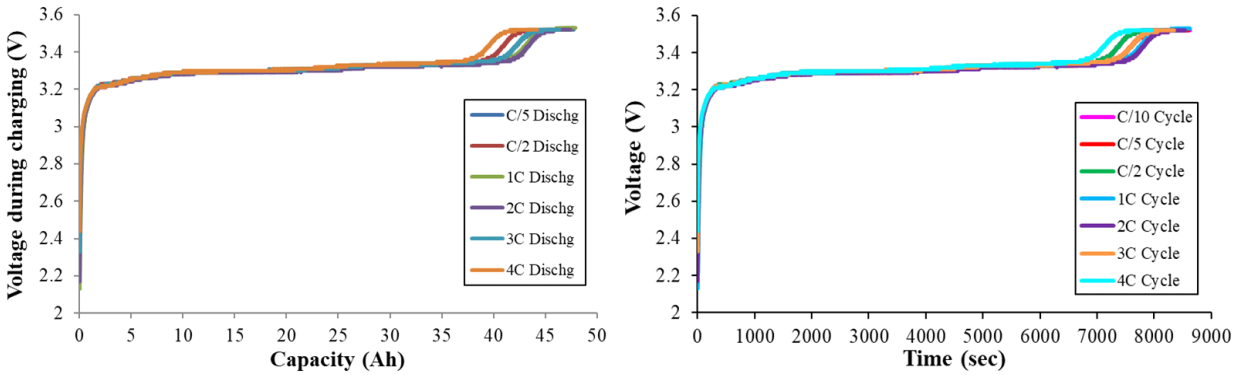

Figure 34: Charge Discharge Profile versus Capacity for A123 Batteries.

4.6.2.2 Open Circuit Voltage

Open circuit voltage as a function of the state of charge for the five operating temperatures tested an is shown in Figure 34. The OCV data indicates that the cell's voltage remains relatively constant throughout much of the SOC window. Across all temperatures the cell's nominal voltage is in the 3.25 to 3.30 V range; however, cell voltage drops sharply below 5% SOC. The higher temperature tests, particularly 25°C and 35°C show a wider range of operating voltage, which indicates the higher usable capacity at these temperatures.

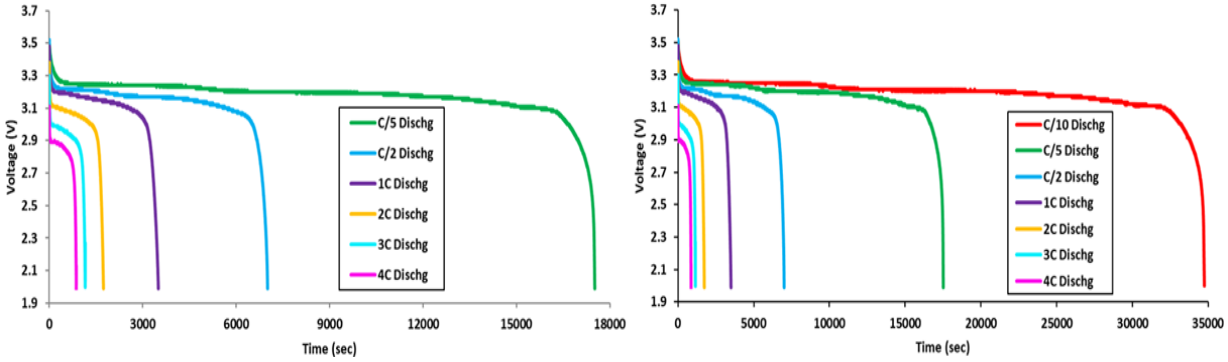

Figure 35: Open Circuit Voltage of A123 Batteries.

4.6.2.3 Charge and Discharge Power

The charge and discharge pulse power of the cell are shown in Figure 36. The absolute values of these power numbers are not that valuable since current limitations from the Maccor prevented testing at the maximum discharge or charge current. Thus, these values will be well below the limits of the cell's discharge or charge power. The most important information from the data below involves the effect of temperature on cell power. The data illustrates that cell power, especially discharge power is a strong function of temperature. The large increases in internal resistance that

occur as the temperature drops below 10°C significantly limit the power of the cold-temperature power cell. Once again, these results illustrate the importance of operating temperature on battery performance.

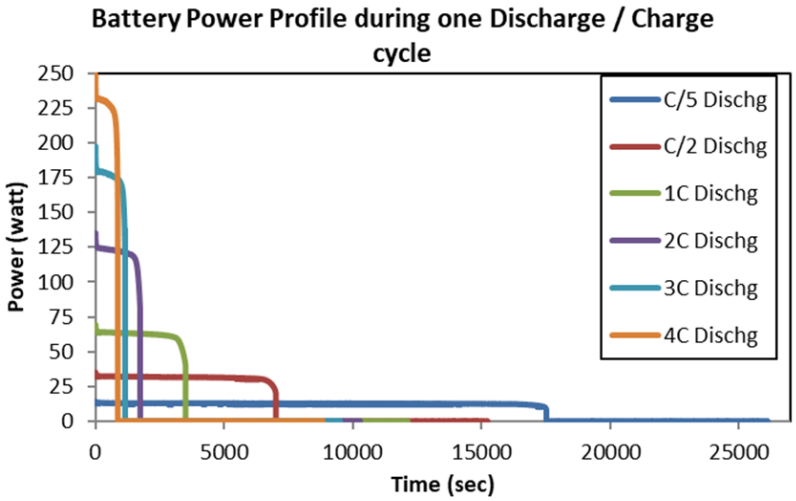

Figure 36: Power versus Time of A123 Batteries.

4.6.3 Battery Degradation Model

Similar to the HEV application and despite to the type of the implemented topology, energy storage systems are the most challenging parts in a HEL. On the other hand, as it has been mentioned so far, the compromising specifications of the Li-Iron phosphate batteries, i.e., the high power density at high specific energy levels, making them as the best choice for the powertrains with an energy storage system. Typically, the life cycle of these types of batteries is highly dependent on the applied duty cycles. Batteries show significant degradation during time and load. For this reason, understanding the chemistry of the batteries is important to estimate the durability and performance of the batteries. Typically, a lithium-Ion battery is constructed with five different layers of which are the positive collector, the positive electrode, separator, negative collector, and negative electrode [79]. Figure 37 shows a brief representative schematic of the chemistry of a Li-Ion battery. In the battery, copper and aluminum are used as anode and cathode collectors, respectively.

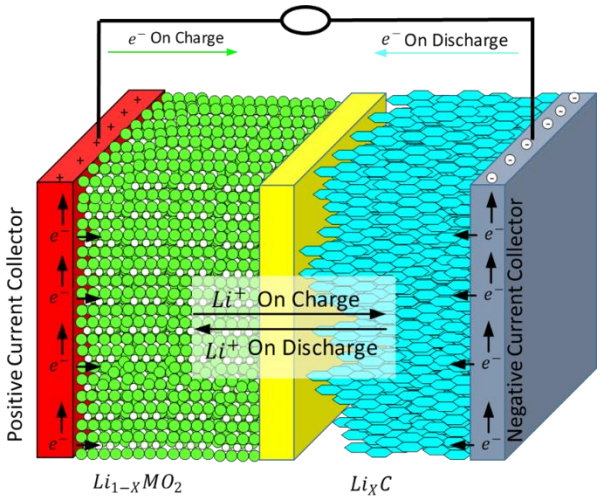

Figure 37: Schematic of the Li-Ion batteries representing battery chemistry.

In the battery cell, copper is used as the anode, and aluminum foil is utilized as the cathode. To scale down and look at the anode in more detail, the structure is the (MCMB) and SFG in PVdf [79]. Talking about materials, several types of polymers are under development. In Figure 37, it was assumed that the cathode composition is nickel-cobalt. The two other components, which are separator and electrolyte, should be a high ion conductive polymer, a good electrical insulator, and also forming a stable ionic conductive passive-interface both at anode and cathode side. In this regards, $LiPF_6$ is the main part of the most common electrolyte structure. $LiPF_6$ in these electrodes always solved in a cyclic alkyl carbonate solvent and a linear alkyl carbonate. The most common separator is also a polypropylene, like Celgard.

Solid electrolyte interface is a common phenomenon in almost all Li-Ion batteries. This passivation layer is formed at the electrolyte anode interface. It's a lithiated alkyl carbonate and forms at the first charging cycle. This layer is considered as the significant source of cyclable lithium loss in the battery cell. A practical way to compensate such loss is to implement the cathode with an excess of lithium [79]. However, observing the electrodes at this scale and analyzing the chemical dynamics of the battery is not in the scope of this research study. In this area, it would suffice to mention that the batteries are exhibiting fades in both power and capacity. To capture this capacity fade, experiments have done in the lab, and the data for the A123 battery were extracted using a customized test stand [79]. However, the battery degradation model developed in our lab can be represented by the modified Ning model, which is shown in (1) to (5) [79]. The battery degradation

fitting data were shown in Table 19 [79]. The battery block is tuned based on the values are extracted through the experiments, battery OCV, VOC, current, and temperature vectors to be used as a subsystem in the Hydrail model.

$$J_{para} = \alpha_{Temp}^{n,avg} \alpha_{SOC}^{n,avg} J_{Para}^{0} \exp\left(\frac{\alpha_c F}{RT}\eta\right) \quad (1)$$

$$\alpha_{Temp}^{n} = \exp\left(\frac{-40498}{RT}\left(\frac{1}{T} - \frac{1}{T^0}\right)\right) \quad (2)$$

$$\alpha_{Temp}^{n,avg} = 0.01 \times (\alpha_{Temp}^{n})^{Z_1} + 0.99 \times \alpha_{Temp}^{n-1,avg} \quad (3)$$

$$\alpha_{SOC}^{n} = \exp\left(\frac{-100}{abs(60 - SOC)}\right) \quad (4)$$

$$\alpha_{SOC}^{n,avg} = 0.01 \times (1 + \beta_1 \times \alpha_{SOC}^{n})^{Z_2} + 0.99 \times \alpha_{SOC}^{n-1,avg} \quad (5)$$

Table 19: Battery Degradation fitting parameters [79]

Parameter	Value
B_1	2
Z_1	0.25
Z_2	4
$J0_{para}$	0.000000008
α_c	0.5

4.7 Hydrogen Fuel Cell Subsystem

The discovery of fuel cells came back to 1839 by William Grove [79]. These electrochemical devices were hypothesized base upon the fact that the hydrogen can be produced by the presence of electrical currents. What Groove suggested was to execute the reaction in reverse side. He demonstrated that hydrogen and oxygen could react in the presence of a catalyst. Fifty years later, Charles Langer and Ludwig Mond implemented the first fuel cell in the shape of the current fuel cells [79]. In the electrochemical scale, the reactions for the half cells are as follows:

$$\text{Anode: } H_2 \longrightarrow 2H^+ + 2e^- \quad (6)$$

$$\text{Cathode: } 2H^+ + 2e^- + \tfrac{1}{2} O_2 \longrightarrow H_2O \quad (7)$$

$$\text{Overall: } H_2 + \tfrac{1}{2} O_2 \longrightarrow H_2O \quad (8)$$

A PEMFC is composed of three components, which are the Membrane Electrode Assembly (MEA), Gas Diffusion Layer (GDL), and bipolar plates [79]. In the fuel cells, the most popular material for the membranes is a commercialized material developed by Dupont named Nafion [79]. The material is a monomer with the base of Perflourosulfonic (PFSA) acid. The molecular structure of PFSA acid is shown in Figure 31. Recently, it is believed that the porous structures can improve the kinetics of reactions [79]. In a fuel cell, collectors are the connection to the external load while the end plates provide the strength which is protecting the stack through mechanical compression.

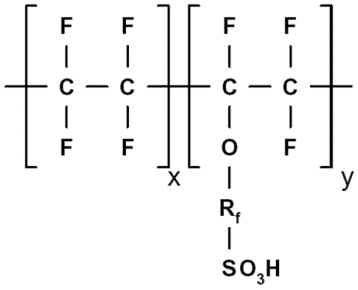

Figure 38: The Structure of PFSA. [80]

A fuel cell should be connected to some other peripherals to work properly. These components are required to provide mandatory pressure, humidity, heat, as well as the reaction streams. To count these components, a fuel cell circuit should have recirculation pump, humidifier, and supply manifold in the anode. In the cathode side, the circuit should have air blower, exhaust and supply manifold, and humidifier. On the other hand, in some cases, the coolant circulatory as well as a sensor and control circuit would be needed additionally. In a fuel cell, the net power output is dependent on the duty cycle. Which means that the fuel cell output fluctuated by an applied change in the duty cycle. The fluctuation was considered in the model for the case that an appropriate model of the inventor can be implemented in the future and keep the model more realistic and complex.

4.6.5 Fuel cell performance

Numerous types of semi-empirical, empirical, and mechanistic models describing fuel cell behavior have been developed so far [79]. The first semi-empirical model developed by Amphlett

and Kim in 1995 [79]. Theoretically, the model was a polarization curve to evaluate the voltage of the cell in terms of current and shown in (9).

$$V = V_0 - \eta_{act} - \eta_{ohmic} \quad (9)$$

In 2000, Mann refined this parameterized form to a model which is called the Generalized Steady State Electrochemical Model (GSSEM). In the proposed model, the loss of mass transfer was split into two overvoltages of activation and ohmic. In this equation, the V_0 referred to as thermodynamic equilibrium overpotential. To calculate this overpotential, Nernst equation might become the best solution:

$$V_0 = E_0 - \frac{RT}{nF} \ln[p^*_{H_2} (p^*_{O_2})^{0.5}] \quad (10)$$

This overvoltage is the voltage drop that happened due to the kinetics of the reaction. The kinetic of hydrogen at the anode is comprehensively faster than the kinetics of oxygen at the cathode [79]. To calculate the term η_{act}, activation overvoltage, is calculated as a sum equation, (11)

$$\eta_{act} = \xi_1 + \xi_2 T + \xi_3 [\ln C^*_{O_2}] + \xi_4 T [\ln(i)] \quad (11)$$

The last term of the polarization equation is the ohmic resistance, which is the resistance of proton transfer in the membrane and electron transfer in the electrodes and collector plates. This overpotential is calculated using the (12)

$$\eta_{ohmic} = i(R^{electronic} + R^{proton}) \quad (12)$$

In this equation, the total proton diffusion resistance is calculated as a function of the membrane cross-sectional area and thickness as well as the membrane resistance and can be calculated (13)

$$R^{proton} = \frac{r_M l}{A} \quad (13)$$

The membrane resistance is also can be given by (4)

$$r_M = \frac{181.6[1 + 0.03\left(\frac{i}{A}\right) + 0.062\left(\frac{T}{303}\right)^2\left(\frac{i}{A}\right)^{2.5}]}{\left[\lambda - 0.634 - 3\left(\frac{i}{A}\right)\right]\exp(4.18\left[\frac{T-303}{T}\right])} \quad (14)$$

4.7.6 Fuel cell degradation model

Like the batteries, fuel cells are also degraded over time. Degradation in fuel cells means that the specific voltage for a given current draw is dropped due to the service time. The degradation in fuel cells is composed of two types of degradation, which are the reversible and irreversible degradation. Observing such changes in the fuel cell polarization curve over time of service may have the benefit of estimating long term voltage drop in a fuel cell package. It also gives an insight into the dominant degradation mechanism [79]. As an example of the degradation models of a fuel cell, the (15) was proposed by Fowler et al., which utilized a fitted term λ to represent the age of a fuel cell and its effect on the voltage drop. In the study, the revised equation r_M is defined as (15)

$$r_M = \frac{181.6[1 + 0.03\left(\frac{i}{A}\right) + 0.062\left(\frac{T}{303}\right)^2\left(\frac{i}{A}\right)^{2.5}]}{\left[\lambda_{age} - 0.634 - 3\left(\frac{i}{A}\right)\right]\exp(3.25\left[\frac{T-303}{T}\right])} \quad (15)$$

Where:

$$\lambda_{age} = \lambda_0 + \lambda_{DR} \times age$$

In (15), λ_{DR} is approximated as a function of operating boundary conditions [79]. To propose the membrane resistance as a function of the boundary conditions and operational situation, giving the option of implementing the high-level control scenario to perform a degradation regulation strategy. There are several studies on modeling the degradation in a PEM fuel cell. Table 20 shows the results of some of these research studies.

Table 20: PEMF degradation Studies.

Test cycle Type/ Researcher	Current Densities (mA/cm^2)	Cell Temperature (°C)	Voltage Decay Rate (μV/hr)
Steady State			
St-Pierre	1076	75	1
St-Pierre	538	75	1.4
Yoshioka	861	75	1.3
Cleghorne	259	75	1.5
cyclic			
Yamazaki	150- 300	70	2.5
Wahdame	0- 700	55	45
Nakayama	0.01- 300	80	75- 114
Miyoshi	0.01- 300	80	210

A casual degradation model of a single cell PEMFC was implemented in this research. In the development of the model, the results of the previous works represented in Table 20 was inspired. These studies assumed different degradation rates as a function of membrane structures, temperature, and duty cycle. However, the dynamic of a Ballard fuel cell stack was modeled. Ballard fuel cells are working in lower temperatures comparing to the other fuel cells. Also, these stacks are working in lower pressures as well. Accordingly, the effect of the temperature is not considered in this study. It means that the weight of tests conducted in lower temperatures is more than those performed in higher temperatures. The rate of degradation was assumed to be ten μV/hr, and the cyclic operation was exhibited as approximately 90 μV/hr [79]. However, the degradation rate, which manifested as the open-circuit voltage drop, is modeled with (16)

$$\frac{\partial V_{decay}}{\partial t} = -\frac{0.000225}{3600} \times stedv(P_{FC}^{N}\ P_{FC}^{N-1} P_{FC}^{N-2} P_{FC}^{N-3} P_{FC}^{N-4}) - \frac{0.0000010}{3600} \qquad (16)$$

In this equation, the degradation rate at each time is approximated in terms of the standard deviation of the drawn power amplitude for the previous five seconds. According to the GSSEM equations, membrane resistance can be derived as a function of time in the form of (17)

$$\frac{\partial r_M^N}{\partial t} = -\frac{A}{ii}\frac{\partial V_{decay}}{\partial t} + \frac{A}{ii^2}\frac{\partial i_{decay}}{\partial t} \tag{17}$$

By assuming that the degradation is solely dependent on the voltage decay, the second term in (19) is considered to be negligible. So the (1) can be rewritten in the shape of:

$$\frac{\partial r_M^N}{\partial t} = \frac{A}{ii}\left(\frac{0.000225}{3600} \times stedv(P_{FC}^N\ P_{FC}^{N-1} P_{FC}^{N-2} P_{FC}^{N-3} P_{FC}^{N-4}) - \frac{0.0000010}{3600}\right) \tag{18}$$

Considering the current decay and also the temperature is remaining constant over time with a negligible differential and taking a derivation of λ with respect to the r_m, it turned out that:

$$\frac{\partial \lambda}{\partial t} = \frac{-181.6\left(1+0.03\left(\frac{i}{A}\right)+0.062\left(\frac{T}{303}\right)^2\left(\frac{i}{A}\right)^{2.5}\right.}{\left(r_M^N\right)^2 \times \exp\left(4.18\left[\frac{T-303}{T}\right]\right)} \times \left[\frac{A}{li} \times \left(\frac{0.000225}{3600} \times \right.\right.$$
$$stedv(P_{FC}^N\ P_{FC}^{N-1} P_{FC}^{N-2} P_{FC}^{N-3} P_{FC}^{N-4}) + \frac{0.0000010}{3600}\Big) \tag{19}$$

This equation gives a relation to calculate the degradation of λ, which approximates the fuel cell age. However, the function can be compared to Fowler's developed relationship.

In this theses, the fuel cell subsystem was used to calculate power and hydrogen fuel consumption rate of our stack. In this block, the hydrogen fuel rate is calculated based on the demanded duty cycle, which manifested as the electrical power. Keeping the power to be constant, as the voltage is dropping off over time, the current drawn should be increased over the same period. This shows that the voltage drop causes an increase in hydrogen consumption as the current directly related to the fuel consumption rate. On the other hand, the fuel cell state of health can be calculated as:

$$SOH_{FC}(t) = \frac{V_{BOL} - V_{decay}(t)}{V_{BOL}} \tag{20}$$

With the aim of this formula, the hydrogen consumption rate can be calculated as

$$\mathrm{H_2(t)} = \frac{H_{2_{BOL}}}{SOH_{FC}(t)} \tag{21}$$

This session explained the relationships were used in modeling the fuel cell dynamics. A degradation model was implemented in this session, as well.

4.8 Power Split Subsystem

Basically, signals have a stochastic and random nature. It means that in a power system, power demand can have any values during a period. When a dynamic system, like a battery or a fuel cell, is excited by a dynamic signal, the output of the system is quantified in terms of two parameters of amplitude and phase. Frequency response is a way of measuring the outputs of a system in the frequency domain. Any discrete signal is composed of number of discrete frequencies. Two different applications of signal processing, which is estimation and detection, comes from the simple definition. In terms of detection, the availability of an individual signal in the observed signal is approximated. On the other hand, in the estimation, necessary parameters are obtained to describe a unique signal [81]. Often a signal is complex and corrupted by noises. To detect, determine, or estimate of the desired signal through a complex initially logged signal, decomposition is the first step. Such decomposition is performed by the classic Fourier transform [81]. An appropriate tool to decompose a signal and estimate the desired second and third signal throughout the initial signal is the Fast Fourier Transform (FFT). FFT has several benefits comparing to the Discrete Fourier Transform (DFT) [82]. In the transportation application, decomposing drive cycles with such transforms are common. As an example, the drive cycle was decomposed to be split in a powertrain [89].

Four different characteristics are important to draw currents from the fuel cell in an electric vehicle [83]. Although in this study, we looked at the power flow as a black box and the dynamics of power electronics were not modeled, these conditions should become satisfied by a customized converter. The converter should regulate the current ripples. The voltage gain ratio should be optimally high, as well. In driving a fuel cell, the compactness and redundancy should be high as well.

Fuel cell conditions are adaptively changed during the vehicles driving modes. Basically, the fuel cell conditions are evaluated based on the vehicles power demands. Such demand is classified as transient demands or long term demands. However, fuel cells have unique characteristics. One of the most important drawbacks of the fuel cells characteristics is the low dynamics and efficiency in high current densities [84]. However, in a vehicle, the load fluctuation is extremely depended

on the topology. The topology should define the power management strategy. As an example, in powertrain with a fuel cell and battery, like the topology we are implementing in this thesis, the battery might face severe bursts. Such transient loads are making the battery life shortened. From another side, batteries show lower energy density comparing to the fuel cells. In this part of the thesis, a power management system is developed for the fuel cell- battery hybrid powertrain. The power management system is similar to the power management strategies in the literature and proposed to protect the fuel cell and improve the fuel economy of it [57]. Splitting the duty cycle in terms of frequency content gives the option of developing precise optimal control strategies. It also gives the opportunity of controlling each power source in a high-level mode, considering each power source dynamic separately. Fuel cells are working under dynamic conditions in a hybrid vehicle. The conditions are stop/start and transient changing in the frequency of the load. These changes in the loads might affect the durability response of the fuel cell which is happening more quickly in mobility applications in comparison to the stationary conditions because that the loads have more dynamic natures in mobile applications [57]. Figure 39 shows that fuel cell H_2 consumption is very high when it works in both low and high power zones [57]. On the other hand, at lower power zones, the efficiency is very low, and the reason is that there are several components (like compressors, valves, etc.) are consuming energy. Frequency domain power splitting is not a new objective. Several studies in the literature have proposed a frequency-domain power split scenario [57]. In a study, three different regions were characterized to split the power according to two different cut off frequency, Figure 40 [57]. These three frequencies are defined according to the fuel cell, battery, and super capacitor's specifications. However, based on these studies [58], and Figure 39, the FC must be fixed to work in its efficient power range. Also, the battery should be working in its intermediate dynamic horizon.

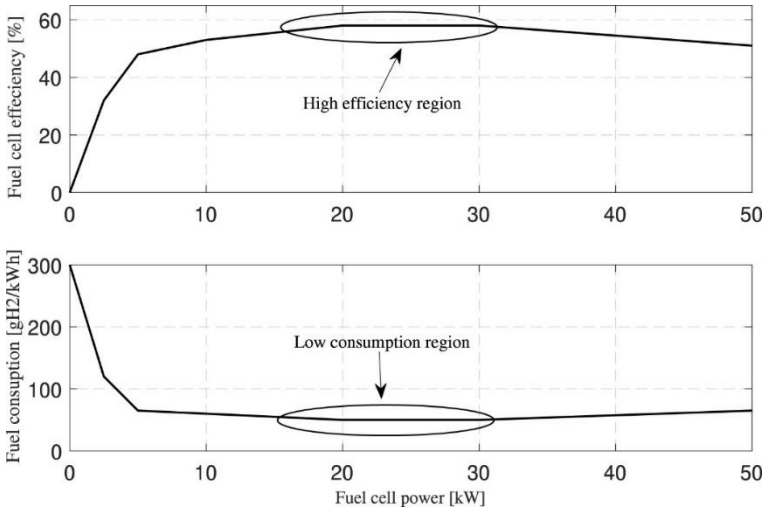

Figure 39: Fuel cell efficiency and fuel consumption in terms of power demand [57].

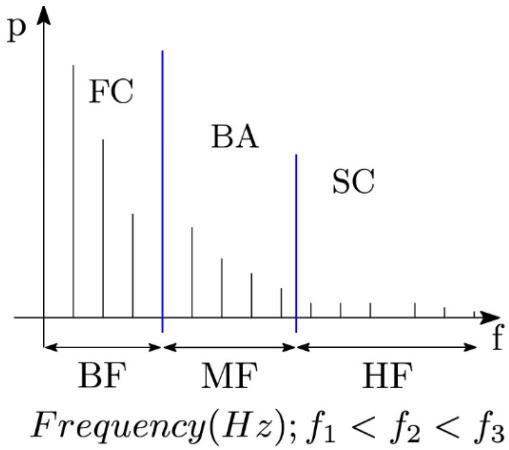

Figure 40: Cut off frequencies for a similar study [57].

After the brief introduction, Frequency Domain Power Splitting (FDPS) is explained in this session. In the scenario, based upon the frequency content of the duty cycle, the key is to split the power into some portions to be distributed between energy sources. The portion is defined based on the dynamic characteristics of each power sources. Figure 41 shows the frequency content of the duty cycle. However, the duty cycle should be separated to the high frequency and low-frequency portions. The low-frequency portion approximates the smooth trajectory of the duty cycle, and the high-frequency part estimates the highly dynamic contents. Technically the amplitude of the duty cycle in the high frequency is smaller than the smooth part. In a recent study [80], a HEL with a fuel cell as a range extender, a battery pack as the first ESS source and a supercapacitor pack as the second source, the fuel cell was designed to work at a near steady-state

condition. The battery supply additional energy demand in acceleration portions, and supercapacitor was used to fill the peaks [80].

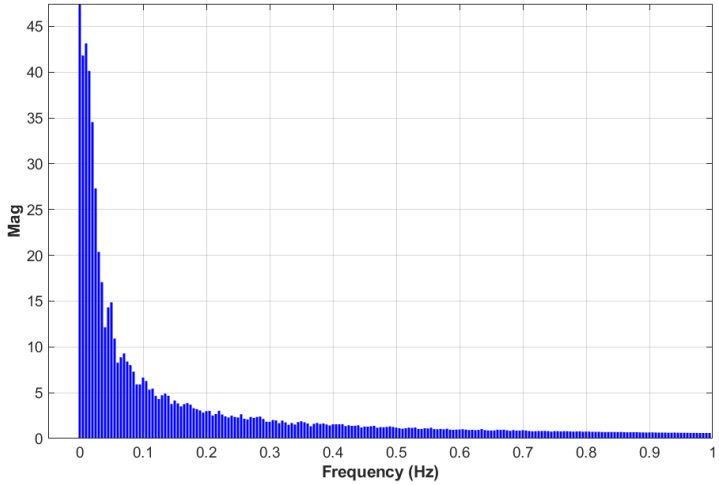

Figure 41: Frequency content of the duty cycle

Starvation is a common phenomenon taking place in the fuel cell membrane and has different reasons [85]. A good gas management system causes a delay in membrane starvation because of reactant depletion. However, in an urban duty cycle similar to the one logged from the UPExpress DMUs, although a good gas management system might give the opportunity of using only fuel cell configuration, such system might not be applicable for several reasons [86]. However, in the development of the model, the UP Express drive cycle was analyzed, and the maximum acceleration and jerk were calculated. The power demand was also analyzed. Based on the calculations, it turned out that the batteries solely can maintain the acceleration trips during the journey, and there would be no need to utilize excess supercapacitors in the configuration. However, the HEL power management system is composed of two parts of the battery and, fuel cell. Figure 42 shows the power split strategy represented in this theses.

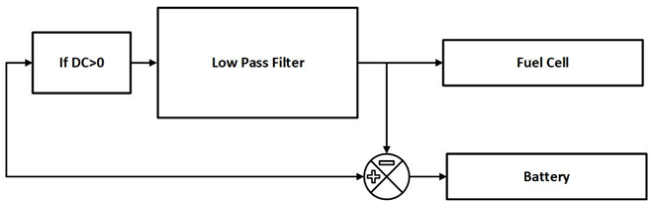

Figure 42: Schematic of the power splitting scenario.

4.7.1 Filter design

A low pas Infinite Impulse Response (IIR) filter, Butterworth, was implemented in the DSP environment of MATLAB, Simulink. Different filters with different orders were investigated to the system, and the best response concerning the order of the filter was characterized. The filters were designed from the first order to fifth-order separately. The duty cycle was applied to each filter, and the filter's characteristics were analyzed based on the performance factor of the filters. The performance is expressed through the gain and phase responses which are corresponding to the cut of frequency and the filter's order, Figure 43.

As it was explained in the last sessions, a sensitivity analysis was performed due to evaluating the long term response of the energy storage system according to different frequencies. In this analysis, the higher-order filters are shown the best attenuation response at the cut off frequencies, but the phase shift is observed to be larger than the lower order filters. This thesis aims to perform a sensitivity analysis in terms of splitting cut of frequency. To split the power, four nominated different frequencies of 0.001 Hz, 0.005 Hz, 0.01 Hz, and 1 Hz were chosen, and the duty cycle was separated based on these four frequencies.

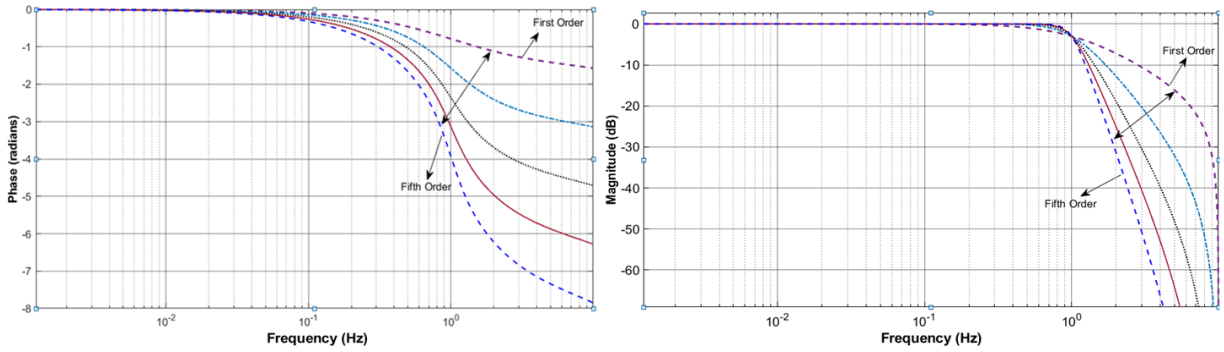

Figure 43: Frequency and phase response of first to fifth order low path filter.

4.9 High-Level Supervisory Control Subsystem

Power management of a HEL may be defined as a set of rules to regulate the operation of the powertrains in a multidirectional sensotronic platform which supports the power management systems feedback demand. The goal of such power management algorithm including but not limited to fuel consumption optimization, charge sustaining or depleting optimization, reducing

emission, and controlling the long-term dynamic response of different components. The number of feasible solutions might be available for these problems are affecting the dynamics of the vehicle in real-time and the levels of applicability of the solutions. Technically, power management scenarios are dividing into two categories of rule-based and optimization-based. In optimization-based algorithms, a set of globally optimal solutions should be found. In the most particular case in real-time applications, instant-wise noncausal decisions are made based on particular cost functions [88]. On the other hand, rule-based control strategies are defined by fuzzy logic or deterministic thermostatic rules. Figure 35 shows the classification of power management scenarios.

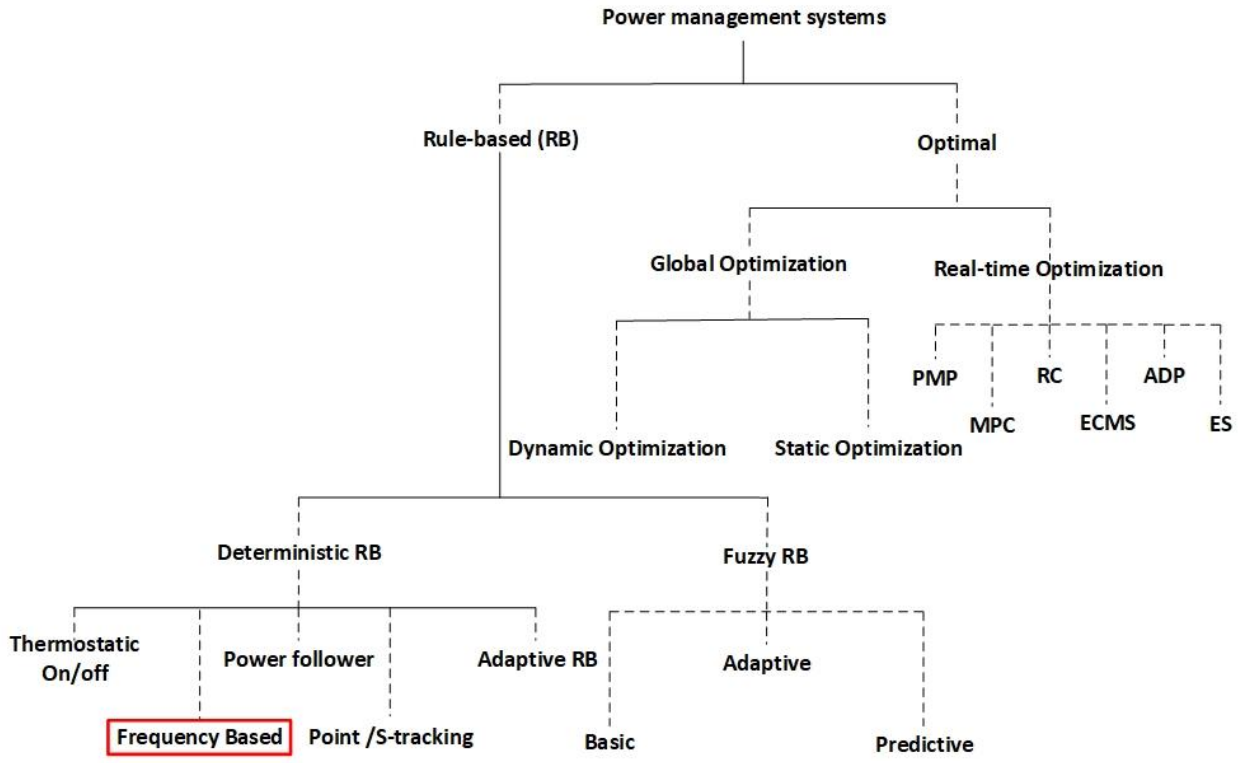

Figure 44: Power Management Systems Classification.

From Figure 44, Rule-based controls are sets of "if-then" rules to assign the appropriate control action based on the control feedbacks received from the sensotronic platform. In the development of such controls, the human expertise and knowledge of the system is the preliminary key point. The low computational cost is the main advantage of these control algorithms. These types of control systems are already used in almost all vehicles. Between the mentioned rule-based

strategies shown in Figure 44, frequency decomposition-based power management systems are shown to apply a 5.9% improvement in fuel economy compared to the thermostatic strategies. It was also clarified that these types of control systems have a 62.7% soot reduction compared to the other rule-based strategies. These control scenarios are also decreasing the battery temperature in HEVs for more than 3 ℃. Based on Ah-processed models, it also is shown that the frequency splitting of the duty cycle increases the lifespan of batteries for more than 23%.

Based on the benefits of the frequency-based power management systems, in the theses, a frequency splitting power management system was developed. The previous session was approximate the basics of the IIR filter based duty cycle decomposition strategy. Figure 45 shows the high-level rule-based control scenario was explained in detail.

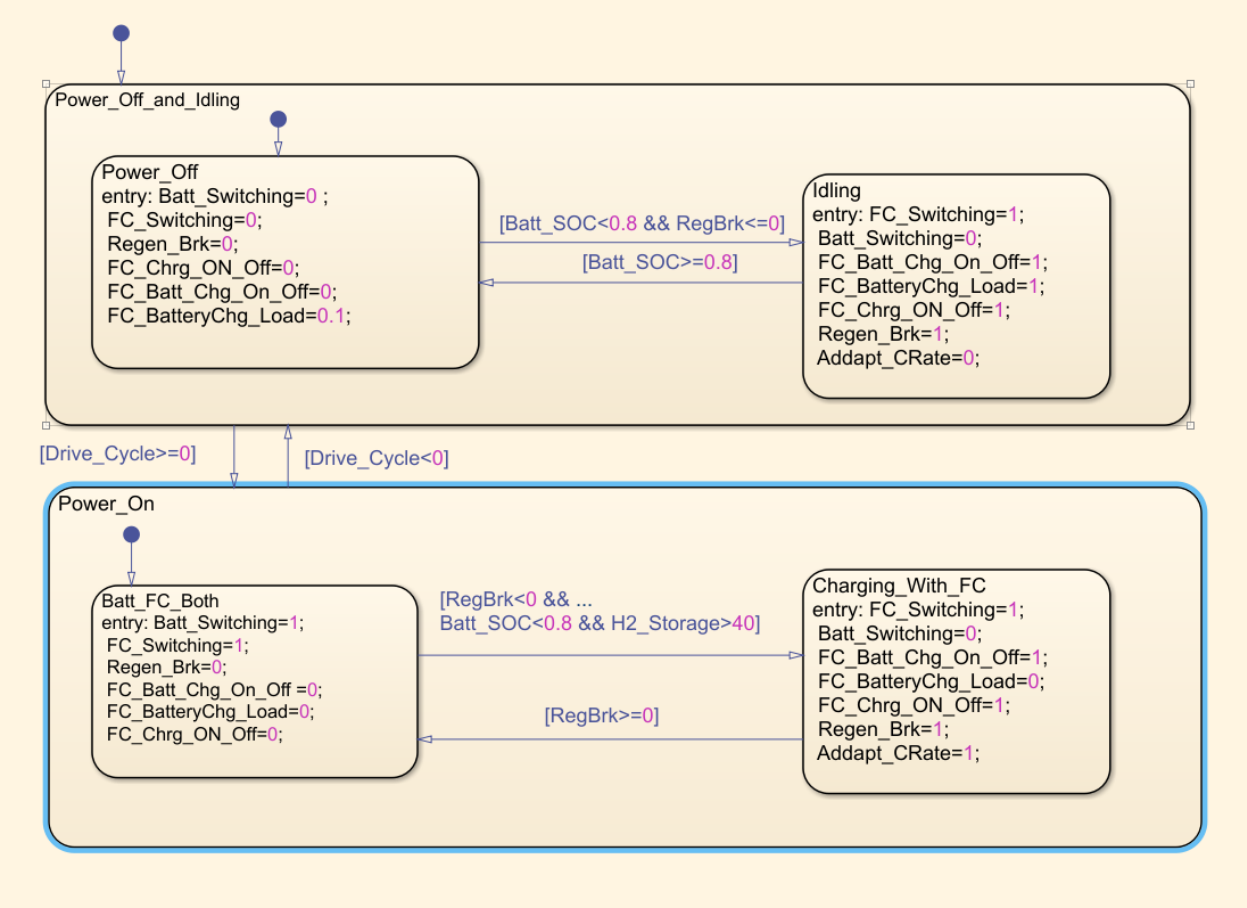

Figure 45: High-level rule-based power management system.

4.10 Results and Conclusion

The duty cycle as shown in Figure 11 and it's the frequency content also justified in Figure 41. On the other side, recent research showed that with the battery system, a frequency of 10 Hz is achievable [87]. So, it turned out that a powertrain with battery and fuel cell packs can satisfy the loads in terms of frequency domain and there would be no need to use supercapacitors. A model of the powertrain was implemented and shown in Appendix 1. The model was developed in MATLAB Simulink. The generic battery and fuel cell model was used in our model. The dataset was used to set up the semi-empirical model of the battery was extracted from the tests conducted on an A123 battery pack using Fowler's Lab test setup [79]. In Fowler's Lab, a test bench was also installed for testing fuel cells due to extracting polarization curves and other necessary data out of fuel cell stacks and cells. A dataset of a Ballard Fuel cell with 80 kW nominal power was available and published before [79]. Using the mentioned extracted datasets of batteries and fuel cells, the battery and fuel cell subsystems were empirically tuned, and the results for a cell was validated by the papers published in our group before [92]. Appendix 2 shows the initialization file was developed to set up the subsystems. In terms of the third subsystem, which is estimating the power demand with respect to the rolling stock characteristics, the block was verified with the Metrolinx DMU's specifications [36]. According to the filter design, the response of the filter, which was implemented in Simulink, was compared with the filter designer toolbox of the MATLAB. The high-level control scenario, also, was implemented in State flow toolbox of the MATLAB and integrated into the filter subsystem to represent a complex two-layer signal processing subsystem to split power flow between the other subsystems.

Although this control scenario, should become a part of a sophisticated customized optimal controller, implementing such power management system needs a good insight of the designer out of the system sensitivity [88]. The high-level control strategy, as mentioned before, is to use a frequency splitting based methodology. To conduct a sensitivity analysis, the first step is to approximate cut off frequencies and approximate the response of the system in terms of this important factor. In this regard, the spectrum of the duty cycle was extracted using FFT toolbox in MATLAB which shown significantly close to the studies performed on drive cycles of vehicles [89]. The drive cycle, as shown in Figure 5, was sampled in 5 Hz. However, the peak frequency has

happened at 0.1 Hz. To evaluate the system response, four different frequencies were chosen. The nominated frequencies were 0.001 Hz, 0.005 Hz, 0.1 Hz, and 1 Hz.

On the other hand, the high-level control was implemented to control the state of charge of the battery as a cost function manipulating the flow of energy between battery pack, fuel cell pack, and the regenerative braking system. In simulating four different scenarios, all the other system factors set to be constant in every scenario and time domains and the only manipulated parameter was the splitting cut off frequency. To start the simulation, the battery and fuel cells were sized for the cut off frequency of 0.001 Hz. Table 21 shows the number of batteries and fuel cells in the desired configuration [38].

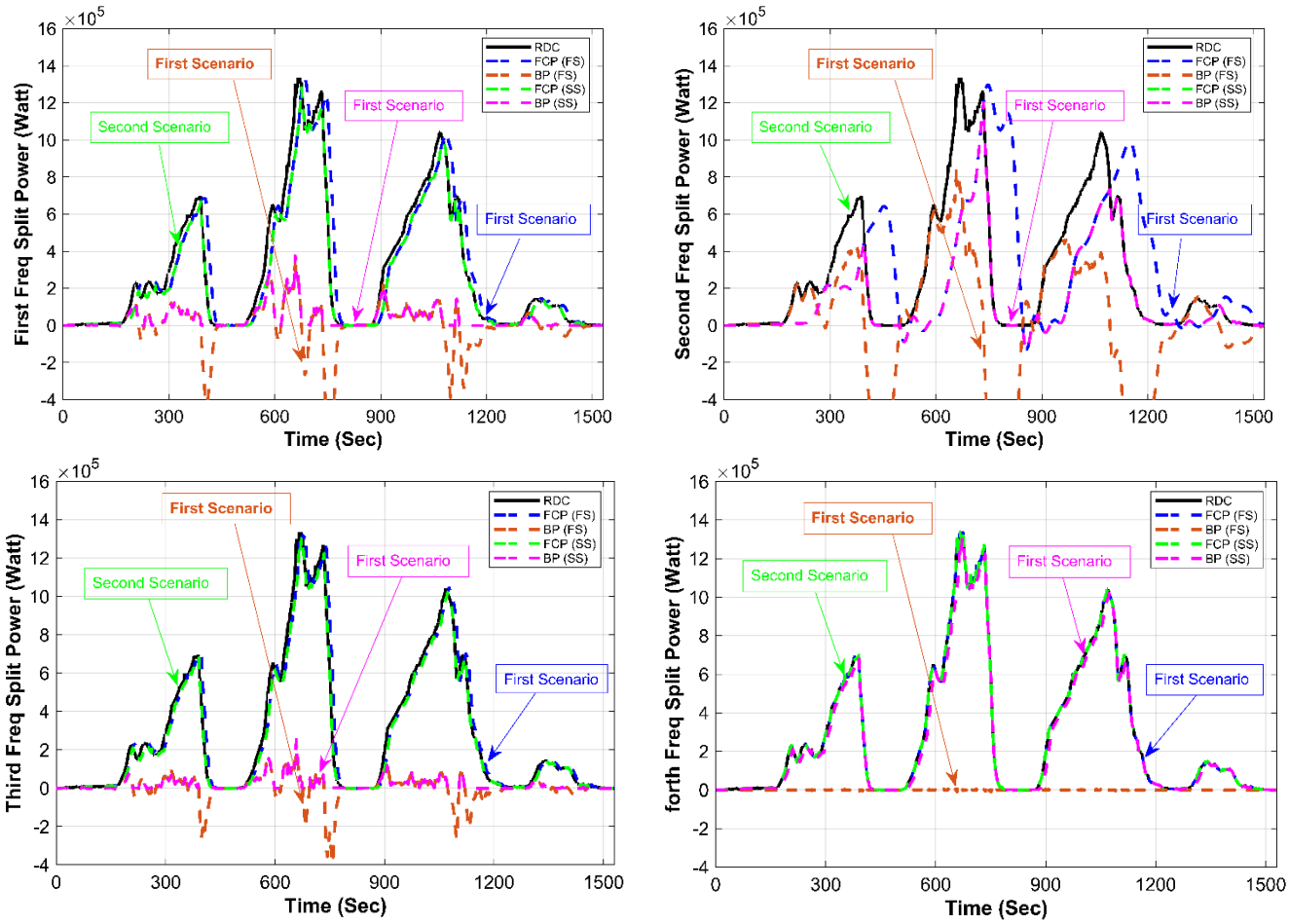

Figure 46: Power Splitting Based on Different Scenarios at four Cut off Frequencies of 0.001 Hz, 0.005 Hz, 0.01 Hz, and 1 Hz.

Table 21: Size of the battery and fuel cell [38].

Description	Number
Number of Parallel Battery String	3
Number of Series Battery Cells	265
Number of Parallel Fuel Cell Strings	38
Number of Series Fuel Cells	1

The first step in analyzing the results and interpreting the system dynamics in terms of different frequencies is to interpret the filters output and the portions of contribution for each part of the ESS. Figure 46 shows the outputs of the filter, designed and explained in detail in previous sections, for mentioned four different cut off frequencies. In the development of the power split subsystem, two different scenarios were implemented; one is more mathematical, but not practical, and the other is purely practical. Figure 42 shows the splitting strategy. In some cases, the power portion assigned to the battery is introduced as a negative intensity value. This negative power might be translated to the current demand and use as a charging value. But the issue is that the negative value should be considered as an imaginary value since, at that moment, the powertrain is not in a recharging situation. The second scenario, which is shown in Figure 46, the value jump to the real zero and the fuel cell command jumps to follow the whole portion of the duty cycle. Both the battery and fuel cell duty timely demands are shown in different colors in Figure 46. This figure is also showing the split duty cycle for four different cut off frequencies.

To evaluate the response of the battery pack in terms of the state of charge, four mentioned different splitting frequencies were applied to the system, and the high-level control response was measured in controlling the SOC during the journey. In this matter, it was assumed that the initial battery state of charge was set to be 80%. The sizing scenario was performed in the way that the designed main bus voltage should be sustained. The standard voltage for a locomotive was defined to be 850V [38]. This voltage approximates the number of series in each string of the battery and fuel cell packs. However, in battery pack it turned out three parallel strings of 265 batteries connecting in series might satisfy the demanded power. Also, it turned out that one string containing 38 series fuel cell stacks can satisfy the fuel cell power demanded. The sizing strategy in this research was published in [38]. Figure 47 shows the SOC of the battery in response to the duty cycle. The maximum range of the state of charge in the figure belongs to when the cut off

frequency set to be 0.001. In this cut off frequency, the whole portion of the load applied to the battery packs, and the fuel cells are only using as the range extender. We also developed an adaptive charging scenario which changes the C-rate based on the SOC and hydrogen level of the tanks. In this adaptive scenario, the controller changes the C-rate when the SOC becomes shorter than 0.75%.

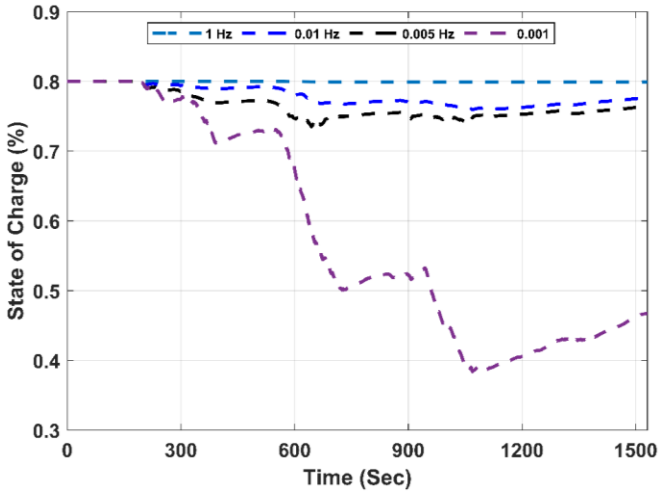

Figure 47: State of Charge versus Time for Different Cut off Frequencies of 1 Hz, 0.01 Hz, 0.005 Hz, and 0.001 Hz.

In terms of energy utilization, increasing the cut off frequency has been interpreted to increase the load portion of the fuel cells. In Figure 48, the ESS energy output, which shown in black, faces a decrease as the cut off frequency reaches its maximum value. Comparing to the Figure 16, which shows the demanded power [38] it is approximated that increasing the cut off frequency, which means the increase of fuel cell load portion can even result in energy shortage during the trip.

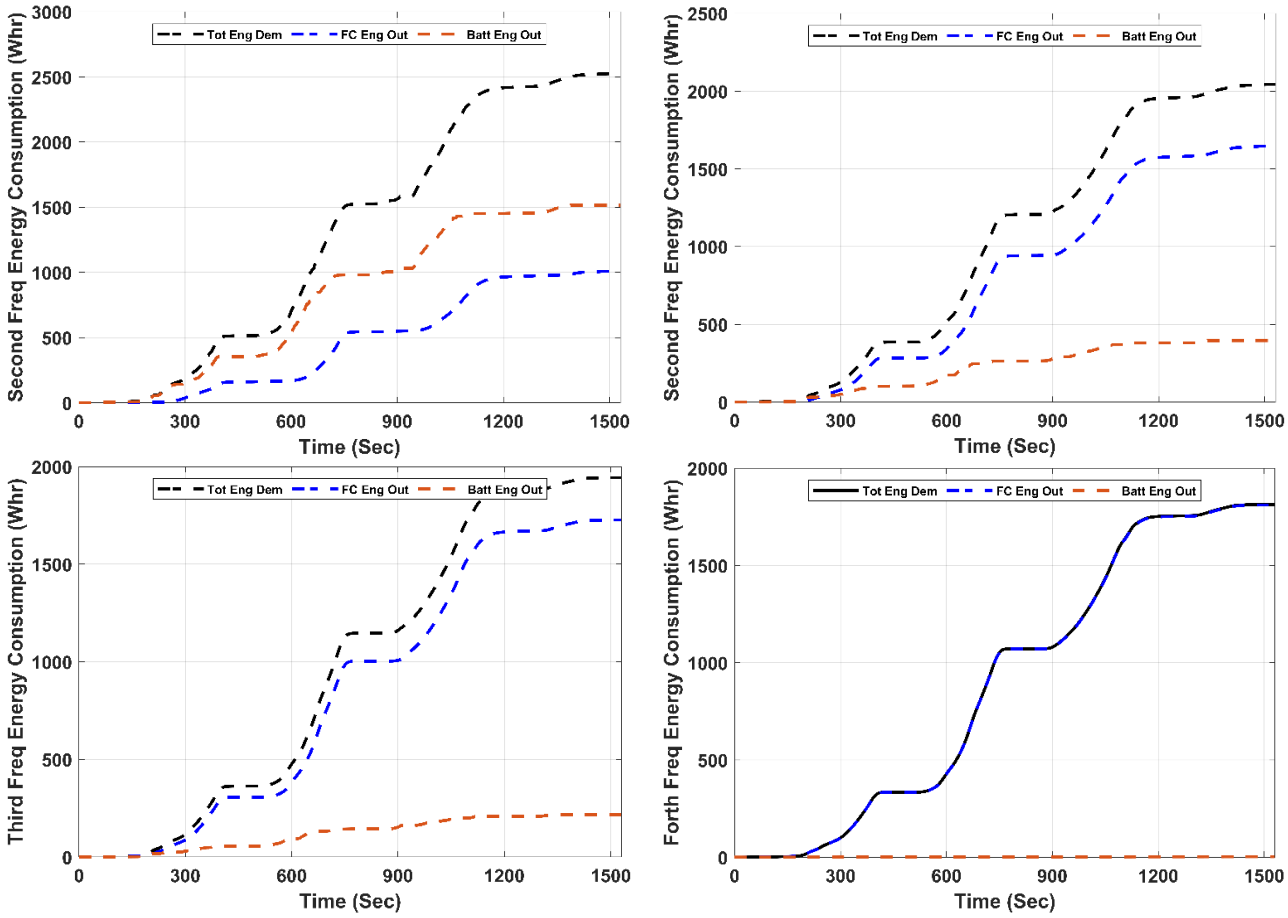

Figure 48: Energy Consumption Split for Different Cut off Frequencies of 1 Hz, 0.01 Hz, 0.005 Hz, and 0.001 Hz.

In terms of hydrogen consumption, Figure 49, shows the hydrogen consumption of the designed Hydrail powertrain. In this figure, the increase in cut off frequency resulted in an increase in hydrogen consumption, which might result in bigger tanks. However, hydrogen consumption varies between 5 Kg to 8 Kg [38]. The maximum hydrogen consumption belongs to when the cut off frequency set to be 1 Hz. It means that the batteries can help to reduce the size of the tank. This parameter might be considered as a designing parameter in finding an optimal value for battery sizes, splitting frequencies, etc.

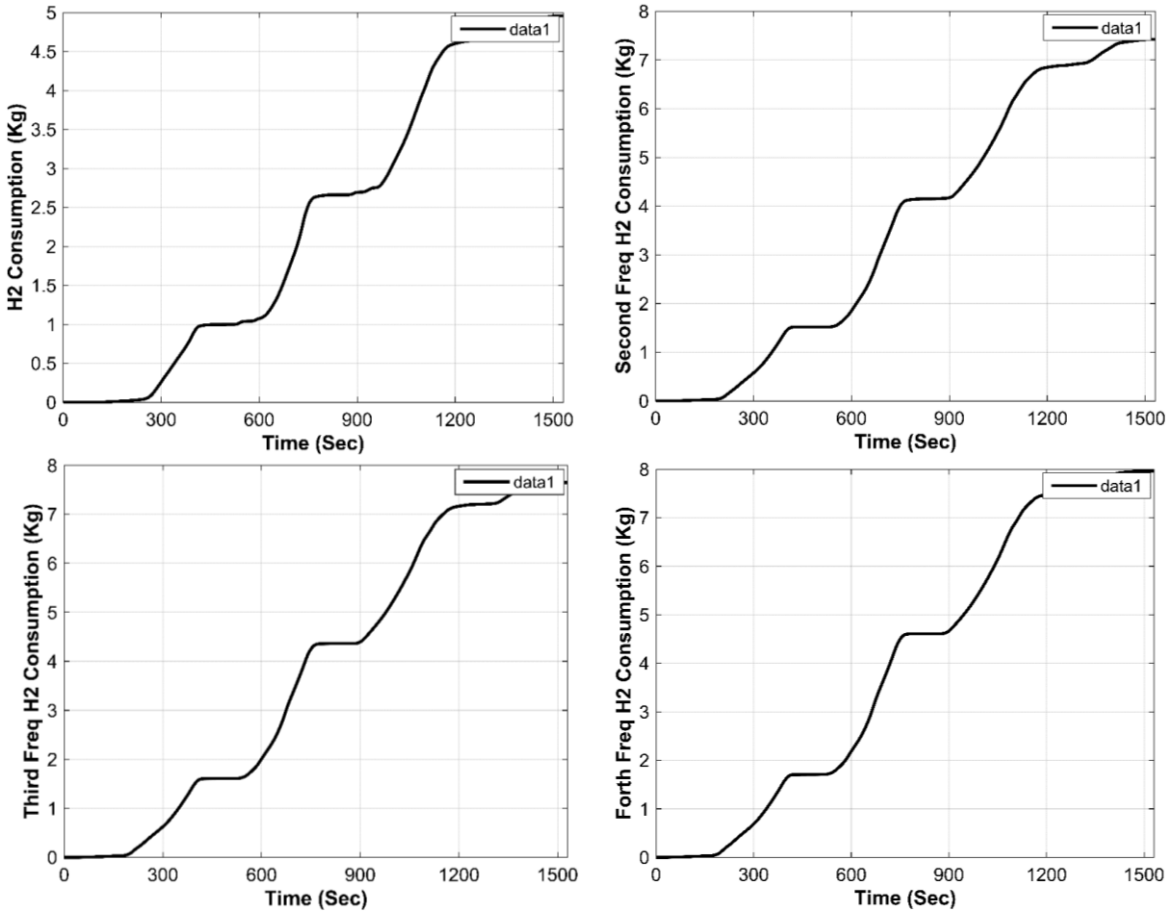

Figure 49: Hydrogen Consumption Split for Different Cut off Frequencies of 1 Hz, 0.01 Hz, 0.005 Hz, and 0.001 Hz.

In the developed model in this study, a simple rule was applied to approximate the dynamic of hydrogen crossover in the PEMFC model in response to the cut off frequency. Figure 52 shows the timely hydrogen consumption rate of the fuel cell stack. The crossover dynamic shows a different frequency as a function of cut off frequency. Red arrows show the dynamic in detail for the fuel cell in a similar region, and the differences are obvious.

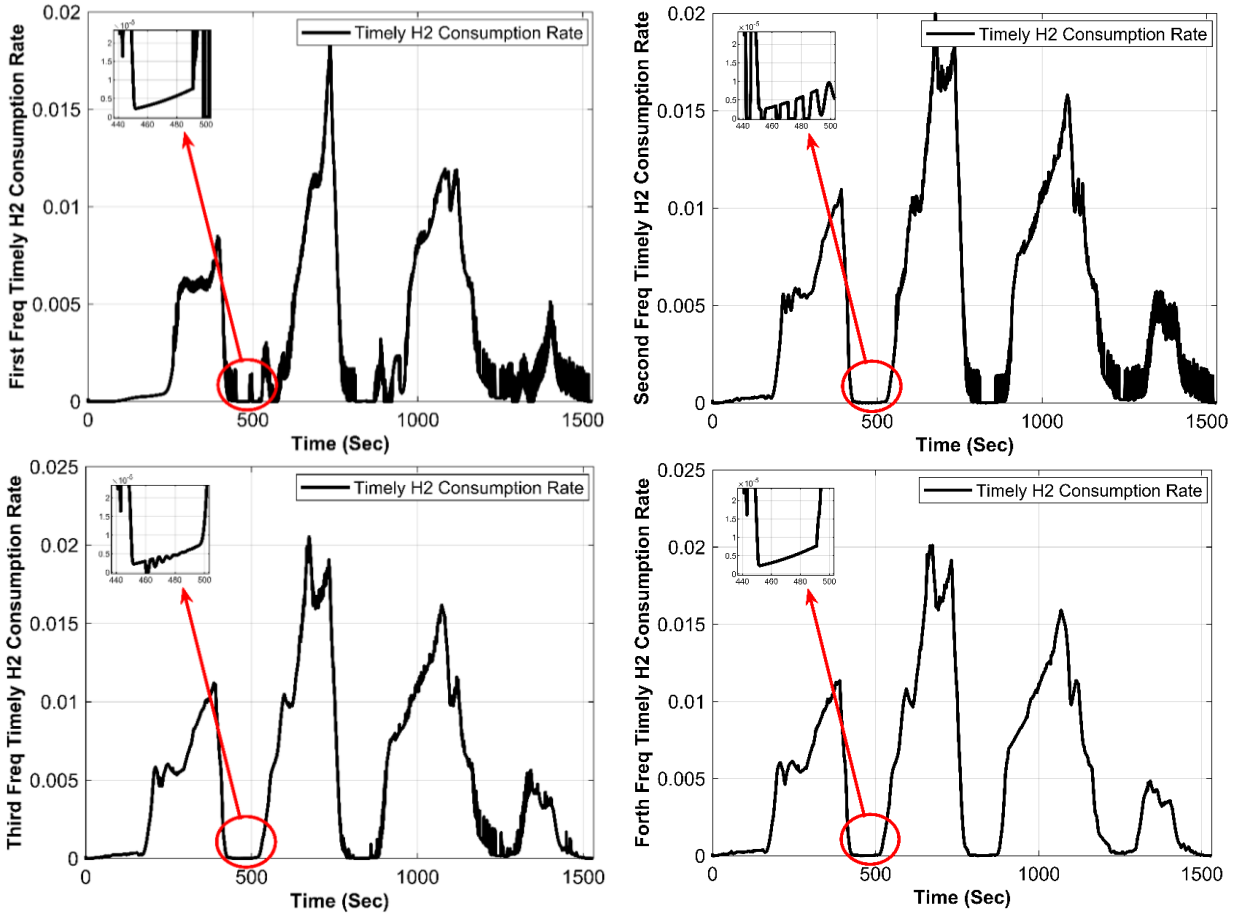

Figure 50: Timely Hydrogen Consumption Split for Different Cut off Frequencies of 1 Hz, 0.01 Hz, 0.005 Hz, and 0.001 Hz.

The model also estimates the temperature of the battery. This part of the subsystem was published in [90]. The temperature response of the battery was shown in Figure 51. The temperature decreases with increase in the cut off frequency. To interpret the response, the contribution of the battery and the portion of drawn current out of the battery is the main reason for such temperature range drop. The ambient temperature was set to be 22˚C. However, the interesting point in the temperature dynamic is that the sensitivity of the battery pack to the drive cycle is extremely high and the temperature reaches even 40˚C and it needs to be damped by means of an effective thermal management system.

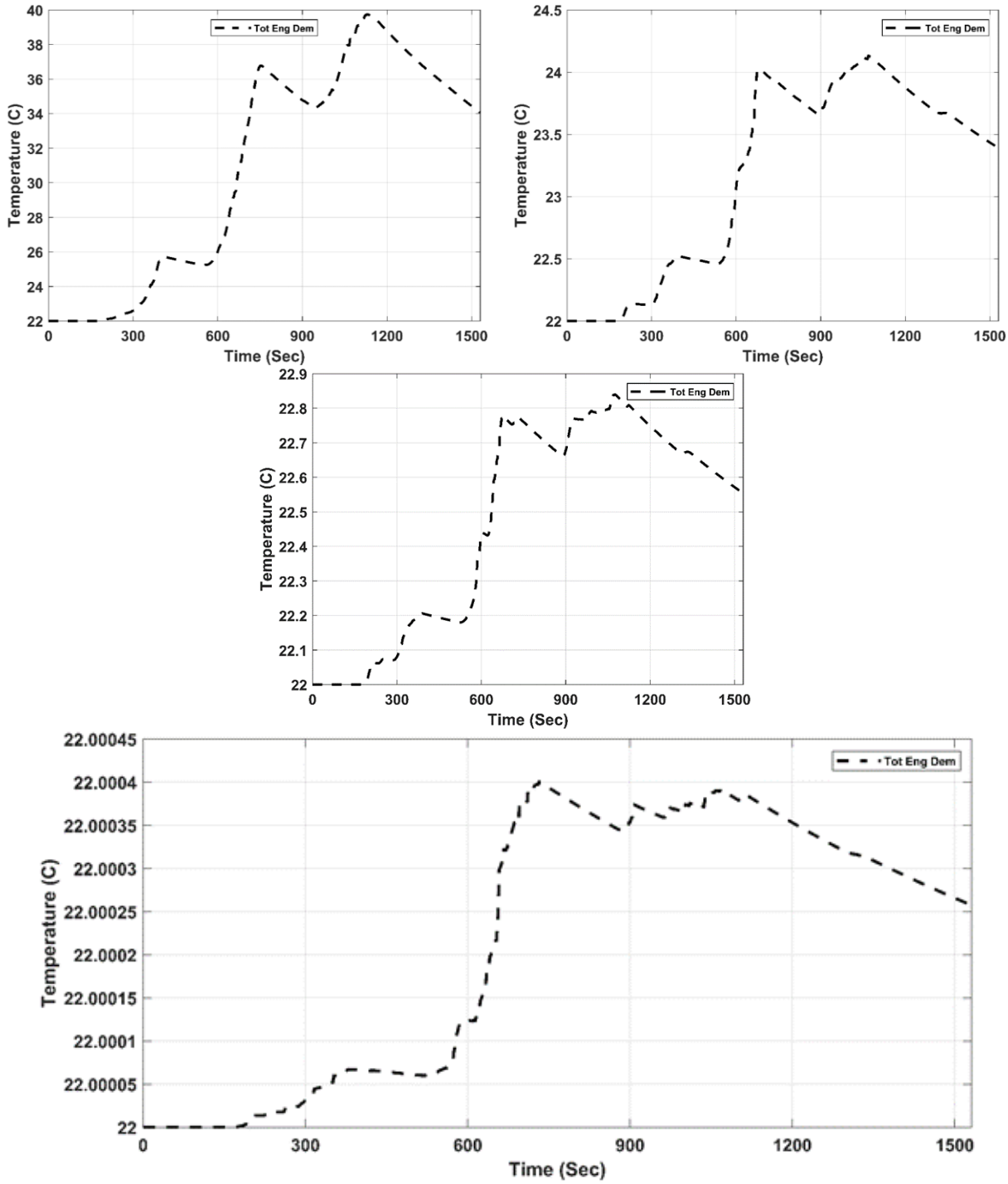

Figure 51: Temperature versus Time for Different Cut off Frequencies of 1 Hz, 0.01 Hz, 0.005 Hz, and 0.001 Hz.

A lifetime degradation analysis was carried out for the fuel cell and battery, considering the effect of different cut off frequencies on the power and capacity fade of the battery as well as the state of health of the fuel cell. Figure 52 shows the power and capacity fade in the battery-package based on the traveled distance. The rule of thumb was to change the battery pack when the battery

capacity fades to its 30% of the initial capacity. Figure 53 also shows the results of the simulation for the fuel cell state of health in terms of the traveled distance. According to Figure 52, the first battery pack change should be performed in 80×10^3 Km. As a result, it was observed that with an increase in cut off frequency, the capacity fade take place sooner. The reason for such prepone is the extra current drawn from the batteries in higher frequencies. Similar to the battery packs, in the fuel cell when the cut of frequency increase, it means that the load portion applied to the fuel cell increases. This would result a higher degradation which is approximately observed in Figure 53.

Table 22: Simulated Capacity fade in Response to Four Different Frequencies.

0.001 Hz	0.005 Hz	0.01 Hz	1 Hz
1	1	1	1
0.897	0.902	0.903	0.903
0.795	0.804	0.806	0.807
0.692	0.707	0.709	0.710
0.590	0.609	0.612	0.614
0.488	0.511	0.515	0.517
0.385	0.414	0.418	0.421
0.283	0.316	0.321	0.324
0.185	0.218	0.224	0.228

Table 23: Simulated Power Fade in Response to Four Different Frequencies.

0.001 Hz	0.005 Hz	0.01 Hz	1 Hz
1	1	1	1
0.990351	0.99079694	0.990862724	0.990912829
0.980703	0.981593881	0.981725447	0.981825659
0.971054	0.972390821	0.972588171	0.972738488
0.961405	0.963187762	0.963450894	0.963651318
0.951757	0.953984702	0.954313618	0.954564147
0.942108	0.944781643	0.945176341	0.945476977
0.932459	0.935578583	0.936039065	0.936389806
0.923256	0.926375524	0.926901789	0.927302635

Table 24: Simulated Fuel Cell State of Health in Response to Four Different Frequencies.

0.001 Hz	0.005 Hz	0.01 Hz	1 Hz
1	1	1	1
0.898117570	0.998400357	0.998400357205724	0.998517570102996
0.899621041	0.996800714	0.996800714411448	0.997014098894167
0.896614099	0.995201072	0.995201071617172	0.995510627685339
0.893607156	0.993601429	0.993601428822896	0.994007156476512
0.892103685	0.992001786	0.992001786028620	0.992503685267637
0.890600214	0.990402143	0.990402143234344	0.991000214058809
0.889096743	0.9888025	0.988802500440022	0.989496742849980
0.887593272	0.987202858	0.987202857645746	0.987993271641152
0.886089800	0.985603215	0.985603214851470	0.986489800432278
0.884586329	0.984003572	0.984003572057194	0.984986329223403
0.883082858	0.982403929	0.982403929262918	0.983482858014575
0.881579387	0.980804286	0.980804286468642	0.981979386805700
0.880075916	0.979204644	0.979204643674366	0.980475915596872
0.878572444	0.977605001	0.977605000880090	0.978972444388044
0.877068973	0.976005358	0.976005358085814	0.977468973179216
0.875565502	0.974405715	0.974405715291538	0.975965501970388
0.874062031	0.972806072	0.972806072497216	0.974462030761513
0.872558560	0.97120643	0.971206429702940	0.972958559552638
0.871055088	0.969606787	0.969606786908664	0.971455088343810

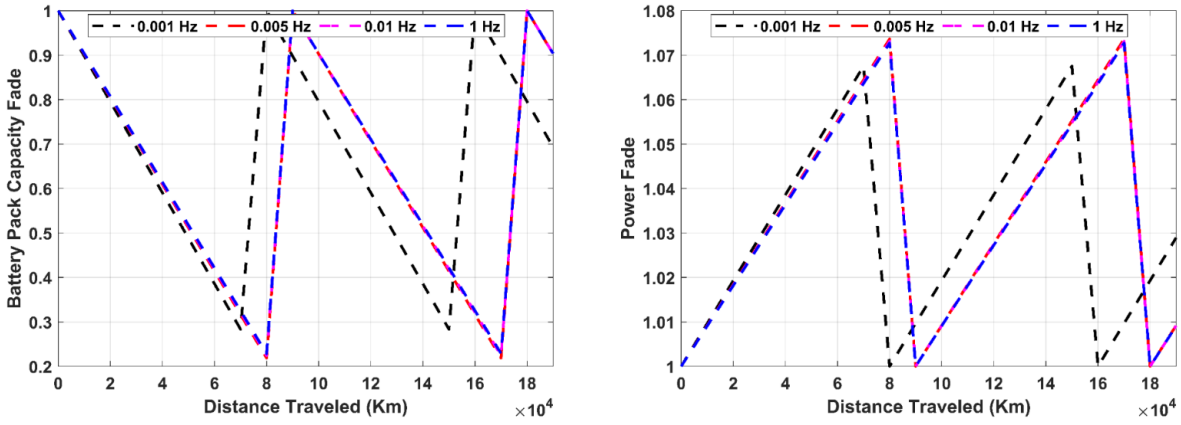

Figure 52: Battery Power and Capacity Fade Response in four different Cut off Frequency of 0.001, 0.005, 0.01, and 1 Hz.

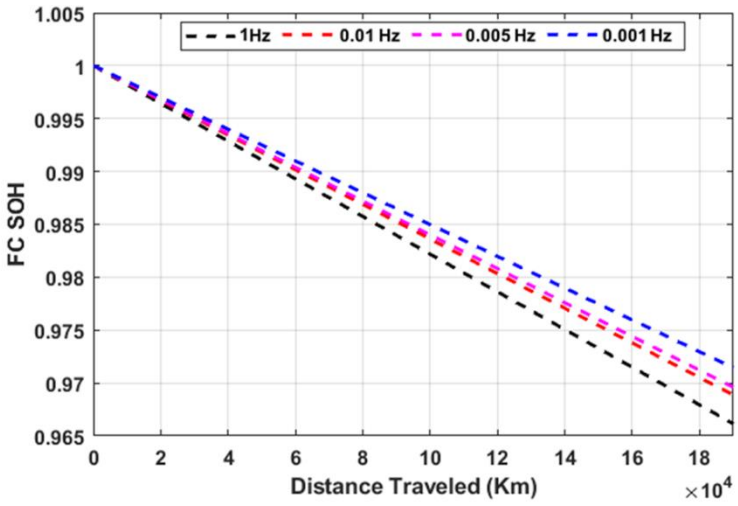

Figure 53: Fuel Cell SOH in response to four different Cut off Frequency of 0.001, 0.005, 0.01, and 1 Hz.

Chapter 5: Conclusion and Future Works

5.1 Introduction

According to the previous chapters, the Hydrail technology was approximately identified in details and the key options, as a case study, were analyzed for an individual track, Union Pearson. Although the applicability of this technology was approximated later in chapter four of this thesis, to justify the necessity of implementing the Hydrail technology, criteria pollutants (NO_x, HC, and PM) are emitted through the current DMUs working in the UP Express route was estimated and emission generated throughout the track was converted to the 24h local concentration using the commercial software, AERMOD. To figure out the risks of the track on human health, according to the estimated concentration in different residencies, the maximum estimated concentrations were compared with the Canadian Ambient Air Quality Standards (CAAQS). To compare a precise conclusion, a significant health risk assessment is needed to be performed to evaluate the impact of different pathways on social health. Such a health assessment can be performed using commercial software packages like "I-Rap View" to show the exact environmental effect for the track. However, conducting a health risk assessment on this scale was not in the scope of this study. In chapter 4, a hydrogen powertrain composed of the battery pack as the energy storage system and hydrogen fuel cell as a range extender was sized to support the estimated power demand. A frequency-domain power splitting algorithm was implemented using IIR filters, and a rule-based high-level control scenario was developed to supervise the energy flow based on the battery and fuel cell state of charge. The sensitivity of the developed model to different parameters was analyzed, and the long term simulation showed the effect of the different power splitting scenarios in terms of cut off frequency on the degradation of the energy sources.

5.2 Study Findings

The major findings after this research can be outlined as follows:

It was showed that the UP Express DMU's might have health impacts, in terms of hydrocarbons, on the buildings located near the track with vulnerable occupants. About 32 buildings were analyzed in this study. Although the effect was not significant, it should be mentioned that the track is considered as a low traffic railway. To evaluate the exact impact of the conventional powertrains in terms of the hydrocarbons, different emission factors for diverse types of

contaminants should be extracted from the QSR-19R engines defining the portion of hydrocarbons released from the engine. In the next step, a precise health impact analysis should be needed to quantify the health risk and life cycle of the exact track using appropriate software like the IRAP-h.

The hydrogen consumption, degradation of the battery packages, the temperature of the battery packages during each journey, and the state of health of the fuel cells were simulated considering four different frequencies. The cut-off frequency was set as the main parameter and based on the calculations, in the highest cut off frequency which means the fuel cell should supply the whole amount of the duty demand, each DMU utilizes 8 kg of H_2 during each trip. According to Table 8, the track has 154 trips per weekday and 146 trips for weekends. This amount means that the daily H_2 consumption of the track for each weekday is about 1232 kg and for a weekend day is 1168 kg. Accordingly, 14656 kg of H_2 is consumed during each week. In Table 17, the accepted hydrogen price for the FCHEVs was shown. In the transportation sector, it was shown that the hydrogen price might be equal to 4.72 CAD × kg^{-1}, and assuming a similar price for the hydrogen supply for trains, the weekly price of the hydrogen demand for this individual track should be 215736 CAD. To calculate this value for the lowest frequency, the H_2 consumption in the 0.001 Hz is 5.1 kg. In this frequency, the batteries are the main suppliers of power. After such calculations, it turned out that the weekly hydrogen consumption is about 5416 kg and the weekly hydrogen investment should become 79723 CAD. With a simple comparison between two different values, it turned out that the splitting frequency has an extreme effect on the economy of transportation.

5.3 Key component Overview and future studies

A Hydrail, as an integrated system, consists of diverse types of components and subsystems. These subsystems, from the production of hydrogen to dispensing of the hydrogen, are modular, which means that the system can be implemented locally with limited traffic as an initial phase of implementation. As an example, in the GO rail corridor, UP Express might be a start for implementing a Hydrail platform as the traffic is very low and implementing a baseline might be considered reasonable. In the next phases, the Hydrail platform can be expanded to the other connected and not connected tracks. However, future expansion of the services, as well as the other designing parameters, might become considered as the cost functions in the development progress. Considering such parameters in modeling a Hydrail platform should be place of research before

running an optimization. However, this part was not defined in the scope of this study. This study aimed to perform a conceptual design on one end of a Hydrail system, which is the rolling stock, and the sensitivity analysis took place.

5.3.1 Power to Gas

Predominately clean Ontario grid has various supply options from solar and hydro-electric to the wind and nuclear, with natural gas to support the peak demand. Such intermittent power resources are utilized as a hydrogen production pathway in Hydrail application. However, these electrolytic hydrogen production strategies would result in 80% GHG emission reduction [93]. But these methods are too expensive [94]. The possibility of combining renewable energy resources with the power to gas facilities to convert the generated surplus power to the hydrogen has been pondered for several years [95]. One important opportunity of the power to gas methods is the ability to work in real-time infrastructures. The platform can be optimized based on grid demand. So the opportunity of generating hydrogen at the moment of lower demand compared to the nominal capacity of the renewable resource could become applicable. Using the produced hydrogen is valuable where the renewable power generation capacity and the electricity price are both periodically fluctuating [94]. As future work, it might be possible to implement a model, as another end of the Hydrail system, to introduce the dynamic of renewables and design power to gas facility to support an individual track's hydrogen demand. In such study, the available power should be optimally controlled based on the microgrid characteristic. Depending on the price, the grids availability, and the hydrogen storage capacity, electrolyzers should draw electricity from the grid to produce hydrogen. With the aim of power to gas, the Ontario grid will allow the GO system's Hydrail to indirectly draw electricity from the grid even in peak time. Also, when the hydrogen demand is more than the storage, in the peak time, the hydrogen to gas concept might be added to the Hydrail concept to compensate the intrinsic grid's fluctuation from one side and the big two sources of intermittency of renewables from another side. Irregularities belong to the random fluctuation of the renewables as well as predictably variable outputs [96]. To optimize the system, several parameters and factors are available. Table 25 shows some of these factors.

Table 25: Electricity subsystem parameters.

Parameters	Description	Significance	Impact
Electricity Price ($\$MWh^{-1}$)	The market cost of electricity, one hour ahead of time.	High, Hourly fluctuated and should be analyzed before ordering the electricity	Operating Cost
Demanded electricity ($GWhd^{-1}$)	The net power demand for Hydrail system	High, showing the amounts of electricity for one application	Operating Cost
Surplus supply (GWh)	Excess electricity	High, lower price of electricity	Operating Cost
Future required electricity (GWh)	Apart from other sectors	Medium, reduce accessible surplus	Operating Cost

5.3.2 Hydrogen Production subsystem

Different strategies might be utilized to support the hydrogen demand of a rail route. From ammonia-based hydrogen production method which has its benefits [97]; to the compressed hydrogen produced in central or distributed hydrogen production pathways. In terms of Hydrail, concentrated pathways have been received more attention so far [93]. The pathway has the following components:

1. Feeding water subsystem,
2. Stacks,
3. Drying subsystem,
4. Cooling subsystems, and,
5. Power and power management subsystem.

In this pathway, the output hydrogen of the electrolyzers is gaseous. Depending on the Hydrail system, the produced hydrogen is sent to the storage system to be utilized in compressed or liquefied phase. However, Table 26 shows the design parameters for this subsystem.

Table 26: Designing parameters for Hydrogen production subsystems.

Parameters	Description	Significance	Impact
Electrolyzer Price ($\$\times kWe^{-1}$)	The significant payment in a Hydrail system	High, numerous modules are needed, and the price can be reduced in a good design	Capital Cost
Electrolyzer Efficiency ($kWh\times kg^{-1}$)	Demanded Energy for 1kg hydrogen	High, affect power consumption to H2 production	Operating Cost
Current density ($A\times cm^{-2}$)	Current can be drawn across the membrane active area	Medium, current density increase rise the power consumption	Operating Cost
H2 production size (Number)	Low-cost hydrogen should be produced	High, the capital cost increase	Operating Cost

5.4 Hydrogen Storage Subsystem

The key equipment of this subsystem includes:

1. Compressor;
2. Flow controller;
3. Regulators;
4. Sensors;
5. Tanks; and,
6. Controls.

These components are only for a Hydrail system working with gaseous hydrogen. For those systems are working with liquid hydrogen, the refrigerant plant should be installed as well. There are some other subsystems should be considered in an end-to-end Hydrail system like distribution and piping subsystem, refueling based subsystems, dispensing subsystems, etc. Although modeling the dynamics of these subsystems are not in the scope of this theses, the model is capable of being updated with any other types of parameters and subsystems.

5.5 Study recommendations

- This sensitivity analysis recommending to implementing the other ends of a Hydrail system to customize different end in an integrated platform based on cost functions and boundary conditions would be defined for an individual track.

- There are only a few studies which considered the health impact of a track on local residencies based on the drive and duty cycle using AERMOD View. The reason is that the Gaussian models, as mentioned before in the thesis, performing the calculations based on the hourly emission rates. This thesis recommends applying timely emissions with higher resolutions instead of hourly emissions. This way, concentration and health risks would be more realistic.
- The developed multilayer system is appropriate to be coupled with an optimization algorithm. This would provide a powertrain with an optimized set of components. In the optimization process, the downstream emission of the Hydrail should be considered as a cost function.
- Modeling an adaptive thermal management system.
- Using other renewables as range extenders in parallel with the implemented hydrogen range extender.
- Modeling onboard ammonium-based hydrogen production system.

References

[1] Metrolinx. (2017). Air Quality Impact Assessment-Metrolinx Georgetown South Service Expansion and Union-Pearson Rail Link. *Toronto Board of Health and the Parks and Environment,* Accessed on Feb. 1. [Online]. Available: www.metrolinx.com.

[2] Ramboll. (2017). Air Quality Technical Report; 303 Baldwin Avenue Development. *San Mateo,* Accessed on Feb. 1. [Online]. Available: https://www.cityofsanmateo.org/.

[3] Hoek, G., Brunekreef, B., Goldbohm, S., Fischer, P., & Van Den Brandt, P. A. (2002). Association between mortality and indicators of traffic-related air pollution in the Netherlands: a cohort study. *The Lancet,* 360 (9341), 1203-1209.

[4] Faiz, A. (1993). Automotive emissions in developing countries-relative implications for global warming acidification and urban air quality. *Transportation Research Part A: Policy and Practice,* 27(3). 167-186.

[5] Yifang, Z. Hinds, W. C. Kim, S. Shen, S., & Sioutas, C. (2002). Study of ultrafine particles near a major highway with heavy-duty diesel traffic. *Atmospheric Environment,* 36 (27), 4323-4335.

[6] Mullner, R. M. Chung, K. Croke, K. G., & Mensah, E. K. (2004). Introduction: Geographic Information Systems in Public Health and Medicine. *Journal of Medical Systems,* 28 (3), 215–221.

[7] Krämer, U. Koch, T. Ranft, U. Ring, J., & Behrendt, H. (2000). Traffic-related air pollution is associated with atopy in children living in urban areas, *Epidemiology,* 11 (1), 64-70.

[8] Venn, A. Lewis, S. Cooper, M. Hubbard, R. Hill, I. Boddy, R. Bell, M., & Britton, J. (2000). Local road traffic activity and the prevalence, severity, and persistence of

wheeze in school children: combined cross sectional and longitudinal study. *Occupational and Environmental Medicine*, 57 (3), 152-158.

[9] Jerrett, M. Burnett, R. T. Kanaroglou, P. Eyles, J. Finkelstein, N., & Giovis, C. (2001). A GIS environmental justice analysis of particulate air pollution in Hamilton, Canada. *Environment and Planning A*, 33, 955-973.

[10] Hoek, G. Fischer, P. Van Den Brandt, P. Goldbohm, S., & Brunekreef, B. (2001). Estimation of long-term average exposure to outdoor air pollution for a cohort study on mortality. *J Expo Anal Environ Epidemiol*, 11 (6), 459-69.

[11] Bellander, T. Berglind, N. Gustavsson, P. Jonson, T. Nyberg, F. Pershagen, G., & Järup, L. (2001). Using geographic information systems to assess individual historical exposure to air pollution from traffic and house heating in Stockholm. *Environ Health Perspect*, 109 (6), 633-639.

[12] Zmirou, D. Gauvin, S. Pin, I. Momas, I. Just, J. Sahraoui, F. Moullec, Y. L. Brémont, F. Cassadou, S. Albertini, M. Lauvergne, N. Chiron, M. Labbé A., & VESTA Investigators. (2002). Five epidemiological studies on transport and asthma: objectives, design and descriptive results. *J Expo Anal Environ Epidemiol*, 12 (3), 186-96.

[13] Sahsuvaroglu, T. Arain, A. Kanaroglou, P. Finkelstein, N. Newbold, B. Jerrett, M. Beckerman, B. Brook, J. Finkelstein, M., & Gilbert, N. L. A. (2006). Land Use Regression Model for Predicting Ambient Concentrations of Nitrogen Dioxide in Hamilton, Ontario, Canada. *Journal of the Air & Waste Management Association*, 56 (8), 1059-1069.

[14] Sahsuvaroglu, T. Jerrett, M. Sears, M. R. McConnell, R. Finkelstein, N. Arain, A. Newbold, B., & Burnett, R. (2009). Spatial analysis of air pollution and childhood asthma in Hamilton, Canada: comparing exposure methods in sensitive subgroups. *Environmental Health*, 8 (1), 14.

[15] Mulholland, J. A. Butler, A. J. Wilkinson, J. G. Russell, A. G., & Tolbert, P.E. (1998). Temporal and spatial distributions of ozone in Atlanta: regulatory and epidemiologic implications. *J Air Waste Manag Assoc*, 48 (5), 418-426.

[16] Nafstad, P. Håheim, L. L. Oftedal, B. Gram, F. Holme, I. Hjermann, I., & Leren, P. (2003). Lung cancer and air pollution: a 27 year follow up of 16209 Norwegian men. *Thorax*, 58 (12), 1071-1076.

[17] Clench-Aas, J. Bartonova, A. Bøhler, T. Grønskei, K. E. Sivertsen, B., & Larssen, S. (1999) .Air pollution exposure monitoring and estimating," *J Environ Monit,* 1 (4), 313-319.

[18] Cimorelli, A. J. Perry, S. G. Venkatram, A. Weil, J. C. Paine, R. J. Wilson, R. B. Lee, R. F. Peters, W. D., & Brode, R. W. (2005). AERMOD: A Dispersion Model for Industrial Source Applications. Part I: General Model Formulation and Boundary Layer Characterization. *Journal of Applied Meteorology,* 44 (5), 682-693.

[19] Hrubá, F. Fabiánov, E. Koppová, K., & Vandenberg, J. J. (2001). Childhood respiratory symptoms, hospital admissions, and long-term exposure to airborne particulate matter. *J Expo Anal Environ Epidemiol,* 11 (1), 33-40.

[20] Nicholls, M. E. Pielke, R. A. Eastman, J. L. Finley, C. A. Lyons, W. A. Tremback, C. J. Walko, R. L., & Cotton, W. R. (1995). Applications of the RAMS Numerical Model to Dispersion over Urban Areas," *Wind Climate in Cities*, 277, 703-732.

[21] Williams, T. I. Schaaf, W. E., & Burnette, A. E. (2000) "A History of Invention: From Stone Axes to Silicon Chips. 18th ed, London, Little, Brown.

[22] Jansson, A. Olander, L. Olofsson, U. Sundh, J. Söderberg, A., & Wahlström, J. (2010). Ultrafine Particle Formation from Wear, *International Journal of Ventilation,* 9 (1), 83-88.

[23] Dincer, I. Hogerwaard, J., & Zamfirescu, C. (2016). Clean Rail Transportation Options. *Green Energy and Technology*.

[24] Fuglestvedt, J. Berntsen, T. Myhre, G. Rypdal, K., & Skeie, R. B. (2008) “Climate forcing from the transport sectors,” Proceedings of the National Academy of Sciences, 105 (2), 454-458.

[25] Steinberg, B. A., & Scott, D. S. (1984). Hydrogen vs diesel fueled locomotives: a technoeconomic appraisal. *International Journal of Hydrogen Energy,* 9 (1), 101-107.

[26] Patil, P. G. (1992). US Department of Energy fuel cell program for transportation applications. *Journal of Power Sources,* 37 (1), 171-179.

[27] Miller, A. R. Hess, K. S. Barnes, D. L., & Erickson, T. L. (2007). System design of a large fuel cell hybrid locomotive. *Journal of Power Sources,* 173(2), 935-942.

[28] Ikeya, T. (2007). Development of fuel-cell and hydrogen technologies and their application to rolling stock in Japan. *Japan Railway Engineers' Association,* 47 (1). 17-19.

[29] Venkatram, A. Brode, R. Cimorelli, A. Lee, R. Paine, R. Perry, S. Peters, W. Weil, J. Wilson, R. (2001). A complex terrain dispersion model for regulatory applications. *Atmospheric Environment,* 35 (24), 4211-4221.

[30] Willis, G. E., & Deardorff, J. W. (1981). A laboratory study of dispersion from a source in the middle of the convectively mixed layer. *Atmospheric Environment,* 15 (2), 109-117.

[31] Hanna, S. R., & Paine, R. J. (1989). Hybrid Plume Dispersion Model (HPDM) Development and Evaluation. *Journal of Applied Meteorology,* 28 (3), 206-224.

[32] Barad, M. L. PROJECT PRAIRIE GRASS, A FIELD PROGRAM IN DIFFUSION. 2014.

[33] Venkatram, A. Strimaitis, D. Dicristofaro, D. (1984). A semiempirical model to estimate vertical dispersion of elevated releases in the stable boundary layer. *Atmospheric Environment,* 18 (5), 923-928.

[34] Venkatram, A. (1992). Vertical dispersion of ground-level releases in the surface boundary layer. *Atmospheric Environment Part A General Topics*, 26 (5), 947-949.

[35] Metrolinx. (2014). Regional Express Rail (RER), A. http://www.metrolinx.com, Editor. [Accessed 22 June 2017].

[36] SMART. (2010). Available online: http://sonomamarintrain.org [accessed on 1 October 2018].

[37] Miller, A. R. Peters, J. Smith, B. E., & Velev, O. A. (2006). Analysis of fuel cell hybrid locomotives. *Journal of Power Sources*, 157 (2), 855-861.

[38] Haji Akhoundzadeh, M. Raahemifar, K. Panchal, S. Samadani, E. Haghi, E. Fraser, R., & Fowler, M. (2019). A Conceptualized Hydrail Powertrain: A Case Study of the Union Pearson Express Route. *World Electric Vehicle Journal*, 10 (2), 32.

[39] Meegahawatte, D. Hillmansen, S. Roberts, C. Falco, M. McGordon, A., & Jennings, P. (2010). Analysis of a fuel cell hybrid commuter railway vehicle. *Journal of Power Sources*, 195 (23), 7829-7837.

[40] Sripad, S., & Viswanathan, V. (2017). Performance Metrics Required of Next-Generation Batteries to Make a Practical Electric Semi Truck. *ACS Energy Letters*, 2 (7), 1669-1673.

[41] Transportation Research Board National Academies of Sciences. Engineering, Medicine. (2019). National Academies of Sciences, and Medicine, Comparison of Passenger Rail Energy Consumption with Competing Modes. *Washington, DC: The National Academies Press,* Accessed on Feb. 1.. [Online]. Available: www.nap.edu.

[42] Metrolinx. https://www.upexpress.com/

[43] Parent, M. E. Rousseau, M. C. Boffetta, P. Cohen, A., & Siemiatycki, J. (2007). Exposure to diesel and gasoline engine emissions and the risk of lung cancer. *Am J Epidemiol,* 165(1), 53-62.

[44] Fuels Assessment Section. Water and Air Quality Bureau, Healthy Environments and Consumer Safety Branch; Health Canada. (2016). “Human Health Risk Assessment for Diesel Exhaust. *Ottawa: Health Canada*, [Online]. Available: http://publications.gc.ca.

[45] Canadian Environmental Law Association, (2008). Environmental Reporting, Disclosure, and Innovation Program in the City of Toronto. [Online]. Available: www.cela.ca.

[46] Perrotta, K., & The City of Toronto. (2002). Ten Key Carcinogens in Toronto Workplaces and Environment: Assessing the Potential Exposure. *Health Promotion & Environmental Protection Office, Toronto Public Health.* [Online]. Available: http://www.city.toronto.on.ca.

[47] California Air Resources Board. (2015). Vision 2.0 Heavy-Duty Vehicles Module. [Online]. Available: www.arb.ca.gov.

[48] Peninsula Corridor Joint Powers Board. (2014). Peninsula Corridor Electrification Project Environmental Impact Report. [Online]. Available: www. http://www.caltrain.com.

[49] EPA. (2009). Technical Highlights Emission Factors for Locomotives. [Online]. Available: https://nepis.epa.gov.

[50] Agarwal, A. K. Gautam, A. Sharma, N., & Singh, A. P. (2019). Methanol and the Alternate Fuel Economy. *Energy, Environment, and Sustainability*.

[51] Sharma, A., & Strezov, V. (2017). Life cycle environmental and economic impact assessment of alternative transport fuels and power-train technologies. *Energy*, 133, 1132-1141.

[52] Hoffrichter, A. Fisher, P. Tutcher, J. Hillmansen, S., & Roberts, C. (2014). Performance evaluation of the hydrogen-powered prototype locomotive Hydrogen Pioneer. *Journal of Power Sources*, 250, 120-127.

[53] Abdelrahman, A. S. Attia, Y. Woronowicz, K., & Youssef, M. Z. (2016). Hybrid Fuel Cell/Battery Rail Car: A Feasibility Study. *IEEE Transactions on Transportation Electrification,* 2 (4), 493-503.

[54] Donnelly, F. W., & Maier, J. E. (2006). Locomotive power train architecture (US20060061307A1). Retrieved from https://patents.google.com/

[55] Din, T., & Hillmansen, S. (2018). Energy consumption and carbon dioxide emissions analysis for a concept design of a hydrogen hybrid railway vehicle. *IET Electrical Systems in Transportation,* 8 (2), 112-121.

[56] Washing, E. M., & Pulugurtha, S. S. (2016). Energy demand and emission production comparison of electric, hydrogen and hydrogen-hybrid light rail trains. *International Journal of Rail Transportation,* 4 (1), 55-70.

[57] Badji, A. Abdeslam, D. O. Becherif, M. Eltoumi, F., & Benamrouche, N. (2019). Analyze and evaluate of energy management system for fuel cell electric vehicle based on frequency splitting. *Mathematics and Computers in Simulation.*

[58] Fragiacomo, P., & Piraino, F. (2018). Numerical modelling of a PEFC powertrain system controlled by a hybrid strategy for rail urban transport. *Journal of Energy Storage,* 17, 474-484.

[59] Wickens, A. H. (1998). The dynamics of railway vehicles-from Stephenson to Carter. *Part F: Journal of Rail and Rapid Transit,* 212 (3), 209-217.

[60] Emadi, A. Rajashekara, K. Williamson, S. S., & Lukic, S. M. (2005). Topological overview of hybrid electric and fuel cell vehicular power system architectures and configurations. *IEEE Transactions on Vehicular Technology,* 54 (3), 763-770.

[61] Cipek, M. Pavković, D. Kljaić, Z., & Mlinarić, T. J. (2019). Assessment of battery-hybrid diesel-electric locomotive fuel savings and emission reduction potentials based on a realistic mountainous rail route. *Energy,* 173, 1154-1171.

[62] Gaskell, G. H. (2015). The Origin of Locomotive Class Names," *The Railway and Locomotive Historical Society Bulletin,* 1952 (87), 83-95.

[63] Myamlin, S. Neduzha, L. Urbutis, Z. (2016). Research of Innovations of Diesel Locomotives and Bogies. *Procedia Engineering,* 134, 469-474.

[64] Graff-Baker, W. S. (1952). Considerations on Bogie Design, with Particular Reference to Electric Railways. *Proceedings of the Institution of Mechanical Engineers,* 166(1), 217-236.

[65] Ronanki, D. Singh, S. A., & Williamson, S. S. (2017). Comprehensive Topological Overview of Rolling Stock Architectures and Recent Trends in Electric Railway Traction Systems. *IEEE Transactions on Transportation Electrification,* 3 (3), 724-738.

[66] Bernet, S. (2000) Recent developments of high power converters for industry and traction applications. *IEEE Transactions on Power Electronics,* 15 (6), 1102-1117.

[67] Jahns, T. M. Blasko, V. (2001). Recent advances in power electronics technology for industrial and traction machine drives. *Proceedings of the IEEE,* 89 (6), 963-975.

[68] Eckel, H. Bakran, M. M. Krafft, E. U. Nagel, A. (2005). A new family of modular IGBT converters for traction applications. *European Conference on Power Electronics and Applications*.

[69] Mermet-Guyennet, M. (2010). New power technologies for traction drives. *Proceeding in SPEEDAM*.

[70] Meng, N. I., & Leung, M. K. H. (2005). Hydrogen storage technology," *Renewable Energy*, 35 (1).

[71] An, E. K., & Zhang, W. (2010). Technical Economic Analysis of Ammonia Based Hydrogen. *Journal of Tongji University (natural science),* 38 (9), 1371-1374.

[72] An, E. K. Yang, X., & Song, Y. (2008). The Application of Ammonia as Hydrogen Carrier and Fuel. *Energy Technology*, 29 (4), 209-211.

[73] Makepeace, J. W. Teng, H. Claudia, W. Torben, J. R. Chang, F. Vegge, T. Ngene, P. Kojima, Y. de Jongh, P. E. Chen, P., & David, W. I. F. (2019). Reversible ammonia-based and liquid organic hydrogen carriers for high-density hydrogen storage: Recent progress. *International Journal of Hydrogen Energy*, 44 (15), 7746-7767.

[74] Tractebel. (2017). Study on early business case for H2 in energy storage and more broadly power to H2 applications. *Fuel cells and hydrogen two joint undertaking*.

[75] Chen, H. Zhao, X. Qu, B. Zhang, T. Pei, P. (2019). Evaluating the Gas Distribution Quality of PEMFC in Dynamic Response: Severe Condition of Delayed Gas Supply," *Energy Procedia,* 158, 2290-2298.

[76] Killer, A. Armstorfer, A. Díez, A.E., & Biechl, H. (2012). Ultracapacitor assisted regenerative braking in metropolitan railway systems. *Proceeding In 2012 IEEE Colombian Intelligent Transportation Systems Symposium (CITSS)*.

[77] Steiner, M., & Scholten, J. (2005). Energy storage on board of railway vehicles. *Proceeding In 2005 European Conference on Power Electronics and Applications*.

[78] Brenna, M. Foiadelli, F. Tironi, E., & Zaninelli, D. (2007). Ultracapacitors application for energy saving in subway transportation systems. *Proceeding In 2007 International Conference on Clean Electrical Power.*

[79] Stevens, M. (2009). Hybrid Fuel Cell Vehicle Powertrain Development Considering Power Source Degradation. *UWSpace*.

[80] Fragiacomo, P., & Piraino, F. (2018) Numerical modeling of a PEFC powertrain system controlled by a hybrid strategy for rail urban transport. *Journal of Energy Storage,* 17. 474-484.

[81] Harris, F.J. (1978). On the use of windows for harmonic analysis with the discrete Fourier transform. *Proceedings of the IEEE*, 66(1), 51-83.

[82] Richardson, L.F., & W.F. Eddy. (2019). Algorithm 991: The 2D Tree Sliding Window Discrete Fourier Transform. *ACM Trans. Math. Softw*, 45(1), 1-12.

[83] Wang, H., Gaillard, A., & Hissel, D. (2019). A review of DC/DC converter-based electrochemical impedance spectroscopy for fuel cell electric vehicles. *Renewable Energy*, 141, 124-138.

[84] Chen, H. Song, Z. Zhao, X. Zhang, T. Pei, P., & Liang, C. (2018). A review of durability test protocols of the proton exchange membrane fuel cells for vehicle. *Applied Energy*, 224, 289-299.

[85] Arora, D. (2019). Direct hybridization of PEMFC and supercapacitors: Effect of excess hydrogen on a single cell fuel cell durability and its feasibility on fuel cell stack. *Electrochimica Acta*, 310, 213-220.

[86] Wei, Z. Song, Y. Wang, L. Zhang, C. Lam, J. C. C. Teng, X. Zhou, E., & Han, M. (2019). Design and energy efficiency analysis of a pure fuel cell vehicle for Shell eco racer. *International Journal of Energy Research*, 43 (7).

[87] Lee, R. Homan, S. Dowell, N. M., & Brown, S. (2019). A closed-loop analysis of grid scale battery systems providing frequency response and reserve services in a variable inertia grid. *Applied Energy*, 236, 961-972.

[88] Ali, A.M., & Söffker, D. (2018). Towards Optimal Power Management of Hybrid Electric Vehicles in Real-Time: A Review on Methods, Challenges, and State-Of-The-Art Solutions. *Energies*, 11 (3), 476.

[89] Kim, Y. Lee, T.K., & Filipi, Z. (2012). Frequency Domain Power Distribution Strategy for Series Hybrid Electric Vehicles. *SAE International*.

[90] Panchal, S. Haji Akhoundzadeh, M. Raahemifar, K. Fowler, M., & Fraser, R. (2019). Heat and mass transfer modeling and investigation of multiple

LiFePO4/graphite batteries in a pack at low C-rates with water-cooling. *International Journal of Heat and Mass Transfer*, 135, 368-377.

[91] Kim, Y. (2014). Hardware-in-the-loop validation of a power management strategy for hybrid powertrains. Control Engineering Practice, 29, 277-286.

[92] Samadani, E. Farhad, S. Scott, W. Mastalia, M. Gimenez, L.E. Fowler, M., & Frasera, R.A. (2015). Empirical Modeling of Lithium-ion Batteries Based on Electrochemical Impedance Spectroscopy Tests. *Electrochimica Acta*, 160, 169-177.

[93] Jacob Engineering Group, Ernst & Young Orenda Corporate Finance, & Canadian Nuclear Laboratories. (2018). Regional express rail program Hydrail feasibility study report. *Metrolinx,* Accessed on Feb. 1, 2019. [Online]. Available: www.metrolinx.com.

[94] Glenk, G., & Reichelstein, S. (2019). Economics of converting renewable power to hydrogen," *Nature Energy*, 4 (3), 216-222.

[95] Shaner, M.R. Atwater, H.A. Lewis, S.N., & McFarland, E.W. (2016). A comparative technoeconomic analysis of renewable hydrogen production using solar energy. *Energy & Environmental Science*, 9 (7), 2354-2371.

[96] Lemmon, J.P. (2015). Energy: Reimagine fuel cells. Nature Comment, 525 (7570), 447–449.

[97] Chu, Y. Wu, Y. Chen, J. Zheng, S., & Wang, Z. (2019). Design of energy and materials for ammonia-based extended-range electric vehicles. *Energy Procedia*, 158, 3064-3069.